이학박사학위청구논문

지방세포 기능 조절에 있어 지방대사물 및 활성산소의 역할 규명

Roles of lipid metabolites and reactive oxygen species in the regulation of adipocyte function

2021년 2월

서울대학교 대학원

생명과학부

손 지 형

지방세포 기능 조절에 있어
지방대사물 및 활성산소의 역할 규명

Roles of lipid metabolites and reactive oxygen species in the regulation of adipocyte function

지도교수 김재범

이 논문을 이학박사 학위논문으로 제출함

2021년 2월

서울대학교 대학원

생명과학부

손 지 형

손지형의 박사학위논문을 인준함

2021년 2월

위 원 장 이건수 (인)

부위원장 김재범 (인)

위 원 김진홍 (인)

위 원 강찬희 (인)

위 원 서종배 (인)

Roles of lipid metabolites and reactive oxygen species in the regulation of adipocyte function

A dissertation submitted in partial fulfillment of

the requirement for degree of

DOCTOR OF PHILOSOPHY

To the Faculty of the

School of Biological Sciences

At

SEOUL NATIONAL UNIVERSITY

By

Jee Hyung Sohn

February, 2021

Data Approved

Dec. 24th, 2020

ABSTRACT

Roles of lipid metabolites and reactive oxygen species in the regulation of adipocyte function

Jee Hyung Sohn

Adipocytes are specialized cells to regulate lipid metabolism, a process that is closely linked to systemic energy homeostasis. In mammals, white adipocytes are responsible for lipid storage and breakdown in response to energy status, whereas brown adipocytes participate in heat production and energy expenditure through fatty acid (FA) oxidation in response to cold. In adipocytes, dysregulation of lipid metabolism is closely associated with metabolic disorders including dyslipidemia, type 2 diabetes, hepatic steatosis, and various inflammatory diseases. Although precise control of lipid metabolism in adipocytes is crucial for systemic energy homeostasis, the patho-physiological roles of each mediator produced during metabolic processes are largely unknown. Emerging evidence suggests that lipid metabolites and reactive oxygen species (ROS), which are products and/or byproducts of lipid metabolism, could act as signaling molecules. For example, lipid metabolites, such as saturated FA and leukotriene B_4, activate

inflammatory responses in white adipose tissue (WAT), resulting in systemic insulin resistance. Further, it has been recently reported that cellular ROS in brown adipocytes has opposite effects on thermogenic activity. While mitochondrial ROS mediates heat production in brown adipocytes upon cold exposure, excessive ROS disrupts the thermogenic action of brown adipocytes. However, the underlying mechanisms by which lipid metabolites and ROS could modulate adipocyte function and whole-body energy metabolism have not been thoroughly understood yet.

In chapter one, I have demonstrated that aberrant lipolysis in white adipocytes induced adipose tissue inflammation and systemic insulin resistance through the secretion of pro-inflammatory lipid metabolites. Increased basal lipolysis in adipocytes by perilipin 1 (PLIN1) deficiency promoted adipose tissue macrophage (ATM) accumulation through elevated prostaglandins, leading to systemic insulin resistance. Thus, it is feasible to speculate that dysregulation of lipolysis in white adipocytes could impair the immune balance in adipose tissue and whole-body energy homeostasis by unnecessary secretion of lipid metabolites.

In chapter two, the regulatory mechanisms of thermogenic activity through ROS clearance in brown adipocytes have been investigated. I observed that redox regulation and the anti-oxidative pathway were more active in brown adipose tissue (BAT) than in WAT. It is of interest to note that glucose-6-phosphate dehydrogenase (G6PD), a nicotinamide adenine

dinucleotide phosphate (NADPH)-producing enzyme, contributed to different roles in BAT and WAT. In brown adipocytes, G6PD defect enhanced cytosolic ROS-induced ERK activation, leading to dysfunction of thermogenesis. Together, these data propose that cellular ROS scavenging by G6PD in brown adipocytes would support heat production upon cold stimulation.

In this thesis study, I suggest that proper regulation of lipid metabolites and cellular ROS in adipocytes is crucial for maintaining adipocyte functions which contribute to systemic energy homeostasis.

Keywords: white adipocyte, brown adipocyte, lipolysis, lipid metabolites, pro-inflammatory responses, insulin resistance, thermogenesis, oxidative stress

Student number: 2012-20314

TABLE OF CONTENTS

LIST OF FIGURES

LIST OF TABLES

BACKGROUNDS

1. Adipocytes

1) White adipocytes

In mammals, adipose tissue is composed of adipocytes and stromal vascular cells (SVCs). Among them, adipocytes are specialized in storing extra energy sources as lipid metabolites in the form of lipid droplets (LDs) and are an essential cell type in the control of whole-body energy homeostasis. For long times, adipocytes have been largely divided into white and brown subtypes (Park et al., 2014). The characteristics of white and brown adipocytes are summarized in Table 1.

The main function of white adipocytes is storage of excess energy as lipid metabolites. White adipocytes anatomically constitute two depots of subcutaneous white adipose tissue (WAT) and visceral WAT. White adipocytes are spherical cells whose variable size depends on the size of the unilocular LDs. In mature white adipocytes, the LDs accounts for the majority of cell volume (Cinti, 2009). Recent studies have demonstrated that white adipocytes release various hormones and metabolites, such as leptin, adiponectin, cytokines, and, fatty acids (FAs) (Scherer et al., 1995; Yore et al., 2014; Zhang et al., 1994). In response to metabolic stimuli, white adipocytes perform paracrine and endocrine functions and regulate adipose tissue and systemic energy metabolism through the secretion of diverse hormones and

Table 1. Characteristics of white and brown adipocytes

	White adipocytes	Brown adipocytes
Location	Subcutaneous, visceral	Interscapular
Development	From $Myf5^-$ progenitor cells	From $Myf5^+$ progenitor cells
Function	Energy storage, endocrine function	Energy expenditure, heat production
LD morphology	Large, unilocular	Small, multilocular
Mitochondria content	Low	High
UCP1 expression	Low	High
Lipid metabolism	Lipid storage, lipolysis	Fatty acid oxidation

metabolites.

2) Brown adipocytes

Compared to white adipocytes, the most distinct features of brown adipocytes are LD morphology and mitochondrial content. Brown adipocytes contain LDs that are small and multilocular, while their mitochondria are numerous, large, and spherical (Cinti, 2009). Uncoupling protein 1 (UCP1) is located in the inner membrane of mitochondria (IMM) in brown adipocytes. UCP1 induces proton conductance through the IMM to dissipate the proton gradient and convert chemical energy into heat, rather than producing ATP (Nicholls and Locke, 1984). During cold exposure, the sympathetic nervous system is activated, and released norepinephrine stimulates brown adipocytes. In response to catecholamines, activated β_3-adrenergic receptors in brown adipocytes turn on the expression of thermogenic genes, including peroxisome proliferator-activated receptor γ coactivator 1-alpha (PGC1α), iodothyronine deiodinase 2 (DIO2), and UCP1. Also, β_3-adrenergic stimulation in brown adipocytes promotes mitochondrial biogenesis as well as the uptake of glucose and lipids (Cannon and Nedergaard, 2004). Thus, brown adipocytes play a key role in the regulation of thermogenesis and energy expenditure through fuel oxidation. Although brown adipocytes have been intensively studied in rodents, it has been considered that brown

adipocytes in humans appeared to be limited to infants. However, it has been recently reported that brown adipocytes contained in brown adipose tissue (BAT) are present and functional in adult humans (Cypess et al., 2009; Virtanen et al., 2009). For instance, metabolically functional brown adipocytes are formed in the cervical, supraclavicular, mediastinal, paravertebral, and suprarenal regions in adult humans (Cedikova et al., 2016).

3) Beige adipocytes

Most recently, beige adipocytes, inducible brown-like adipocytes in WAT, are identified. At room temperature or thermoneutrality, beige adipocytes resemble white adipocytes which do not express UCP1. However, upon cold or β-adrenergic stimulation, beige adipocytes have small and multilocular LDs and mitochondria that express UCP1 (Sidossis and Kajimura, 2015). Thus, similar to brown adipocytes, beige adipocytes have a thermogenic activity. However, it is still unclear whether beige adipocytes arise through *de novo* differentiation of precursor cells or through the transition from white adipocytes.

2. Lipid metabolism in adipocytes

1) Regulation of lipid metabolism in adipocytes

Adipocytes are specialized for lipid metabolism including uptake,

storage, lipogenesis, and lipolysis. LD is a pivotal subcellular organelle in the regulation of lipid metabolism in adipocytes. LD is consist of neutral lipids such as triglycerides (TGs) and cholesteryl esters surrounded by a phospholipid monolayer (Carman, 2012; Kimmel and Sztalryd, 2016). Various proteins associated with the regulation of lipid metabolism are present on the surface of LD. An energy surplus leads adipocytes to store extra glucose and FAs in the form of LD, whereas TGs stored in the LD are hydrolyzed and released upon energy deprivation.

In the postprandial state, insulin stimulates both lipids uptake from the blood and *de novo* lipogenesis, while it represses lipid breakdown. Circulating TGs packed with lipoproteins are hydrolyzed by lipoprotein lipase and absorbed by adipocytes (Merkel et al., 2002). Also, free FAs (FFAs) enter adipocytes through transporters such as CD36 and fatty acid transport protein-1 (Endemann et al., 1993; Wu et al., 2006). In addition, insulin promotes glucose uptake, which drives *de novo* lipogenesis through sterol regulatory element-binding protein and carbohydrate response element-binding protein (Song et al., 2018). Upon fasting or starvation, glucagon and catecholamines stimulate the mobilization of accumulated lipids through lipolysis in adipocytes to meet the energy demand of other organs. Lipolysis is defined as a catabolic process leading to TG hydrolysis into FFAs and glycerol through interactions between lipases, including adipose triglyceride lipase (ATGL) and hormone-sensitive lipase (HSL), and LD-associated proteins, including

Perilipin 1 (PLIN1) and comparative gene identification (CGI)-58 (Tansey et al., 2001) (Brasaemle et al., 2000; Miyoshi et al., 2006) (Granneman et al., 2009) (Figure 1). In adipocytes, lipid storage and hydrolysis are highly regulated processes upon various physiological conditions (Saponaro et al., 2015). Thus, dysregulation of lipid metabolism is closely linked to pathological conditions such as obesity, lipodystrophy, insulin resistance, and inflammatory diseases.

2) Lipid dysregulation and metabolic diseases

Impaired lipid metabolism in adipocytes is correlated with metabolic disorders. In adipocytes, extra energy intake without enough energy expenditure causes excessive lipid accumulation, leading to obesity. Moreover, chronic overnutrition which exceeds the maximal capacity of lipid storage results in obesity-related metabolic disorders such as insulin resistance, dyslipidemia, and cardiovascular disease. In particular, enlarged adipocytes often fail to absorb excess lipids in the blood and/or frequently show increased lipolysis, resulting in ectopic fat accumulation. Aberrantly increased lipid accumulation in liver and skeletal muscle impairs insulin sensitivity (Samuel and Shulman, 2012). Further, diacylglycerol suppresses the insulin signaling pathway through activation of protein kinase C (Shulman, 2014). It has also been reported that lipid metabolites trigger immune

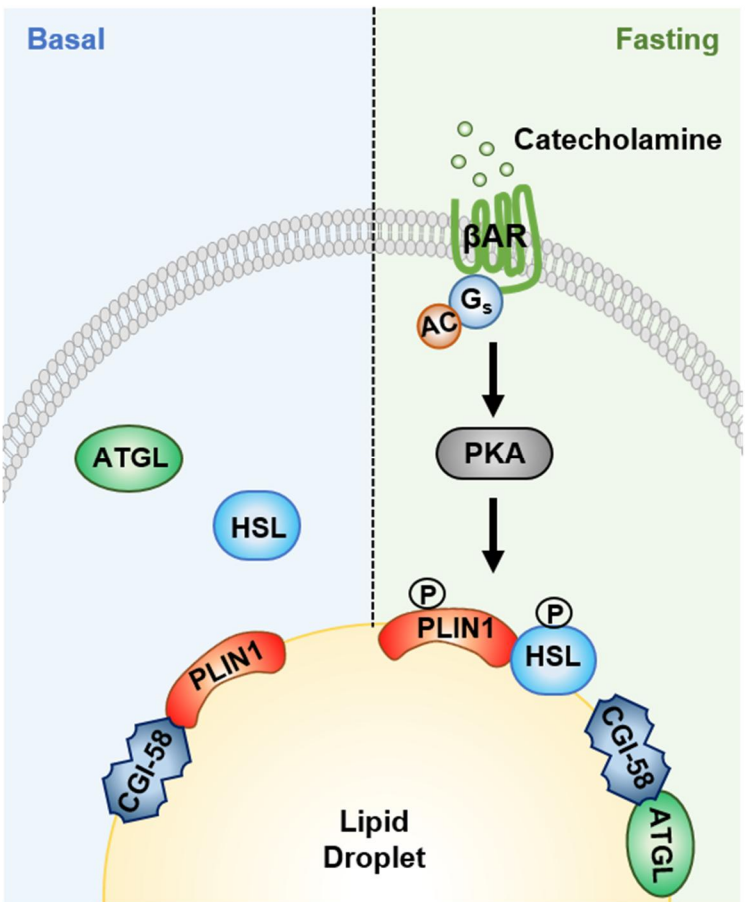

Figure 1. Schematic model of lipolysis upon fasting. In adipocytes, PLIN1 surrounds LDs and inhibits lipolysis during feeding condition. On the other hand, fasting signal induces phosphorylation of PLIN1, thereby regulating the interactions between LD proteins and lipases. Thus, these interactions promote lipolysis.

responses. In immune cells, saturated FAs and ceramides promote inflammatory responses and insulin resistance (Lackey and Olefsky, 2016; Shi et al., 2006) (Chaurasia and Summers, 2015). Lipodystrophy is a pathological state of adipose tissue deficiency that can be acquired or genetically inherited (Garg, 2004). In addition to obesity, dysfunction adipocytes which fail to efficiently store lipids cause lipodystrophy. In lipodystrophy, mature adipocyte numbers are reduced, leading to a reduction of storage capacity in adipose tissue associated with ectopic fat accumulation in liver and skeletal muscle. The consequences of this disorder include abnormalities in insulin sensitivity and serum lipid levels (Huang-Doran et al., 2010; Savage, 2009).

Even though lipodystrophy and obesity show opposite phenomena in the aspect of adipose tissue mass, both pathological conditions are accompanied by similar metabolic complications (Huang-Doran et al., 2010; Kahn and Flier, 2000; Savage, 2009). Obesity-induced chronic low-grade inflammation is one of the major factors in the pathogenesis of insulin resistance (Donath and Shoelson, 2011; Olefsky and Glass, 2010). Obese adipocytes are characterized by increased expression of inflammatory genes, such as tumor necrosis factor (TNF) α, interleukin (IL)-6, and monocyte chemoattractant protein (MCP)-1, and also by promoted infiltration of immune cells, particularly macrophages (Hotamisligil et al., 1993; Weisberg et al., 2003; Xu et al., 2003). However, the underlying mechanisms by which factors directly

induce systemic insulin resistance in patients with lipodystrophy have not been largely understood.

3) Lipid metabolites and inflammatory responses

Lipid metabolites are associated with numerous human diseases, including atherosclerosis, rheumatoid arthritis, and other inflammation-linked metabolic diseases (Shimizu, 2009). Historically, lipid metabolites have been considered as energy sources. However, the importance of lipid metabolites as signaling molecules in immune responses has also been recognized (Funk, 2001; Shimizu and Wolfe, 1990). Eicosanoids, certain FAs, and FA derivatives can act as signaling lipid metabolites (Shimizu, 2009). Accumulating evidence suggests that lipid metabolites involved in the regulation of inflammatory responses are produced from ω-6 (n-6) and ω-3 (n-3) long-chain polyunsaturated fatty acids. For instance, arachidonic acid (20:4, ω-6) is subjected to oxidation by the cyclooxygenase, lipoxygenase, and cytochrome P450 enzymes, resulting in production of eicosanoids. Among these eicosanoids, prostaglandin (PG) E_2 has pro-inflammatory roles, acting to recruit immune cells, such as macrophages, neutrophils, and mast cells, to the sites of infection or injury (Wallace, 2001). PGE_2 binds to E prostanoid (EP) receptors in plasma membrane and stimulates the production of pro-inflammatory cytokines (Zoccal et al., 2016). In contrast to PGE_2,

PGD_2 and PGJ_2 suppress cytokine secretion and immune cell activation, acting on macrophages, lymphocytes, and dendritic cells (Faveeuw et al., 2003; Pereira et al., 2018). Leukotriene also acts as a chemoattractant that stimulates immune cell recruitment and promotes inflammatory responses (Scott and Peters-Golden, 2013). In addition, treatment with 12-hydroperoxyeicosatetraenoic acid (HPETE) and 12- hydroxyeicosatetraenoic acid (HETE) upregulates pro-inflammatory genes such as TNFα, IL-6, and MCP-1 in 3T3-L1 adipocytes (Chakrabarti et al., 2009). Although it has been recognized that lipid metabolites could modulate immune responses, it remains elusive how lipid metabolites involved in inflammation would be regulated under physiological or pathological conditions.

3. Reactive oxygen species (ROS) in adipocytes

1) Regulation of ROS homeostasis

ROS are radical and non-radical oxygen species produced by partial reduction of oxygen and include hydroxyl radicals (OH^-), superoxide radicals (O_2^-), singlet oxygen ($^1O_2$), and hydrogen peroxide (H_2O_2). For long time, ROS have been considered a mere byproduct of metabolism. However, accumulating evidence suggests that ROS supports cellular functions by acting as signaling molecules or damaging cues by inducing oxidative stress. In this regard, production and scavenging of cellular ROS seem to be crucial

for cellular homeostasis.

ROS are primarily produced from mitochondria by respiratory complex I and complex III during oxidative phosphorylation (Rigoulet et al., 2011). Superoxide is either rapidly converted to hydrogen peroxide by superoxide dismutase 2 (SOD2) or passes through the mitochondrial membrane via a voltage-dependent anion channel (VDAC) (Bolisetty and Jaimes, 2013; Han et al., 2003). Hydrogen peroxide also easily diffuses to the cytosol through aquaporin (Chauvigné et al., 2015). In addition, cytosolic ROS is generated by enzymatic reactions such as nicotinamide adenine dinucleotide phosphate (NADPH) oxidase (NOX), inducible nitric oxide synthase (iNOS), cyclooxygenase 2 and 5-lipoxygenase (Gorrini et al., 2013). Among pro-oxidative enzymes, NOX generates superoxides by transferring one electron to oxygen from NADPH.

Cells have antioxidant systems to prevent excessive ROS accumulation and oxidative stress. Antioxidant systems consist of enzymatic and non-enzymatic pathways. Enzymatic antioxidant system includes SOD, catalase, glutathione peroxidases, and thioredoxin. In the non-enzymatic pathway, antioxidants such as vitamins and glutathione (GSH) reduce the oxidative state. In particular, GSH, the major soluble antioxidant in cells, detoxifies hydrogen peroxides and lipid peroxides via glutathione peroxidases. Glutathione reductase reduces oxidized glutathione (GSSG) to GSH by using NAD(P)H as the electron donor. Since both pro-oxidative and anti-oxidative

enzymes use NADPH, it is likely that NADPH would be crucial for the regulation of ROS homeostasis as a cofactor and electron donor.

2) Physiological role of ROS on adipocyte function

Emerging evidence suggests that adipocytes use ROS as second messengers. It has been reported that hydrogen peroxide has similar effects to insulin in adipocytes. For example, it induces glucose uptake and lipid synthesis and reduces lipid breakdown (Kono et al., 1982; Little and de Haën, 1980; May and de Haën, 1979). Hydrogen peroxide also stimulates adipocyte differentiation through upregulated peroxisome proliferator-activated receptor gamma (PPARγ) expression and mitochondrial ROS-specific scavengers impair adipogenesis (Lee et al., 2009; Tormos et al., 2011). Recently, it has been reported that mitochondrial ROS supports thermogenic function in brown adipocytes. Administration of mitochondria-specific antioxidant disrupts cold-induced thermogenesis and systemic energy expenditure in mice (Chouchani et al., 2016). It has been reported that genetic ablation of mitochondrial anti-oxidative genes such as Sestrin2 and SOD2 results in increased UCP1 expression in adipose tissue (Han et al., 2016; Ro et al., 2014). Thus, ROS would play essential roles in the regulation of various adipocyte functions.

3) Oxidative stress and adipocyte dysfunction

Despite the necessity of ROS for adipocyte function, prolonged and excessive ROS accumulation is associated with adipocyte dysfunction. In obesity, cellular ROS levels are increased in WAT (Furukawa et al., 2004). It has been proposed that increased ROS accumulation associated with obesity can impair adipocyte function, including adipogenesis, insulin signaling, and expression of adipokines and thermogenic genes (Carrière et al., 2003; Shimizu et al., 2014; Wang et al., 2013). For instance, the activity of NOX4, the major isoform in adipocytes, is enhanced by high concentrations of glucose and palmitate (Han et al., 2012). Knockdown of NOX4 reduces high glucose- and palmitate-induced cellular ROS levels and MCP-1 expression in 3T3-L1 adipocytes (Han et al., 2012). In addition, the pentose phosphate pathway is involved in redox control and ROS homeostasis through production of cytosolic NADPH. Glucose-6-phosphate dehydrogenase (G6PD), the rate-limiting enzyme in the pentose phosphate pathway, catalyzes the oxidation of glucose-6-phosphate to 6-phosphogluconolactone and the reduction of NADP+ to NADPH (Figure 2). In white adipocytes, G6PD expression is upregulated in obese mice (Park et al., 2005). Overexpression of G6PD in 3T3-L1 adipocytes increases ROS-induced inflammatory responses, probably leading to adipose tissue inflammation and insulin resistance (Park et al., 2006). Conversely, G6PD inhibition or

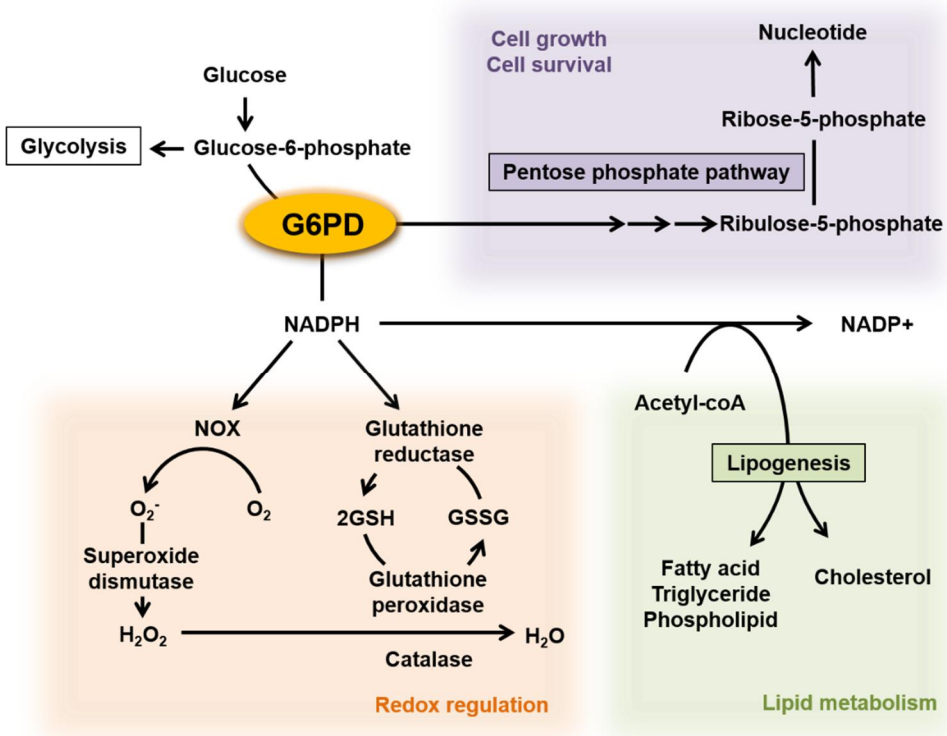

Figure 2. Roles of G6PD in the regulation of diverse cellular metabolisms. G6PD produces NADPH and ribulose-5-phosphate, the latter providing intermediates used for nucleic acid production. NADPH supports the NOX-mediated ROS generation. Meanwhile, glutathione reductase also uses NADPH to reduce GSSG to GSH for use by glutathione peroxidase that reduces H_2O_2 to H_2O (Park et al., 2017).

knockdown reduces ROS accumulation and pro-inflammatory gene expression in 3T3-L1 adipocytes upon high glucose and palmitate treatment (Han et al., 2012). In fact, G6PD-deficient mutant ($G6PD^{mut}$) mice show increased adipose tissue inflammation and improved insulin resistance upon high fat diet (HFD) feeding compared with wild type (WT) mice (Ham et al., 2016). Although it is likely that adipocyte function requires the balance between generation and clearance of ROS, it has not been fully elucidated how cellular ROS in adipocytes are regulated to normal physiological levels without oxidative stress.

4. Purpose of this study

Adipocyte dysfunction is one of the causal factors in the pathogenesis of metabolic disorders. It has been reported that lipid dysregulation in white adipocytes, which specialize for lipid metabolism causes obesity-associated insulin resistance, ectopic fat accumulation, and various inflammatory diseases. Although lipid metabolism has been implicated in the regulation of adipocyte functions and whole-body energy homeostasis, how the dysregulation of lipid metabolism in adipocytes could mediate and/or cause metabolic dysregulation has not been fully elucidated. To elucidate regulatory mechanisms of adipocyte functions depending on lipid metabolism, I have focused on the roles of products and/or byproducts during processes of lipid metabolism.

In this study, I have investigated the contribution of lipid metabolites and cellular ROS in the regulation of adipocyte functions. In the first chapter, I have demonstrated that increased lipolysis in adipocytes stimulated the release of pro-inflammatory lipid metabolites from adipocytes and elevated migration of monocytes/macrophages into adipose tissue, which leads to systemic insulin resistance. In the second chapter, I have revealed that elevated cytosolic ROS in brown adipocytes damaged thermogenic activity and mitochondrial oxygen consumption under cold or β-adrenergic stimulation. Collectively, I suggest that proper regulation of lipid metabolites

and ROS is critical for adipocyte function upon various metabolic stimuli.

CHAPTER ONE:

PLIN1 deficiency promotes inflammatory responses in lean adipose tissue through lipid dysregulation

1. Abstract

Lipid droplets are specialized cellular organelles that contain neutral lipid metabolites and play dynamic roles in energy homeostasis. Perilipin 1 (PLIN1), one of the major lipid droplet-binding proteins, is highly expressed in adipocytes. In mice, *Plin1* deficiency impairs peripheral insulin sensitivity, accompanied with reduced fat mass. However, the mechanisms underlying insulin resistance in lean *Plin1* knockout (*Plin1*$^{-/-}$) mice are still elusive. Here, I demonstrate that PLIN1 deficiency promotes inflammatory responses and lipolysis in adipose tissue, resulting in insulin resistance. M1-type adipose tissue macrophages (ATMs) were higher in *Plin1*$^{-/-}$ than in *Plin1*$^{+/+}$ mice on normal chow diet (NCD). Moreover, *Plin1*$^{-/-}$ adipocytes promoted secretion of pro-inflammatory lipid metabolites such as prostaglandins, which potentiated monocyte migration. In lean *Plin1*$^{-/-}$ mice, insulin resistance was relieved by macrophage depletion with clodronate, implying that elevated pro-inflammatory ATMs might be attributable for insulin resistance under *Plin1* deficiency. Together, these data suggest that *Plin1* is required to restrain fat loss and pro-inflammatory responses in adipose tissue by reducing futile lipolysis to maintain metabolic homeostasis.

2. Introduction

Chronic, low-grade inflammation is a major factor in the pathogenesis of insulin resistance (Kwon and Pessin, 2013; Olefsky and Glass, 2010). Macrophages play an important role in the modulation of inflammation through their capacity to secrete a variety of chemokines and cytokines. Monocyte-originated macrophages polarize to classically activated macrophages (M1) or alternatively activated macrophages (M2) in certain tissue niches and upon environmental stimuli (Lumeng et al., 2008). In fact, alteration of adipose tissue macrophages (ATMs) contributes to elevated adipose tissue inflammation in obesity (Weisberg et al., 2003; Xu et al., 2003). In obesity, macrophages are recruited into adipose tissue and show pro-inflammatory properties compared to resident ATMs (Lumeng et al., 2007). Thus, M1-type macrophages, which secrete pro-inflammatory cytokines such as tumor necrosis factor (TNF) α, interleukin (IL)-6, and monocyte chemoattractant protein (MCP)-1, are the predominant ATM population in obese adipose tissue (Hotamisligil et al., 1993; Weisberg et al., 2003; Xu et al., 2003). Adipose tissue inflammation is also observed in lipodystrophic and cachectic subjects, accompanied with fat loss (Batista et al., 2016; de Matos-Neto et al., 2015; Gandotra et al., 2011; Herrero et al., 2010; Martin et al., 2012). ATM infiltration has been reported in several lipodystrophic animal models and human patients (Gandotra et al., 2011; Herrero et al., 2010; Martin et al., 2012). Moreover, cachexia is associated with elevated pro-

inflammatory gene expression, macrophage infiltration, and fibrosis in adipose tissue of cancer patients (Batista et al., 2016; de Matos-Neto et al., 2015).

Lipid dysregulation is closely related to various pathophysiologies, such as rheumatoid arthritis, multiple sclerosis, and obesity-induced insulin resistance (Bensinger and Tontonoz, 2008; Shimizu, 2009). While lipid metabolites have been considered as simple energy sources, recent findings have revealed that lipid metabolites can also act as signaling molecules for immune responses (Gartung et al., 2016; Yore et al., 2014). In obesity, elevated fatty acids are a potential trigger for macrophage activation (Suganami et al., 2007). For instance, saturated fatty acids stimulate toll-like receptor (TLR) 4 in ATMs, resulting in the activation of inflammatory signaling cascades mediated by nuclear factor-κB (Suganami et al., 2007). Also, leukotriene B_4 (LTB_4) promotes chemotactic activity of macrophages, which contribute to whole-body insulin resistance (Li et al., 2015).

Lipid droplets are metabolically dynamic cellular organelles specialized in storing free fatty acids (FFAs) and sterols in the form of triglycerides (TG) and cholesterol esters, respectively (Carman, 2012; Kimmel and Sztalryd, 2016). This sequestration of lipid metabolites into lipid droplets contributes to relieve from toxic effects of excess FFAs or sterols that can lead to insulin resistance and inflammation (Hoo et al., 2017; Iyer et al., 2010). Perilipin 1 (PLIN1), the most abundant lipid droplet coat protein in

adipocytes, is required for optimal lipid homeostasis (Greenberg et al., 1991). In basal state, PLIN1 encloses lipid droplets and inhibits lipolysis in adipocytes (Tansey et al., 2001). On the contrary, catecholamine promotes lipolysis by inducing the translocation of hormone-sensitive lipase (HSL) onto lipid droplets (Brasaemle et al., 2000; Miyoshi et al., 2006). While PLIN1 binds to comparative gene identification-58 (CGI-58), a coactivator of adipose triglyceride lipase (ATGL) in the basal state, PLIN1 liberates CGI-58 to induce lipolysis upon protein kinase A (PKA) activation during the stimulated state (Granneman et al., 2009). It has been reported that *Plin1*$^{-/-}$ mice are lean and exhibit glucose intolerance and insulin resistance in the absence of any metabolic stress (Tansey et al., 2001). However, the molecular mechanisms of insulin resistance in normal chow diet (NCD)-fed lean *Plin1*$^{-/-}$ mice have not been fully elucidated.

In this study, I investigated NCD-fed lean *Plin1*$^{-/-}$ mice to understand the molecular mechanisms underlying insulin resistance under *Plin1* deficiency. I demonstrate that *Plin1* deficiency stimulates pro-inflammatory responses in adipose tissue by secreting pro-inflammatory lipid metabolites, which exacerbate adipose tissue inflammation. Using lipidomics analysis, I found that elevated prostaglandins (PGs) from *Plin1*$^{-/-}$ adipocytes potentiated monocyte migration. In addition, depletion of ATMs with clodronate alleviated insulin resistance in *Plin1*-deficient mice, implying that an increase in pro-inflammatory ATMs is one of the major inducers for insulin resistance

in *Plin1*$^{-/-}$ mice. Together, these data suggest that *Plin1* is an important protective regulator against adipose tissue inflammation and insulin resistance by restricting futile lipolysis.

3. Materials and Methods

Animals and treatments

The animal study and experimental procedures were approved by the Seoul National University Institutional Animal Care and Use Committee. Plin1$^{-/-}$ mice in a pure C57BL/6 background were obtained from Alan R. Kimmel (US National Institute of Health). Mice were housed under a 12-h light/12-h dark cycle. Heterozygous mice were bred to generate *Plin1*$^{+/+}$ and *Plin1*$^{-/-}$ littermates. *Plin1*$^{+/+}$ and *Plin1*$^{-/-}$ mice were maintained on NCD. Nine- to 12-week-old male mice were used for experiments, except where indicated. At 9-11 weeks of age, *Plin1*$^{+/+}$ and *Plin1*$^{-/-}$ mice were intraperitoneally injected with vehicle (1% DMSO in PBS), NS398 (10 mg/kg body weight, Cayman chemical) or orlistat (50 mg/kg body weight, Sigma-Aldrich) daily for 8 or 9 days, respectively. For intraperitoneal GTT, 17-week-old mice were fasted overnight and then administered glucose (1 g/kg body weight). For ITT, mice were intraperitoneally injected with insulin (0.75 unit/kg body weight). To test insulin signaling in vivo, mice were fasted overnight and killed 15 min after injection of PBS or insulin (0.75 unit/kg body weight). Adipose tissue, skeletal muscle, and liver were isolated and quickly frozen for western blot analysis. For macrophage depletion, clodronate liposomes (FormuMax Scientific) were intraperitoneally injected once.

Serum profiling

Serum FFA, TG, and cholesterol levels were assessed using FFA (Roche), TG (Thermo Fischer Scientific), and cholesterol (Thermo Fischer Scientific) quantification kit. Serum insulin, MCP-1, and TNFα levels were measured using insulin (Morinaga Institute of Biological Science Inc.), MCP-1 (Invitrogen), TNFα (Invitrogen) ELISA kit.

Adipose tissue fractionation

eWAT was dissected out, chopped, incubated in collagenase buffer (0.1 M HEPES, 0.125 M NaCl, 5 mM KCl, 1.3 mM $CaCl_2$, 5 mM glucose, 1.5% (w/v) glucose, and 0.1% (w/v) collagenase I) for 20 min at 37°C with shaking, and centrifuged. Supernatants containing adipocytes were used for primary cell culture. Pelleted SVC fractions were used for flow cytometry and SVC-derived adipocyte differentiation.

Flow cytometry

Flow cytometric analysis was performed as described previously (Huh et al., 2017). SVC fractions were separated from red blood cells by adding lysis buffer (155 mM NH_4Cl/0.1 M Tris-HCl (pH 7.65) (9:1)). SVCs were stained with monoclonal antibodies against CD11b (BD Biosciences), F4/80, CD11c, and CD206 (eBioscience) for macrophage analysis using a FACS Canto II (BD Biosciences).

SVC-derived adipocyte differentiation

Pre-adipocytes were grown to confluence (day 0) in induction medium consisting of Dulbecco's modified Eagle's medium (DMEM), 10% fetal bovine serum (FBS), 167 nM insulin, 1 μM 3,3′,5-triiodo-L-thyronine (T3), 2 μM rosiglitazone, 52 μM isobutylmethylxanthine, and 1 μM dexamethasone. After 2 day incubation in induction medium, the cells were transferred to differentiation medium (DMEM, 10% FBS, 167 nM insulin, 1 μM T3, and 2 μM rosiglitazone), which was changed every other day. For siRNA transfection, differentiated adipocytes were transfected by Lipofectamine 2000 (Invitrogen) according to the manufacturer's protocol.

Isolation of peritoneal macrophages

Mice were intraperitoneally injected with sterile thioglycollate solution (3 ml/mouse). After 3 days, peritoneal cells were harvested by washing the peritoneal cavity with PBS. Primary peritoneal macrophages were cultured in DMEM containing 10% FBS to allow the cells to adhere. Nonadherent cells were removed by washing.

Co-culture and CM preparation

Co-culture experiments were conducted as described previously

(Choe et al., 2014). For indirect co-culture experiments, chopped eWAT or primary adipocytes were placed in the lower chambers of Transwell plates (0.4 μm pore size) and co-cultured with peritoneal macrophages in the upper chambers. After 48 h incubation, the macrophages were used for RNA extraction. For CM preparation, chopped eWAT or primary adipocytes were incubated in serum-free DMEM for 48 h and CM was collected. To test THP-1 or peritoneal macrophage migration, Transwell inserts (8 μm pore size) were used. THP-1 monocytes or macrophages were loaded in the upper chambers and CM was placed in the lower chambers. After 6 h, the degree of cell migration was determined as the number of cells in the lower chambers.

Global metabolome profiling

Lipids were extracted from CM using conventional procedures (Folch et al., 1957). A liquid chromatography-mass spectrometry system equipped with Ultimate3000 (Dionex), Orbitrap XL (Thermo Fischer Scientific), and reverse phase column (Pursuit 5 200 × 2.0 mm) was used. Mobile phase A was 0.1 % formic acid in H_2O, and mobile phase B was 0.1 % formic acid in methanol. The flow rate was 400 μl/min and the column temperature was 25°C. Data were analyzed using Seive 2 and MetaboAnalyst. Metabolite features containing m/z and retention time were extracted using Seive 2.2. Data were statistically analyzed using MetaboAnalyst. Metabolite features were identified using METLIN DB with mass accuracy of 10 ppm.

Eicosanoid analysis

Eicosanoids were extracted from CM, cells, and eWAT using solid-phase extraction (SPE), as described (Yang et al., 2009). A liquid chromatography-tandem mass spectrometry system equipped with 1290 HPLC (Agilent), Qtrap 5500 (ABSciex) and reverse phase column (Pursuit 5 200 × 2.0 mm) was used. Mobile phase A was 0.1 % acetic acid in H_2O and mobile phase B was 0.1 % acetic acid in ACN/MeOH (84/16, v/v). The flow rate was 250 μl/min and the column temperature was 25°C. The multiple reaction monitoring (MRM) mode was used in negative ion mode, and the extracted ion chromatogram corresponding to the specific transition of each analyte was used for quantification. The calibration range for each analyte was 0.1–1000 nM ($r^2 \geq 0.99$).

COX activity assay and PGE_2 measurement

The COX activity was assayed using a colorimetric assay kit (Cayman Chemical) according to the manufacturer's guidelines. PGE_2, selective COX2 inhibitor NS398, and PGE_2 ELISA kit were purchased from Cayman Chemical.

Quantitative reverse transcription (qRT)-PCR

Total RNA was isolated from eWAT, macrophages, and SVC-derived

adipocytes. cDNA was synthesized using a reverse transcriptase kit (Thermo Fisher Scientific) according to the manufacturer's instructions. Primers used for qRT-PCR were obtained from Bioneer (South Korea).

Western blot analysis

eWAT, skeletal muscle, liver, and SVC-derived adipocytes were lysed with TGN lysis buffer (50 mM Tris (pH 7.5), 150 mM NaCl, 1% Tween-20, 0.2% NP-40, 1 mM PMSF, 1 mM NaF, 1 mM Na_3VO_4 and protease inhibitor mixture from GenDEPOT). Proteins in the lysates were separated by SDS-PAGE and transferred to polyvinylidene fluoride membranes (Millipore). The blots were blocked with 5% nonfat milk and probed with anti-pAKT (S473; Cell Signaling Technology), anti-AKT (BD Bioscience), or anti-PLIN1 (Greenberg et al., 1991).

Statistical analysis

All data were analyzed using Student's *t*-test or analysis of variance (ANOVA) in Excel (Microsoft) or GraphPad Prism; p values of <0.05 were considered significant.

4. Results

CD11b-positive cells are increased in adipose tissue of *Plin1*$^{-/-}$ mice

PLIN1 expression is decreased in adipose tissue from insulin resistant animals (Gaidhu et al., 2010). Consistent with this finding, the levels of *Plin1* mRNA and protein were lower in adipocytes from *db*/*db* mice and adipose tissue from high fat diet (HFD)-fed mice than in those from *db*/+ mice and NCD-fed mice (Figure 3). Nonetheless, it remained unclear how *Plin1* deficiency could influence whole-body energy homeostasis. To address this, I investigated various physiological parameters in *Plin1*$^{-/-}$ mice in C57BL/6J background (Tansey et al., 2001) in comparison with littermate wild-type mice (*Plin1*$^{+/+}$). Under NCD-fed condition, body weights were not significantly different between *Plin1*$^{+/+}$ and *Plin1*$^{-/-}$ mice (Figure 4A). However, inguinal WAT (iWAT) and epididymal WAT (eWAT) weights, but neither liver nor BAT weights, were lower in *Plin1*$^{-/-}$ than in *Plin1*$^{+/+}$ mice (Figure 4B). In addition, serum TG and FFAs, but not cholesterol, were slightly higher in *Plin1*$^{-/-}$ than in *Plin1*$^{+/+}$ mice (Figure 4C–E). Hematoxylin and eosin (H&E) staining of eWAT revealed that lipid droplets were smaller in size in *Plin1*$^{-/-}$ than in *Plin1*$^{+/+}$ mice (Figure 5A). Interestingly, the intensity of CD11b staining in eWAT of NCD-fed *Plin1*$^{-/-}$ mice was markedly increased (Figure 5B), suggesting that PLIN1 deficiency might be associated with adipose tissue inflammation in lean animals.

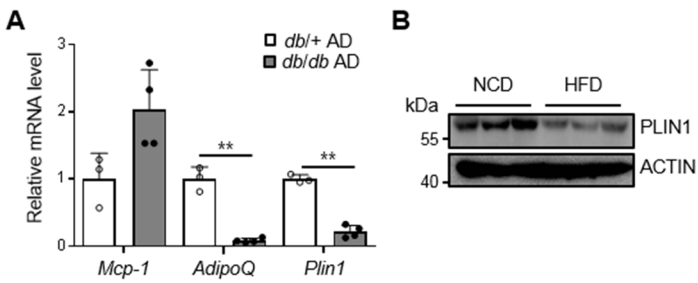

Figure 3. PLIN1 expression level is downregulated in adipose tissue from obese mice. (A) Expression levels of *Plin1* mRNA in adipocytes (AD) of *db*/+ and *db/db* mice were determined by qRT-PCR. $^{**}P < 0.01$ vs. *db*/+ group by Student's *t*-test. (B) C57BL/6J mice were fed normal chow diet (NCD) or high fat diet (HFD) for 20 weeks. eWATs were obtained and subjected to immunoblot analysis using anti-PLIN1 and anti-ACTIN antibodies. Data represent the mean ± standard error of the mean (SEM).

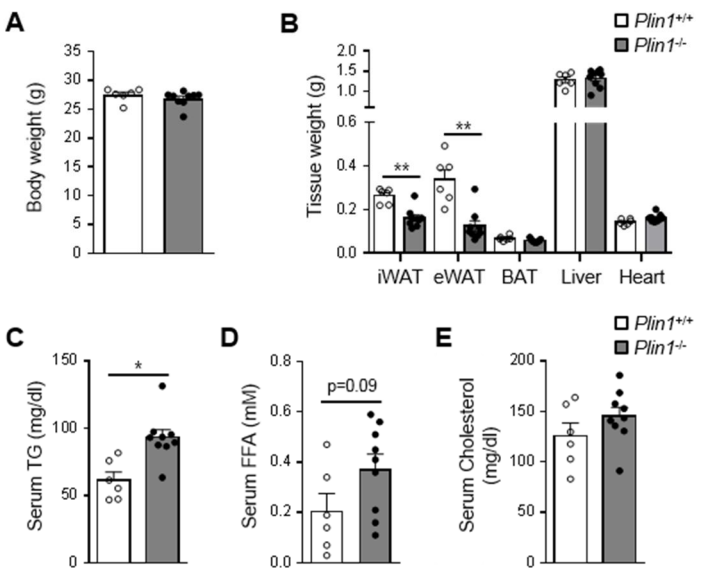

Figure 4. WAT mass is specifically decreased in *Plin1*$^{-/-}$ mice. Body weight (A), the weights of various tissues (B), and the levels of serum TG (C), serum free fatty acids FFAs (D), and serum cholesterol (E) from NCD-fed *Plin1*$^{+/+}$ and *Plin1*$^{-/-}$ mice were measured. Data represent the mean ± SEM. $^{*}P < 0.05$, $^{**}P < 0.01$ vs. *Plin1*$^{+/+}$ group by Student's *t*-test.

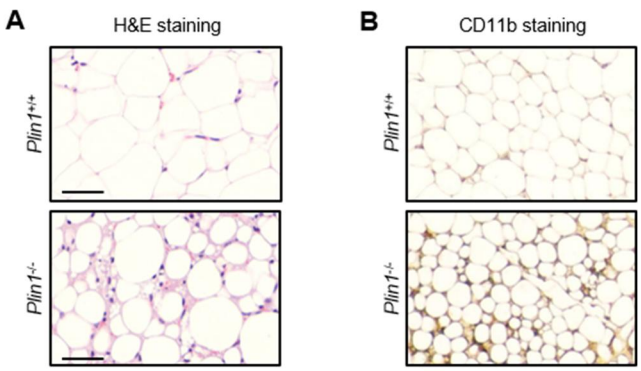

Figure 5. *Plin1*$^{-/-}$ mice show hypotrophy of adipose tissue with elevated macrophages. (A) Adipocyte morphology of eWAT from NCD-fed *Plin1*$^{-/-}$ and *Plin1*$^{+/+}$ mice was assessed by hematoxylin and eosin (H&E) staining. Scale bars, 50 μm. (B) Myeloid cells were detected in eWAT from *Plin1*$^{+/+}$ and *Plin1*$^{-/-}$ mice by DAB staining with an anti-mouse CD11b antibody. 100× magnification. Data represent the mean ± SEM.

PLIN1 deficiency induces macrophage accumulation and adipose tissue inflammation

In adipose tissue, macrophages are one of the abundant cell types and determine the degree of adipose tissue inflammation (Weisberg et al., 2003; Xu et al., 2003). To investigate whether PLIN1 deficiency might be related with adipose tissue inflammation, I examined inflammatory gene expression and macrophage accumulation in eWAT from NCD-fed *Plin1*$^{+/+}$ and *Plin1*$^{-/-}$ mice. As shown in Figure 6, PLIN1-deficient eWAT had markedly increased mRNA levels of the pro-inflammatory cytokine genes including *Mcp-1* and *Tnf*α as well as of the macrophage marker genes such as *F4/80* and *Cd11c*. In addition, serum levels of pro-inflammatory cytokines such as MCP-1 and TNFα were induced in *Plin1*$^{-/-}$ mice (Figure 7). In eWAT of *Plin1*$^{-/-}$ mice, CD11b^{+} and CD11c^{+} cells were increased (Figure 8). Also, PLIN1 deficiency elevated the percentages of F4/80^{+}CD11b^{+} (macrophages) and F4/80^{+}CD11b^{+}CD11c^{+} cells (M1-type macrophages) among stromal vascular cells (SVCs) from eWAT (Figure 9A and B). Total numbers of F4/80^{+}CD11b^{+} and F4/80^{+}CD11b^{+}CD11c^{+} cells (Figure 9C and D) were higher in eWAT of *Plin1*$^{-/-}$ than in that of *Plin1*$^{+/+}$ mice. Moreover, the percentage of M1-type CD11c^{+} cells in F4/80^{+}CD11b^{+} macrophages was higher in *Plin1*$^{-/-}$ than in *Plin1*$^{+/+}$ mice (Figure 9E), whereas the fraction of M2-type CD206^{+} macrophages in F4/80^{+}CD11b^{+} cells was lower in *Plin1*$^{-/-}$ mice (Figure 9F). Collectively, these results suggested that PLIN1 might play certain roles in

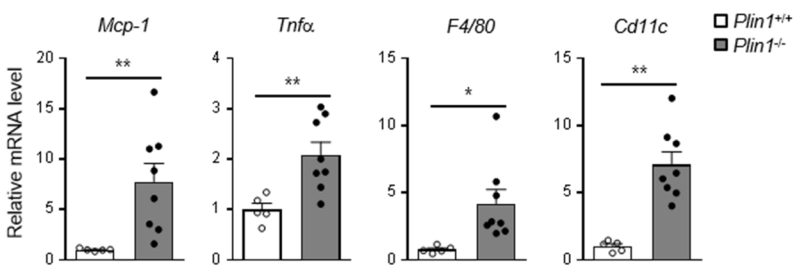

Figure 6. PLIN1 deficiency induces the mRNA level of pro-inflammatory genes in eWAT. Relative mRNA levels of inflammatory cytokine genes (*Mcp-1* and *Tnf*α) and macrophage markers (*F4/80* and *Cd11c*) were measured in eWAT by qRT-PCR. Data represent the mean ± SEM. All data represent the mean ± SEM. $^{*}P < 0.05$, $^{**}P < 0.01$ vs. $Plin1^{+/+}$ group by Student's *t*-test. qRT-PCR data were normalized to the mRNA level of *cyclophilin*.

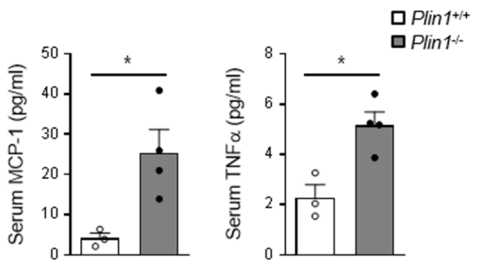

Figure 7. PLIN1 deficiency increases serum cytokine level. Serum levels of MCP-1 and TNFα were assessed by ELISA. All data represent the mean ± SEM. $^{*}P < 0.05$ vs. *Plin1*$^{+/+}$ group by Student's *t*-test.

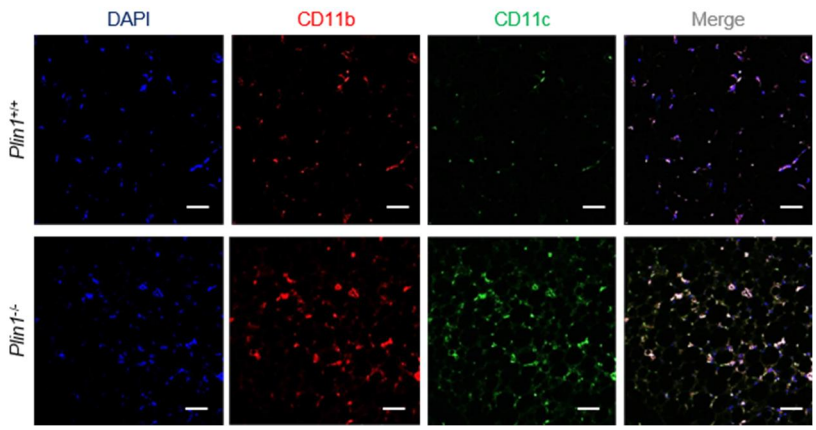

Figure 8. PLIN1 deficiency augments ATM contents. Macrophage accumulation was detected in eWAT from *Plin1*$^{+/+}$ and *Plin1*$^{-/-}$ mice by immunohistochemistry analysis of the nuclei (blue), CD11b (red), and CD11c (green). Scale bars, 50 μm.

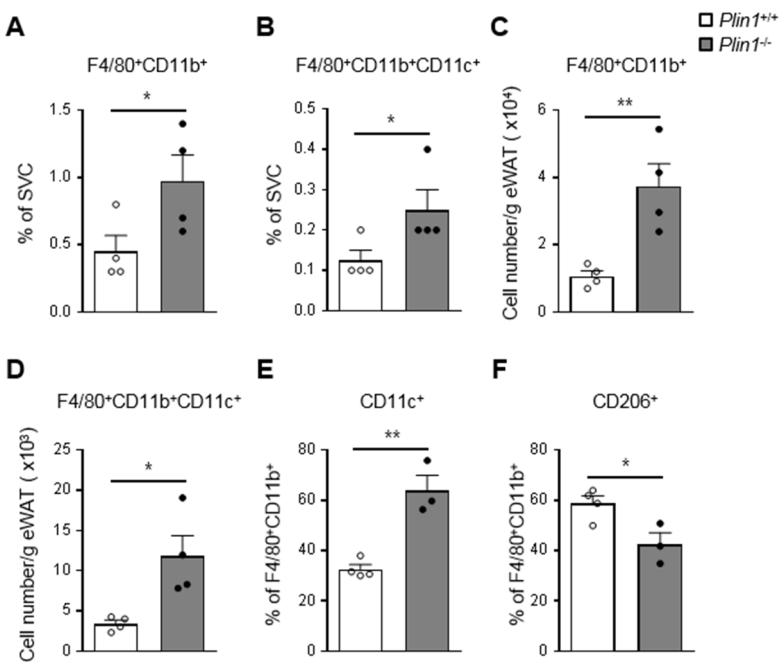

Figure 9. Accumulation of M1-type macrophages is enhanced in adipose tissue from *Plin1*$^{-/-}$ mice. Macrophage accumulation was measured in eWAT by flow cytometric analysis. The percentages of F4/80^{+}CD11b^{+} (A) and F4/80^{+}CD11b^{+}CD11c^{+} (B) cells in the SVCs of eWAT are shown in the graphs. Total numbers of F4/80^{+}CD11b^{+} (C) and F4/80^{+}CD11b^{+}CD11c^{+} (D) cells in SVCs per gram of eWAT were determined. Percentages of CD11c^{+} (E) and CD206^{+} (F) cells in the F4/80^{+}CD11b^{+} cells were measured. All data represent the mean ± SEM. $^{*}P < 0.05$, $^{**}P < 0.01$ vs. *Plin1*$^{+/+}$ group by Student's *t*-test.

the regulation of adipose tissue inflammation as well as ATM recruitment.

PLIN1-deficient adipocytes stimulate monocyte migration and pro-inflammatory cytokine expression in macrophages

In adipose tissue, infiltration of immune cells including monocytes or macrophages and increased pro-inflammatory responses in macrophages are prominent in insulin resistant animals (Fujisaka et al., 2009; Oh et al., 2012). To determine whether PLIN1 deficiency might be involved in the regulation of monocyte/macrophage migration, conditioned media (CM) obtained from *ex vivo* cultured eWAT of *Plin1*$^{-/-}$ and *Plin1*$^{+/+}$ mice were incubated with THP-1 monocytes or peritoneal macrophages (Figure 10A). As shown in Figure 10B and 10C, the degrees of THP-1 and macrophage migration were higher in CM from *Plin1*$^{-/-}$ eWAT than in CM from *Plin1*$^{+/+}$ eWAT. Similarly, stimulatory effects were observed when CM were collected from primary *Plin1*$^{-/-}$ adipocytes in monocyte migration assays (Figure 10D). Next, I used a Transwell co-culture system to test whether macrophage gene expression might be affected by *Plin1* deficiency in eWAT or adipocytes (Figure 11A). Relative mRNA levels of the pro-inflammatory response genes including *Il-6*, *iNOS*, and *Il-1*β were stimulated in macrophages when they were indirectly co-cultured with eWAT from *Plin1*$^{-/-}$ mice (Figure 11B). Primary adipocytes from *Plin1*$^{-/-}$ mice also promoted the mRNA levels of these factors in macrophages (Figure 11C). However, *Plin1*$^{-/-}$ macrophages

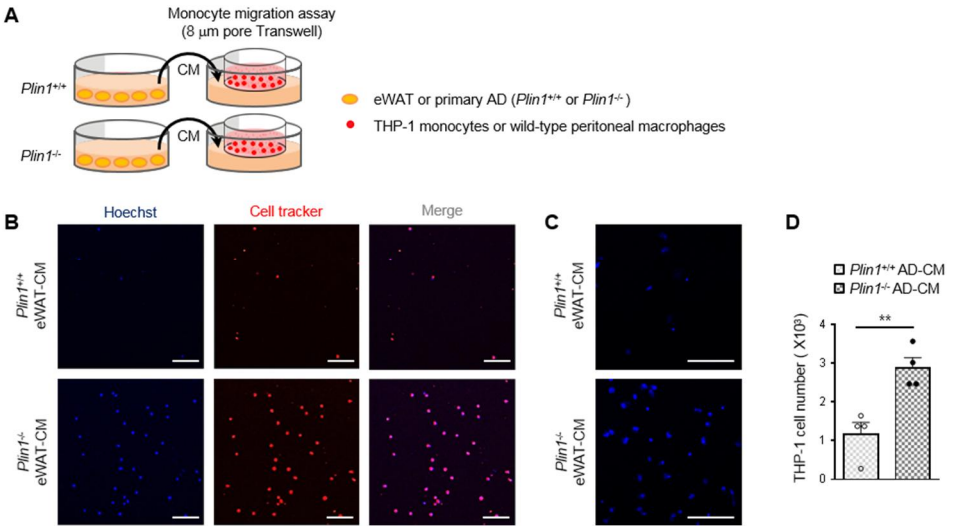

Figure 10. *Plin1*$^{-/-}$ adipocytes enhance monocyte migration. (A) eWAT or primary adipocytes from *Plin1*$^{+/+}$ and *Plin1*$^{-/-}$ mice were incubated with culture medium for 48 h. Collected CM was tested for Transwell culture. THP-1 monocytes were prestained with CellTracker (red), and incubated for 6 h in Transwell plates (8 μm pore size) with CM. Peritoneal macrophages were incubated with CM for 6 h, and stained with Hoechst (blue). (B and C) Migrated monocytes (B) or macrophages (C) upon incubation with eWAT CM were assessed by confocal microscope. Scale bars, 100 μm. (D) The number of migrated cells upon incubation with primary adipocytes CM was measured. All data represent the mean ± SEM. $^{*}P < 0.05$, $^{**}P < 0.01$ vs. *Plin1*$^{+/+}$ group by Student's *t*-test. AD., adipocytes.

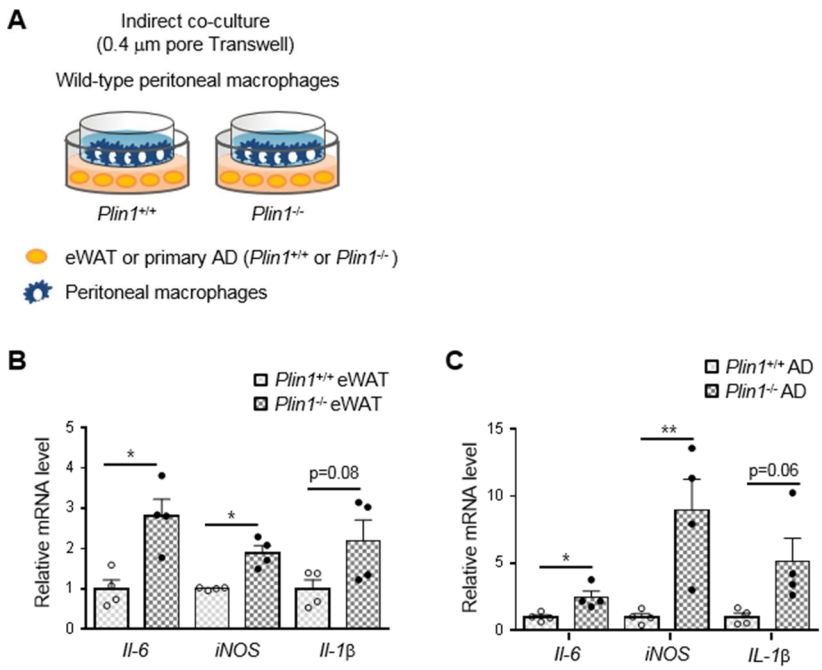

Figure 11. *Plin1*$^{-/-}$ adipocytes potentiate macrophage activation. (A) Peritoneal macrophages were co-cultured with chopped eWAT or primary adipocytes of *Plin1*$^{+/+}$ and *Plin1*$^{-/-}$ mice in Transwell plates (0.4 μm pore) for 48 h. (B and C) Total RNA was isolated from peritoneal macrophages co-cultured with eWAT (B) or primary adipocytes (C) for determining the mRNA levels of *Il-6*, *iNOS*, and *Il-1*β. All data represent the mean ± SEM. $^{*}P < 0.05$, $^{**}P < 0.01$ vs. *Plin1*$^{+/+}$ group by Student's *t*-test. qRT-PCR data were normalized to the mRNA level of *cyclophilin*. AD., adipocytes.

and *Plin1*$^{+/+}$ macrophages did not show any difference in inflammatory gene expression (Figure 12). These results indicated that PLIN1 would act as a protective factor against adipose tissue inflammation, at least in part by inhibiting the secretion of certain signaling molecule(s) that promote the expression of pro-inflammatory cytokines and monocyte migration.

In PLIN1-deficient adipocytes, enhanced lipolysis promotes monocyte migration

In adipocytes, PLIN1 is a key player to modulate lipolysis (Granneman et al., 2009; Tansey et al., 2001). To determine whether the inhibitory effect of PLIN1 on lipolysis might be associated with monocyte migration, I first examined the effect of PLIN1 deficiency on the release of lipolytic metabolites in culture media. As expected, *Plin1*$^{-/-}$ adipocytes secreted higher amounts of glycerol and FFAs than *Plin1*$^{+/+}$ adipocytes (Figure 13A and 13B). On the other hand, PLIN1-deficient adipocytes showed little or no effect on MCP-1 secretion (Figure 13C). Moreover, to examine whether increased monocyte migration upon PLIN1 deficiency depends on secretory proteins from adipocytes, CM from SVC-derived adipocytes was subjected to heat inactivation (Ayache et al., 2006). Heat-inactivated CM from *Plin1*$^{-/-}$ adipocytes did not significantly alter the degree of monocyte migration compared with CM from *Plin1*$^{-/-}$ adipocytes (Figure 13D). These data imply that increased monocyte migration upon PLIN1

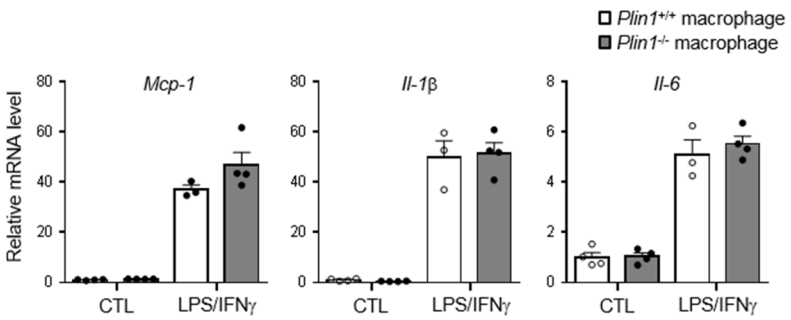

Figure 12. Intrinsic characteristics are not different between *Plin1*$^{+/+}$ and *Plin1*$^{-/-}$ macrophages. Peritoneal macrophages were treated 17 h with LPS (5 ng/ml) and interferon (IFN) γ (100 units/ml) and subjected to qRT-PCR to determine the expression of the indicated inflammatory genes. All data represent the mean ± SEM. qRT-PCR data were normalized to the mRNA level of *cyclophilin*.

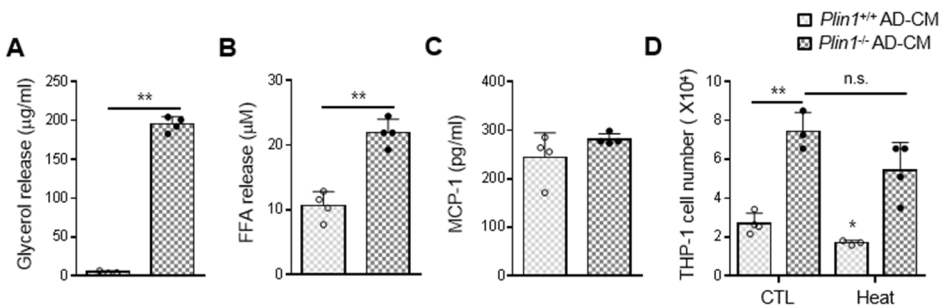

Figure 13. *Plin1*$^{-/-}$ adipocytes induce secretion of lipid metabolites, not chemokines. (A-C) The levels of glycerol (A), FFAs (B), and MCP-1 (C) released from *Plin1*$^{+/+}$ or *Plin1*$^{-/-}$ primary adipocytes for 48 h were measured. $^{**}P < 0.01$ vs. *Plin1*$^{+/+}$ group by Student's *t*-test. (D) CM were collected from SVC-derived adipocytes for 48 h and subjected to heat inactivation (70°C, 10 min). The number of migrated cells upon incubation with each CM was measured. $^{*}P < 0.05$, $^{**}P < 0.01$ vs. *Plin1*$^{+/+}$, CTL group by two-way ANOVA followed by Bonferroni's post-hoc test. All data represent the mean ± SEM. AD., adipocytes.

deficiency might not be associated with secreted chemokines from adipocytes.

To investigate whether enhanced lipolysis in PLIN1-deficient adipocytes might be attributable to monocyte migration, two key lipases, *Atgl* and *Hsl*, were knocked down via siRNA in SVC-derived adipocytes (Figure 14A and 14B). Basal lipolysis was markedly higher in *Plin1*$^{-/-}$ SVC-derived adipocytes than in *Plin1*$^{+/+}$ SVC-derived adipocytes (Figure 14C). In *Plin1*$^{-/-}$ SVC-derived adipocytes, knockdown of *Atgl* and *Hsl* attenuated basal lipolysis (Figure 14C). Intriguingly, the degree of monocyte migration was lower upon suppression of these lipases (Figure 14D). In addition, to verify lipolysis could be responsible for adipose tissue inflammation in *Plin1*$^{-/-}$ mice, *Plin1*$^{-/-}$ mice were administered with orlistat, a lipase inhibitor (50 mg/kg body weight). Serum levels of FFAs and glycerol were decreased in orlistat-treated *Plin1*$^{-/-}$ mice compared to vehicle-treated *Plin1*$^{-/-}$ mice (Figure 15A and 15B). As shown in Figure 15C, orlistat treatment also alleviated mRNA levels of macrophage marker genes and pro-inflammatory cytokines in eWAT of *Plin1*$^{-/-}$ mice. Together, these results suggested that adipocyte PLIN1 would suppress adipose tissue inflammation through repressing basal lipolysis.

Elevated prostaglandins secreted from *Plin1*$^{-/-}$ adipocytes potentiate monocyte migration

Certain lipid metabolites, including LTB_4 and PGD_2 promote

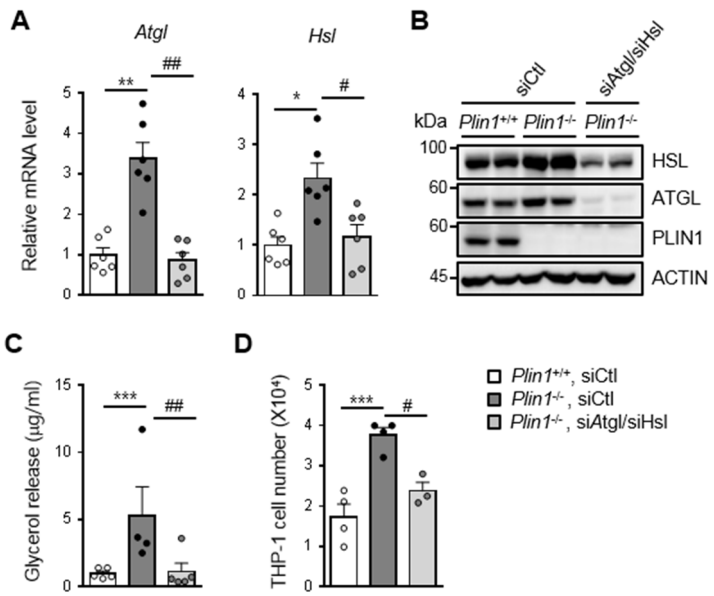

Figure 14. Suppression of enhanced lipolysis in *Plin1*$^{-/-}$ adipocytes alleviates monocyte migration. SVC-derived adipocytes were transfected with control siRNA (siCtl) or *Atgl*-specific siRNA (siAtgl) and *Hsl*-specific siRNA (siHsl). After 48 h, total RNA or protein was extracted and conditioned medium (CM) was collected from siRNA-transfected SVC-derived adipocytes. The mRNA levels of *Atgl* and *Hsl* were analyzed by qRT-PCR (A) and protein levels of ATGL and HSL were analyzed by western blot (B). The released glycerol (C) was measured. The number of migrated cells upon incubation with each CM was measured (D). $^{*}P < 0.05$, $^{**}P < 0.01$, $^{***}P < 0.001$ vs. *Plin1*$^{+/+}$, siCtl group; $^{\#}P < 0.05$, $^{\#\#}P < 0.01$ vs. *Plin1*$^{-/-}$, siCtl group by one-way ANOVA followed by Tukey's post-hoc test. All data represent the mean ± SEM. qRT-PCR data were normalized to the mRNA level of *cyclophilin*. AD., adipocytes.

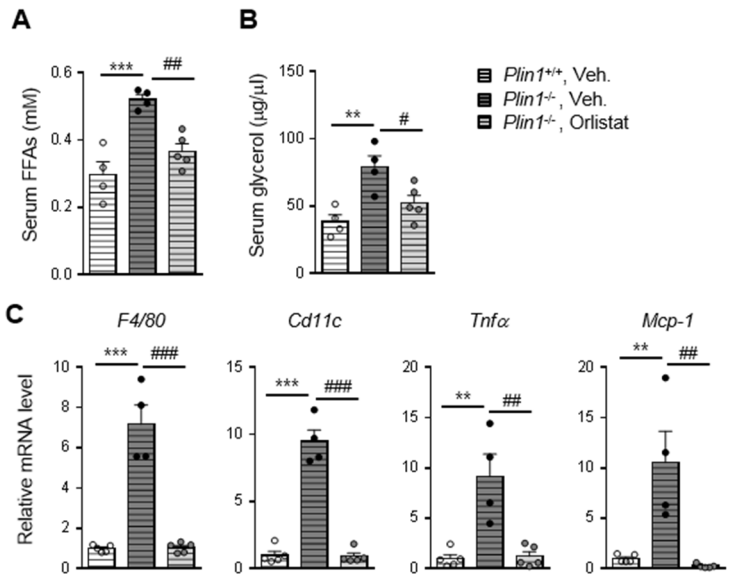

Figure 15. Suppression of enhanced lipolysis in *Plin1*$^{-/-}$ mice attenuates adipose tissue inflammation. *Plin1*$^{+/+}$ or *Plin1*$^{-/-}$ mice were intraperitoneally administered daily with orlistat (50 mg/kg body weight) for 9 days. (A) Serum FFAs and (B) serum glycerol were measured. (C) Relative mRNA levels of pro-inflammatory genes were determined in eWAT by qRT-PCR. $^{**}P < 0.01$, $^{***}P < 0.001$ vs. *Plin1*$^{+/+}$, vehicle group; $^{\#}P < 0.05$, $^{\#\#}P < 0.01$, $^{\#\#\#}P < 0.001$ vs. *Plin1*$^{-/-}$, vehicle group by one-way ANOVA followed by Tukey's post-hoc test. All data represent the mean ± SEM. qRT-PCR data were normalized to the mRNA level of *cyclophilin*. Veh., vehicle.

monocyte/macrophage migration (Hu et al., 2016; Li et al., 2015). To identify potential secreted mediator(s) that can potentiate monocyte migration in adipose tissue of *Plin1*$^{-/-}$ mice, CM of adipocytes was subjected to lipidomic analysis by non-targeted LC-MS/MS (Table 2). The level of eicosanoids appeared to be higher in CM of *Plin1*$^{-/-}$ adipocytes than in that of *Plin1*$^{+/+}$ adipocytes. I took a targeted lipidomics approach to determine the relative quantity of eicosanoids secreted from adipocytes (Figure 16A). The level of PGE_2 was higher in CM of *Plin1*$^{-/-}$ adipocytes than in that of *Plin1*$^{+/+}$ adipocytes (Figure 16B).

Since cyclooxygenase (COX) isoenzymes produce PGs from arachidonic acid (AA) (Figure 17A), intracellular AA was examined in adipocytes. As indicated in Figure 17B, the level of AA appeared to be higher in *Plin1*$^{-/-}$ than in *Plin1*$^{+/+}$ adipocytes. Eukaryotic COX has two isoforms, COX1 and COX2. While COX1 is constitutively expressed and is involved in cellular homeostasis, COX2 is inducible and produces numerous PGs under pathophysiological conditions (Vane et al., 1998). To investigate whether PLIN1 deficiency might affect COX2 activity, I measured the enzymatic activity of COX from SVC-derived adipocytes. While total COX activity was higher in *Plin1*$^{-/-}$ than in *Plin1*$^{+/+}$ adipocytes (Figure 17D), suppression of COX2 via siRNA (Figure 17C) downregulated total COX activity in *Plin1*$^{-/-}$ adipocytes and suppressed the degree of monocyte migration (Figure 17D and 17E).

Table 2. Fold changes of lipid metabolites released from SVC-derived adipocytes.

Metabolite feature (MW/rt)	METLIN Search	Class	Fold change (Log_2 *Plin1*$^{-/-}$/*Plin1*$^{+/+}$)
455.391/31.24	Arachidyl carnitine	Fatty acyls (acyl carnitines)	1.181536
340.2932/29.95	Glycidyl stearate, 2-oxo-heneicosanoic acid		1.159548
770.5644/30	PC(35:2), PE(38:2)	Glycerophospholipids	1.068222
337.33/29.63	13Z-Docosenamide	Fatty acyls (fatty amides)	1.04465
768.5683/29.89	PA(41:3)	Glycerophospholipids	1.025215
769.5718/30.29	PC(35:3), PE(38:3)	Glycerophospholipids	1.024059
380.2851/21.28	24-Nor-5β-cholane-3α,7α,22,23-tetrol, MG(20:3)		0.857633
756.531/31.1	PG(O-36:4), PG(P-36:3)	Glycerophospholipids	0.822948
757.5348/31.05	PS(P-35:2)	Glycerophospholipids	0.803131
256.2366/21.45	Palmitic acid	Fatty acyls (fatty acids and derivatives)	0.68305
299.2787/20.34	Sphingosine, 3-ketosphinganine, Palmitoyl Ethanolamide	Organonitrogen compounds	0.666305
602.3848/2.28	PA(29:2)	Glycerophospholipids	0.597865
298.2469/17.77	9-hydroxy-13Z-octadecenoic acid, Ricinoleic acid	Fatty acyls (fatty acids and derivatives)	0.561922
720.4832/2.58	PA(28:6), PG(32:1)	Glycerophospholipids	0.454224
554.35/1.92	PG(21:0/0:0)	Glycerophospholipids	0.428229
740.5373/21.15	PA(39:3)	Glycerophospholipids	0.404163
712.4059/1.95	PI(25:0)	Glycerophospholipids	0.374166
370.3035/22.59	Docosanedioic acid	Fatty acyls (fatty acids and derivatives)	0.338426
620.295/16.36	PI(20:4)	Glycerophospholipids	0.319366
336.2963/20.9	5,13-docosadienoic acid	Fatty acyls (fatty acids and derivatives)	0.31618
328.2933/23.9	3R-hydroxy-eicosanoic acid	Fatty acyls (fatty acids and derivatives)	0.313408
364.1452/2.11	N-Acetylmuramoyl-Ala		0.303871
753.4682/2.39	PS(34:5)	Glycerophospholipids	0.28537
498.2883/2.12	PG(17:0/0:0)	Glycerophospholipids	0.284992
276.094/2.11	Glutamyl-glutamic acid		0.244705
215.1131/2.01	2-amino-8-oxo-9,10-epoxy-decanoic acid	Fatty acyls (fatty acids and derivatives)	0.234206
347.2755/21.3	Arachidonoyl Ethanolamide	Organonitrogen compounds Direct Parent N-acylethanolamines	0.233468
698.3905/1.94	PI(24:0)	Glycerophospholipids	0.218434
349.1957/2.1	Coutaric acid	Amino acids, peptides, and analogues	0.218434
282.252/15.83	Oleic Acid	Fatty acyls (fatty acids and derivatives)	0.210324
354.1423/4.15	S-Adenosylmethioninamine	5'-deoxyribonucleosides	0.207633
316.204/2.02	15-deoxy-δ-12,14-PGJ2, 19-Hydroxy-13-cis-retinoic acid	Fatty acyls (eicosanoids and derivatives)	0.184757
767.52/1.88	PS(O-36:5), PS(P-36:4)	Glycerophospholipids	0.173124
392.2848/22.78	1α,3α-Dihydroxy-5β-cholan-24-oic Acid		0.169472
282.1066/3.78	2,3-Diphenyl-1-indanone		0.157641
190.0968/10.09	Diaminopimelic acid, Alanyl-Threonine	Carboxylic acids and derivatives	0.157112
270.216/10.12	16-hydroxy-5-hexadecenoic acid, 5-keto palmitic acid	Fatty acyls (fatty acids and derivatives)	0.140856
368.1704/6.03	Testosterone sulfate	Steroids and steroid derivatives	0.139633
270.216/8.28	16-hydroxy-6-hexadecenoic acid	Fatty acyls (fatty acids and derivatives)	0.115991
444.3002/9.7	Stearyl citrate		0.115675
470.2931/2.67	PG(O-16:0)		0.112739
174.1021/8.45	N2-Acetyl-L-ornithine, Valyl-Glycine	Carboxylic acids and derivatives	0.11045
252.2057/8.41	7,10-hexadecadienoic acid	Fatty acyls (fatty acids and derivatives)	0.109846
220.1072/6.45	N-Acetyl-b-glucosaminylamine	Organooxygen compounds	0.105796
254.2211/13.54	cis-9-palmitoleic acid, 11-hexadecenoic acid	Fatty acyls (fatty acids and derivatives)	0.101884
378.293/9.86	cholesta-5,7,8(14),22E-tetraen-3-one		0.097712
298.2468/11.26	9-hydroxy-12Z-octadecenoic acid, Ricinoleic acid	Fatty acyls (fatty acids and derivatives)	0.097421
280.2365/12.52	Linoleic acid	Fatty acyls (fatty acids and derivatives)	0.094585
351.1579/7.05	Phenylalanyl-Tryptophan	Carboxylic acids and derivatives	0.086142
356.2492/9.56	PGF1α, 13,14-dihydro PGF2α	Fatty acyls (eicosanoids and derivatives)	0.076672
357.2623/15.32	Leucyl-leucyl-norleucine		0.073382
386.1804/5.59	6-bromo-eicosa-5E,9Z-dienoic acid		0.039522
400.147/2.61	N-Monodesmethyldiltiazem		0.03026
636.2893/14.35	Thalsimine		0.021127
164.0663/3.03	β-D-Fucose	Organooxygen compounds	0.011422
368.1578/3.6	PA(12:0)	Glycerophospholipids	-0.08932

Metabolites were identified by matching accurate mass (MW) data to METLIN database. Only data with *p* value less than 0.05 were represented. P value was calculated by Mann-Whitney U test (*n*=3 per group). rt., retention time.

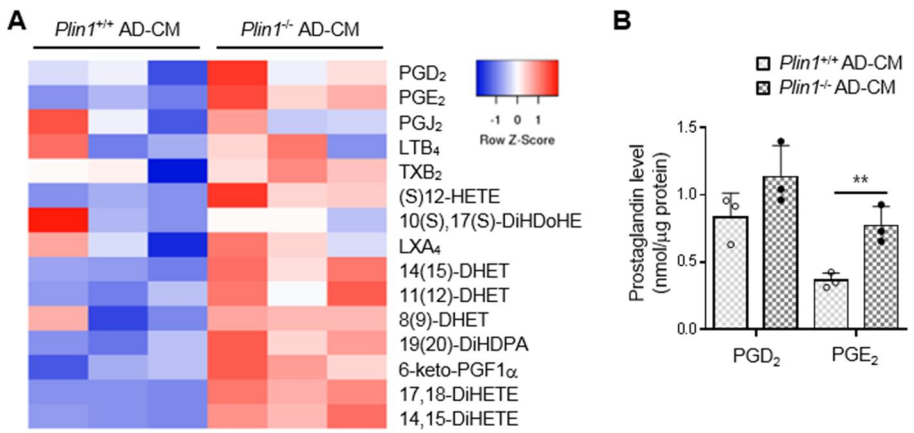

Figure 16. Secretion level of prostaglandins from *Plin1*$^{-/-}$ adipocytes is enhanced. (A) CM of SVC-derived adipocytes was collected and analyzed by LC-MS/MS lipidomic methods. Eicosanoids profiles were displayed as a heat map. (B) The contents of PGD_2 and PGE_2 in the CM were assessed. All data represent the mean ± SEM. $^{**}P < 0.01$ vs. *Plin1*$^{+/+}$ group by Student's *t*-test. AD., adipocytes.

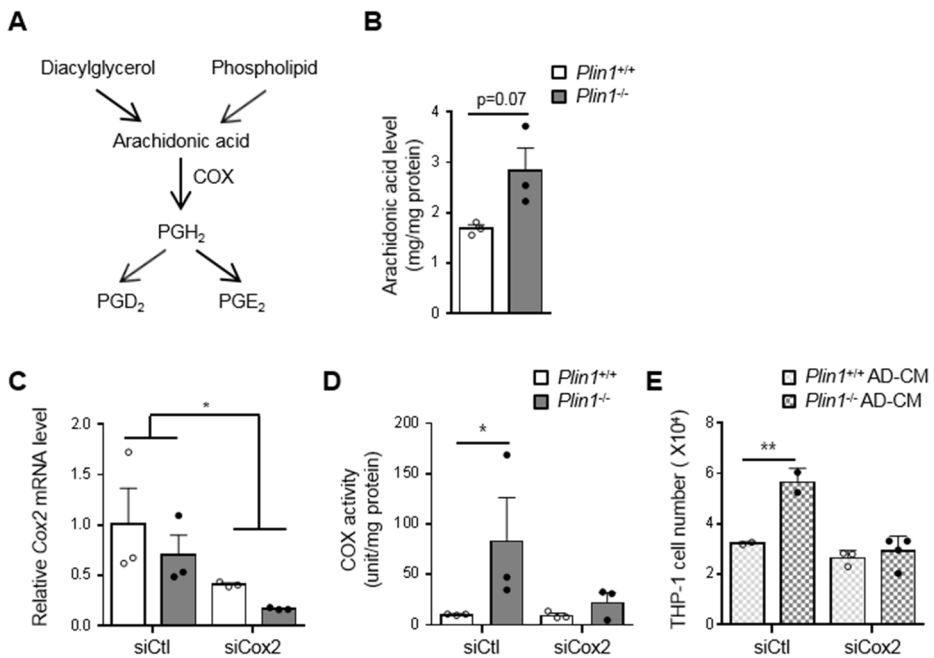

Figure 17. PLIN1 deficiency increases COX activity in adipocytes. (A) Pathway of prostaglandin synthesis from arachidonic acid (AA), and the involvement of COX. (B) The level of intracellular AA in *Plin1*$^{+/+}$ or *Plin1*$^{-/-}$ adipocytes was measured by LC-MS/MS. $^{**}P < 0.01$ vs. *Plin1*$^{+/+}$ group by Student's *t*-test. (C-E) SVC-derived adipocytes were transfected with control siRNA (siCtl) or C*ox2*-specific siRNA (siCox2). After 48 h, total RNA was extracted from siRNA-transfected SVC-derived adipocytes. The mRNA level of *Cox2* was analyzed by qRT-PCR. $^{*}P < 0.05$ vs. siCtl group by two-way ANOVA followed by post hoc Bonferroni test (C). The level of intracellular COX activity in *Plin1*$^{+/+}$ or *Plin1*$^{-/-}$ adipocytes was measured (D) and CM was collected from siRNA-transfected SVC-derived adipocytes. The number of migrated cells upon incubation with each CM was measured (E). $^{*}P < 0.05$, $^{**}P < 0.01$ vs. *Plin1*$^{+/+}$, siCtl group by two-way ANOVA followed by post hoc Bonferroni test. All data represent the mean ± SEM. qRT-PCR data were normalized to the mRNA level of *cyclophilin*.

Next, to examine the effect of elevated PGs on monocyte migration, SVC-derived adipocytes were treated with NS398, COX2-selective inhibitor (Figure 18A). As indicated in Figure 18B, the degree of monocyte migration was mitigated by pharmacological inhibition of COX2 and restored by PGE_2 supplementation in CM. To further investigate PGs might contribute to adipose tissue inflammation in *Plin1*$^{-/-}$ mice, I measured intracellular levels of PGE_2 and AA in eWAT from *Plin1*$^{+/+}$ and *Plin1*$^{-/-}$ mice. While the levels of PGE_2 and AA in eWAT of *Plin1*$^{-/-}$ mice were increased (Figure 19A and 19B), serum PGE_2 level was not altered upon PLIN1 deficiency (Figure 19C). Moreover, in eWAT of NS398-treated *Plin1*$^{-/-}$ mice, pro-inflammatory gene expression profiles were significantly downregulated compared to vehicle-treated *Plin1*$^{-/-}$ mice (Figure 19D). These data proposed that increased PGs released from *Plin1*$^{-/-}$ adipocytes would stimulate monocyte migration.

Plin1$^{-/-}$ mice exhibit impaired insulin sensitivity via lipid dysregulation

To determine whether PLIN1 deficiency might alter systemic glucose homeostasis, the serum levels of glucose and insulin were measured. Compared to *Plin1*$^{+/+}$ mice, *Plin1*$^{-/-}$ mice exhibited higher fasting glucose and *ad libitum* insulin concentrations (Figure 20A and 20B). To investigate whether PLIN1 deficiency would indeed influence whole-body insulin sensitivity, I performed glucose tolerance test (GTT) and insulin tolerance test (ITT). *Plin1*$^{-/-}$ mice were more glucose intolerant and insulin insensitive than

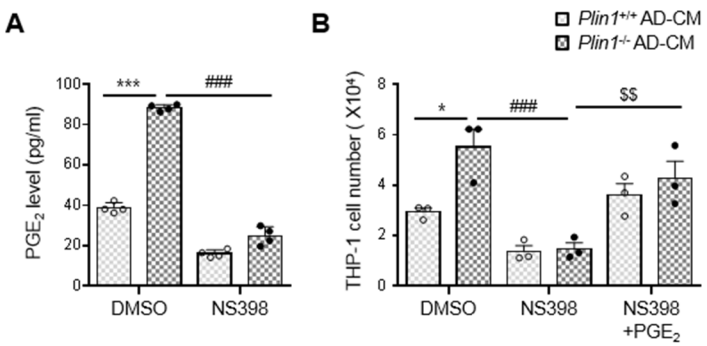

Figure 18. Prostaglandins produced by *Plin1*$^{-/-}$ adipocytes promote monocyte migration. CM was collected from COX2 inhibitor, NS398 (1 μM), pretreated SVC-derived adipocytes. (A) The level of secreted PGE_2 was measured by ELISA. $^{***}P < 0.001$ vs. *Plin1*$^{+/+}$, DMSO; $^{\#\#\#}P < 0.001$ vs. *Plin1*$^{-/-}$, DMSO group by two-way ANOVA followed by Bonferroni's post-hoc test. (B) Migrated cells upon incubation with PGE_2 (0.1 μM) supplemented CM were assessed. $^{*}P < 0.05$, $^{***}P < 0.001$ vs. *Plin1*$^{+/+}$, DMSO group; $^{\#\#\#}P < 0.001$ vs. *Plin1*$^{-/-}$, DMSO group; $^{\$\$}P < 0.001$ vs. *Plin1*$^{-/-}$, NS398 group by two-way ANOVA followed by Bonferroni's post-hoc test. AD., adipocytes.

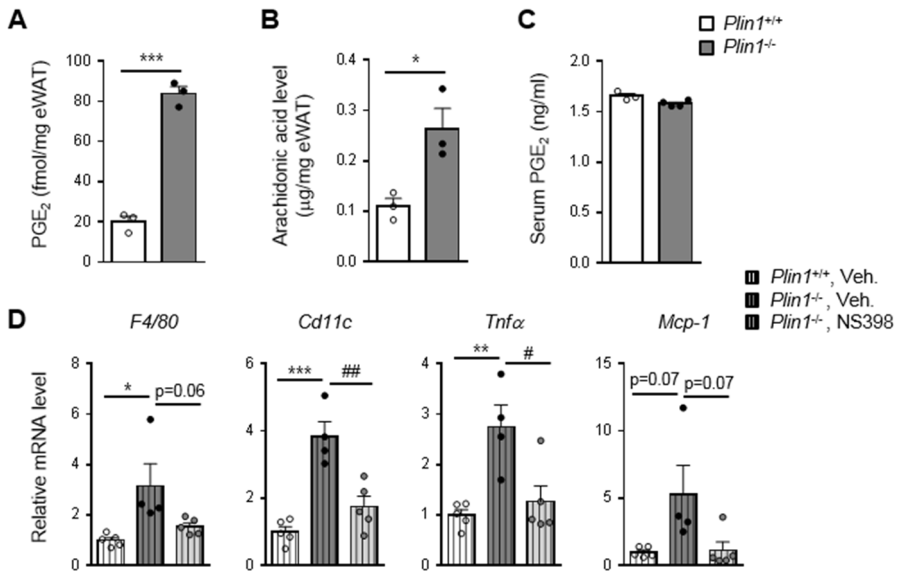

Figure 19. Suppression of prostaglandin production in *Plin1*$^{-/-}$ mice attenuates adipose tissue inflammation. The levels of PGE_2 (A) and AA (B) in eWAT and serum PGE_2 level (C) were measured. $^{*}P < 0.05$, $^{***}P < 0.001$ vs. *Plin1*$^{+/+}$ group by Student's *t*-test. (D) *Plin1*$^{+/+}$ or *Plin1*$^{-/-}$ mice were intraperitoneally administered daily with NS398 (10 mg/kg body weight) for 8 days. Relative mRNA levels of pro-inflammatory genes were determined in eWAT by qRT-PCR. $^{*}P < 0.05$, $^{**}P < 0.01$, $^{***}P < 0.001$ vs. *Plin1*$^{+/+}$, vehicle group; $^{\#}P < 0.05$, $^{\#\#}P < 0.01$ vs. *Plin1*$^{-/-}$, vehicle group by one-way ANOVA followed by Tukey's post-hoc test. All data represent the mean ± SEM. qRT-PCR data were normalized to the mRNA level of *cyclophilin*. Veh., vehicle.

than *Plin1*$^{+/+}$ mice (Figure 20C and 20D). In accordance with these, the homeostatic model assessment-insulin resistance (HOMA-IR) index, a quantitative indicator of insulin resistance, was higher in *Plin1*$^{-/-}$ mice than *Plin1*$^{+/+}$ mice (Figure 20E). Since orlistat administration reduced basal lipolysis and adipose tissue inflammation in *Plin1*$^{-/-}$ mice (Figure 15), I further determined whether orlistat might alleviate insulin resistance in *Plin1*$^{-/-}$ mice. To address this, ITT was performed with vehicle- or orlistat-treated *Plin1*$^{-/-}$ mice. As indicated in Figure 21A, orlistat improved insulin intolerance in *Plin1*$^{-/-}$ mice during ITT. Next, to investigate decrease of adipose tissue inflammation by NS398 might also contribute to insulin resistance, I performed ITT. As shown in Figure 21B, NS398-treated *Plin1*$^{-/-}$ mice seemed to be less insulin intolerant. These data propose that abnormally upregulated lipid metabolism would induce adipose tissue inflammation and insulin resistance in *Plin1*$^{-/-}$ mice.

I also examined whether PLIN1 deficiency might modulate insulin signaling cascades in metabolic organs. Insulin-stimulated AKT phosphorylation was lower in adipose tissue of *Plin1*$^{-/-}$ mice as well as in skeletal muscle of *Plin1*$^{-/-}$ mice (Figure 22A and 22B). In contrast, the level of AKT phosphorylation in the liver of *Plin1*$^{-/-}$ mice was not different from that in *Plin1*$^{+/+}$ mice (Figure 22C). In addition, intracellular levels of TG and FFAs appeared to be increased in skeletal muscle of *Plin1*$^{-/-}$ mice but not in liver of *Plin1*$^{-/-}$ mice compared to *Plin1*$^{+/+}$ mice (Figure 23). These results

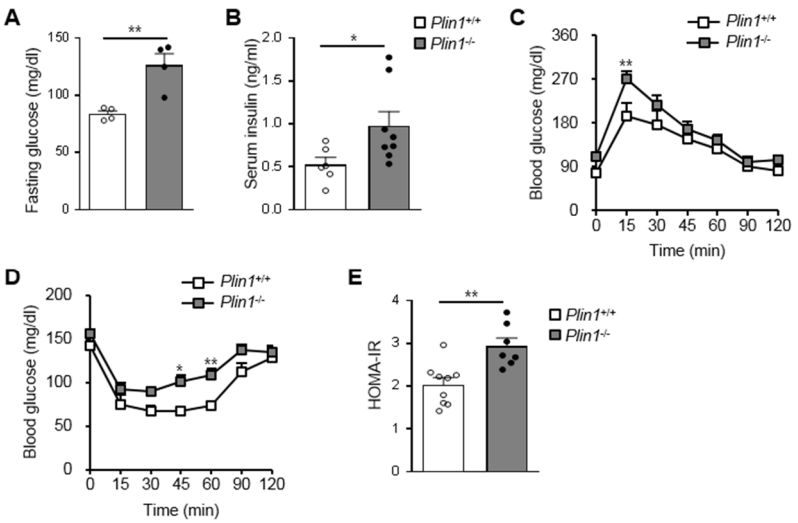

Figure 20. PLIN1 deficiency disrupts systemic insulin sensitivity. (A and B) *Plin1*$^{+/+}$ and *Plin1*$^{-/-}$ mice were fasted for 15 h. Fasting serum glucose (A) and *ad libitum* insulin (B) were measured in *Plin1*$^{+/+}$ and *Plin1*$^{-/-}$ mice. $^{*}P < 0.05$, $^{**}P < 0.01$ vs. *Plin1*$^{+/+}$ group by Student's *t*-test. (C and D) Intraperitoneal glucose tolerance test (GTT) (C) and insulin tolerance test (ITT) (D) were performed on *Plin1*$^{+/+}$ and *Plin1*$^{-/-}$ mice. $^{*}P < 0.05$, $^{**}P < 0.01$ vs. *Plin1*$^{+/+}$ group by repeated-measures ANOVA (RM-ANOVA) followed by Bonferroni's post-hoc test. (E) HOMA-IR was measured in *Plin1*$^{+/+}$ and *Plin1*$^{-/-}$ mice. $^{**}P < 0.01$ vs. *Plin1*$^{+/+}$ group by Student *t*-test.

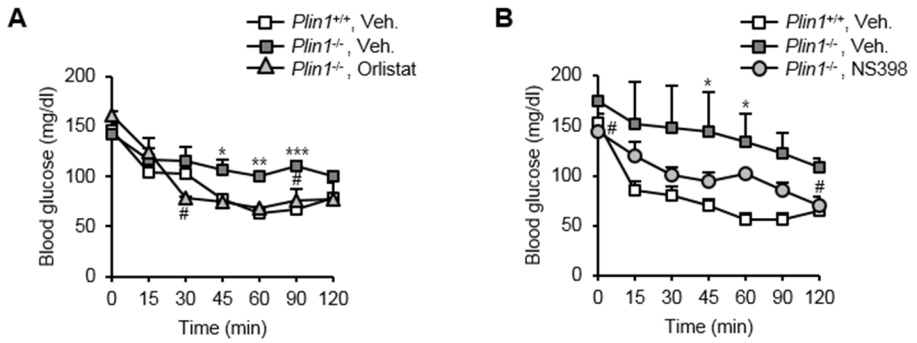

Figure 21. *Plin1*$^{-/-}$ mice show insulin resistance through lipid dysregulation. ITT was performed after treatment with orlistat (50 mg/kg body weight) (A) or with NS398 (10 mg/kg body weight) for 7 days (B). $^{*}P < 0.05$ vs. *Plin1*$^{+/+}$, vehicle group; $^{\#}P < 0.05$ vs. *Plin1*$^{-/-}$, vehicle group by RM-ANOVA followed by Bonferroni's post-hoc test.

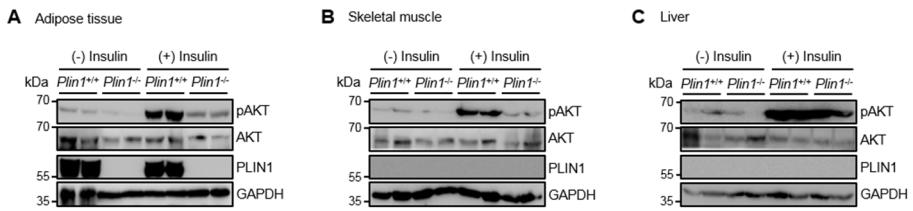

Figure 22. PLIN1 deficiency impairs insulin signaling in adipose tissue and skeletal muscle. *Plin1*$^{+/+}$ and *Plin1*$^{-/-}$ mice were injected with saline or insulin (0.75 units/kg body weight). Insulin signaling in eWAT (A), skeletal muscle (B), and liver (C) was assessed by immunoblot analysis using antibodies against pAKT (S473), AKT, PLIN1 and GAPDH.

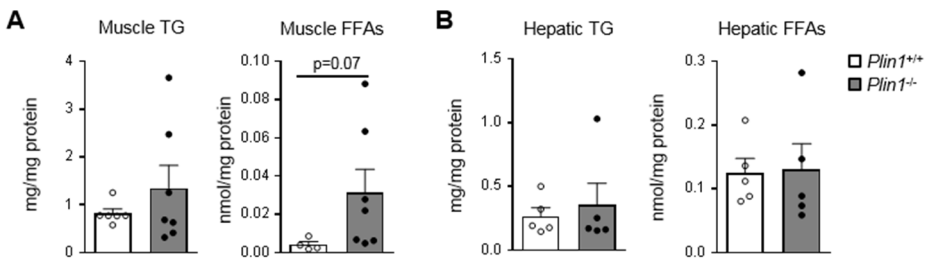

Figure 23. Intracellular lipid contents are increased in skeletal muscle of *Plin1*$^{-/-}$ mice. Levels of TG and FFAs in skeletal muscle (A) or in liver (B) were measured. *p* value vs. *Plin1*$^{+/+}$ mice by Student's *t*-test. All data represent the mean ± SEM.

suggested that PLIN1 would directly or indirectly influence the insulin signaling cascades, at least, in adipose tissue and skeletal muscle.

Macrophage depletion improves insulin resistance in *Plin1*$^{-/-}$ mice

Given that *Plin1* deficiency increased ATM numbers (Figure 9) and induced insulin resistance (Figure 20), I asked whether increased ATMs would be attributable for reduced insulin sensitivity in *Plin1*$^{-/-}$ mice. Clodronate liposomes successfully deplete phagocytic macrophages in peripheral tissues (Choe et al., 2014; Feng et al., 2011). In eWAT from both *Plin1*$^{+/+}$ and *Plin1*$^{-/-}$ mice, clodronate treatment decreased the mRNA levels of *F4/80* and *Cd11c*, while the mRNA level of *Plin1* was not altered (Figure 24A). Accordingly, microscopic analysis revealed that ATM accumulation was decreased by clodronate, and the difference in ATM contents between *Plin1*$^{+/+}$ and *Plin1*$^{-/-}$ mice was insignificant (Figure 24B). As shown in Figure 24C and 24D, clodronate-mediated macrophage depletion improved insulin resistance of *Plin1*$^{-/-}$ mice to levels comparable to those observed in *Plin1*$^{+/+}$ mice. Together, these data suggested that enhanced macrophage recruitment and pro-inflammatory ATMs could mediate impaired insulin sensitivity in *Plin1*$^{-/-}$ mice.

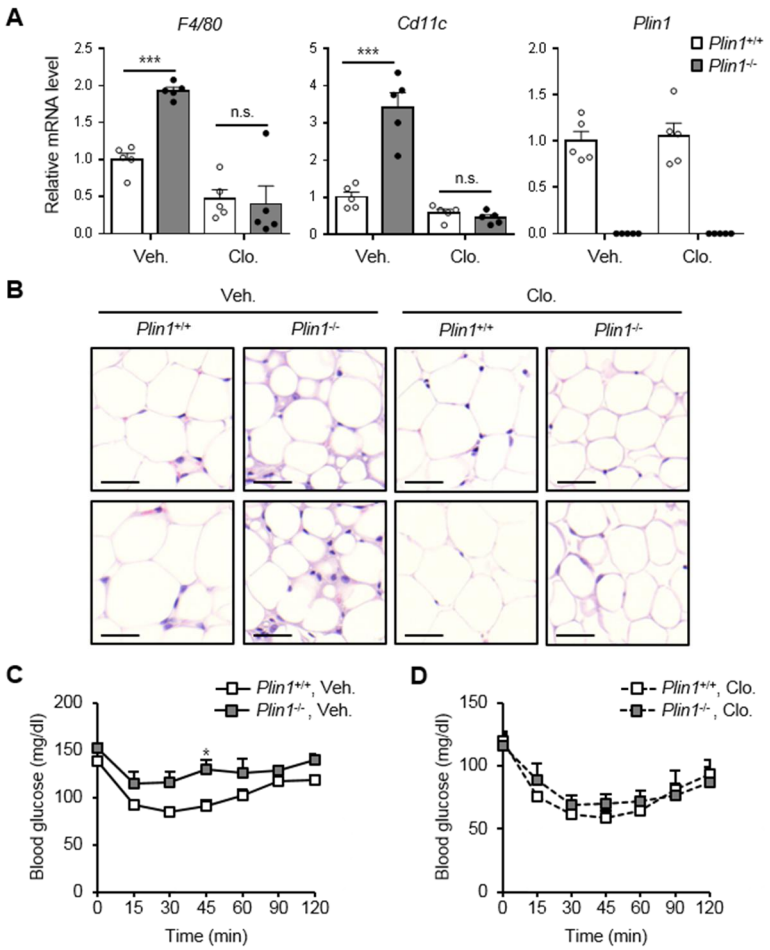

Figure 24. *Plin1*$^{-/-}$ mice exhibit improved insulin resistance upon macrophage depletion. Clodronate (100 µl dose for 20–25 g mouse) was intraperitoneally injected to *Plin1*$^{+/+}$ or *Plin1*$^{-/-}$ mice. Gene expression by qRT-PCR: macrophage markers (A) and histological analysis (B). Scale bars, 50 µm. $^{***}P < 0.001$ vs. *Plin1*$^{+/+}$, vehicle group by two way-ANOVA followed by Bonferroni's post-hoc test. (C and D) Insulin tolerance test (ITT) was performed 4 days after the injection of clodronate. $^{*}P < 0.05$ vs. *Plin1*$^{+/+}$, vehicle group by RM-ANOVA followed by Bonferroni's post-hoc test. All data represent the mean ± SEM. All qRT-PCR data were normalized to the mRNA level of *cyclophilin*. Veh., vehicle; Clo., clodronate; n.s., not significant.

5. Discussion

Immune cells are recruited to white adipose tissue (WAT) under conditions that stimulate lipolysis. For instance, after overnight fasting, macrophage contents in WAT are increased (Kosteli et al., 2010; Schoiswohl et al., 2015). Activation of adipocyte lipolysis with β_3-adrenergic agonists increases ATMs (Kosteli et al., 2010; Schoiswohl et al., 2015). Inhibition of lipolysis by genetic ablation of *Atgl* prevents recruitment of macrophages to WAT (Kosteli et al., 2010; Schoiswohl et al., 2015). However, it is not completely understood how lipolytic activation in adipocytes can increase ATMs. In this study, several lines of evidence supported that adipocyte *Plin1* represses pro-inflammatory responses in adipose tissue by restricting lipolysis. Firstly, pro-inflammatory cytokine expression was higher in adipose tissues of $Plin1^{-/-}$ than in those of $Plin1^{+/+}$ mice. Secondly, macrophage contents were higher in adipose tissue of $Plin1^{-/-}$ mice. Thirdly, *Plin1*-deficient adipocytes potentiated monocyte recruitment and macrophage activation. Lastly, suppression of the key lipases *Atgl* and *Hsl* in *Plin1*-deficient adipocytes alleviated monocyte migration, accompanied with reduced basal lipolysis.

Upon metabolic states, adipose tissue secretes adipokines, which affect functional roles in several metabolic organs such as the liver, pancreas, skeletal muscle, brain, and immune system to modulate whole-

body energy homeostasis. In obese animals, increased chemokines and inflammatory cytokines secreted from adipose tissue facilitate the recruitment of M1-type macrophages into adipose tissue (Hotamisligil et al., 1993). MCP-1 is a crucial chemokine for macrophage infiltration into adipose tissue. For example, adipocyte-specific *Mcp-1* transgenic mice exhibit increased ATMs and whole-body insulin resistance (Kanda et al., 2006). It has been demonstrated that several lipid metabolites released from adipocytes or adipose tissue participate in inflammatory cell activation (Cao et al., 2008; Chan et al., 2015; Gartung et al., 2016; Hu et al., 2016; Yore et al., 2014). Eicosanoids produced from adipocytes promote recruitment of immune cells (Gartung et al., 2016; Hu et al., 2016), whereas palmitoleate and palmitic acid-9-hydroxy stearic acid from adipose tissue reduce pro-inflammatory response in immune cells (Cao et al., 2008; Chan et al., 2015; Yore et al., 2014).

By-products of lipolysis, such as FFAs and eicosanoids, can induce adipose tissue inflammation. FFAs can activate pro-inflammatory responses in adipocytes and myeloid cells (Suganami et al., 2007; Yeop Han et al., 2010). FFAs stimulate adipose tissue inflammation through the TLR4 signaling pathway, resulting in insulin resistance (Suganami et al., 2007; Yeop Han et al., 2010). When adipocytes are treated with β_3-adrenergic agonists or forskolin to stimulate lipolysis, lipid metabolites generated from COX are elevated (Gartung et al., 2016; Hu et al., 2016).

Administration of β_3-adrenergic agonist increases macrophage infiltration into WAT, which can be abrogated by COX2 inhibitor (Gartung et al., 2016). Since PLIN1 in adipocytes plays an important role in the regulation of basal lipolysis (Tansey et al., 2001), I assessed whether PLIN1 deficiency in adipocytes would change the repertoire of released lipid metabolites. The levels of secreted PGs such as PGE_2 were higher in *Plin1*-deficient adipocytes. Further, I observed that suppression of PG production reduced monocyte migration. These data suggest that lipolytic by-products from *Plin1*$^{-/-}$ adipocytes could induce monocyte recruitment and macrophage activation to stimulate adipose tissue inflammation. Given that PGs are one of the potential mediators for pro-inflammatory responses in *Plin1*$^{-/-}$ mice, it is plausible to speculate that PLIN1 in adipose tissue could play a pivotal role in maintaining immune balance, which might eventually contribute to metabolic homeostasis.

It has been suggested that PLIN family could be associated with inflammatory responses (Langlois et al., 2011; McManaman et al., 2013; Montgomery et al., 2018; Najt et al., 2016; Yamamoto et al., 2018; Zhang et al., 2018; Zhou et al., 2017; Zou et al., 2016). For example, PLIN1 ablation in *Ldlr*$^{-/-}$ mice led to an increase in atherosclerotic lesion area when compared to *Ldlr*$^{-/-}$ mice (Langlois et al., 2011). In addition, Zou et al. (Zou et al., 2016) reported that 20-week-old *Plin1*$^{-/-}$ mice in 129/SvEv background developed spontaneous hypertension with perivascular adipose tissue (PVAT)

dysfunction. The anti-contractile effect was impaired in PVAT of *Plin1*$^{-/-}$ mice compared to that of *Plin1*$^{+/+}$ mice. Moreover, pro-inflammatory gene expression and macrophage markers of PVAT were upregulated by *Plin1* deletion (Zou et al., 2016). However, it remains unclear which factors could regulate the inflammatory response in PVAT of *Plin1*$^{-/-}$ mice. We found that NCD-fed lean *Plin1*$^{-/-}$ mice showed enhanced adipose tissue inflammation, which would reduce whole-body insulin sensitivity. In adipose tissue of *Plin1*$^{-/-}$ mice, total macrophages and the CD11c^{+} M1-type macrophage population were elevated. Moreover, it is very likely that certain lipid metabolites secreted from *Plin1*$^{-/-}$ adipocytes would enhance monocyte recruitment and pro-inflammatory responses in macrophages. Furthermore, macrophage depletion using clodronate restored insulin sensitivity in *Plin1*$^{-/-}$ mice. Collectively, these data suggest that ATM stimulation by PLIN1 deficiency seems to be critical for systemic insulin resistance in *Plin1*$^{-/-}$ mice (Figure 25). Nevertheless, I cannot exclude the possibility that *Plin1* ablation might induce systemic insulin resistance through alternative pathways. For instance, COX2 inhibition ameliorated adipose tissue inflammation (Figure 19) even though COX2 inhibition did not thoroughly improve insulin resistance in *Plin1*$^{-/-}$ mice (Figure 21). Further, elevation of circulating TG and FFAs has deleterious effects in non-adipose tissue by inducing lipotoxicity. Impaired insulin signaling reportedly is associated with increased uptake of FFAs into muscle (Petersen and Shulman, 2002). In this

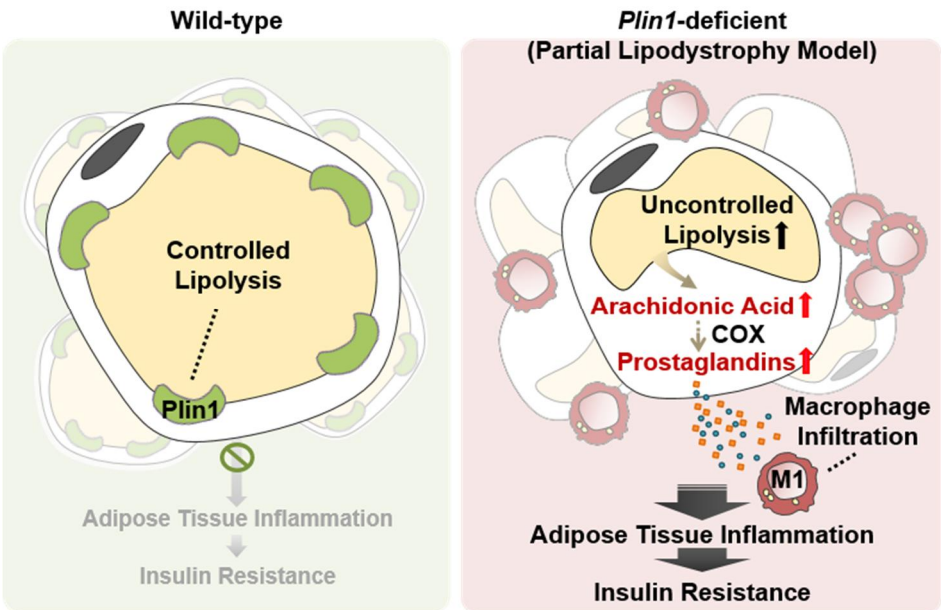

Figure 25. Proposed model of chapter one. In PLIN1-deficient adipose tissue, lipolytic by-products such as prostaglandins promote adipose tissue inflammation, contributing to whole-body insulin resistance.

regard, I observed that serum levels of TG and FFAs were elevated in *Plin1*$^{-/-}$ mice. Moreover, in skeletal muscle of *Plin1*$^{-/-}$ mice, intracellular TG and FFA levels were slightly higher and insulin signaling pathways were impaired (Figure 22 and 23). Thus, it remains to be elucidated whether deteriorated insulin sensitivity in *Plin1*$^{-/-}$ mice might, at least in part result from lipotoxicity in peripheral tissues.

Several pathological conditions, such as lipodystrophy and cachexia, are closely linked to insulin resistance, lipid dysregulation, and inflammation, accompanied with decreased adiposity (Porporato, 2016; Savage, 2009). Interestingly, studies on human PLIN1 deficiency have suggested that mutations in PLIN1 could be responsible for autosomal dominant partial lipodystrophy. Gandotra et al. (Gandotra et al., 2011) identified two heterozygous frameshift mutations in PLIN1. Both mutations result in insulin resistance, severe dyslipidemia, and partial lipodystrophy (Gandotra et al., 2011). Compared to healthy subjects, adipocyte size is significantly decreased, and macrophage infiltration is elevated in adipose tissues of lipodystrophic patients (Gandotra et al., 2011). I found that lean *Plin1*$^{-/-}$ mice showed phenotypes similar to those of PLIN1 mutant patients. In particular, *Plin1*$^{-/-}$ mice exhibited decreased fat mass, dyslipidemia, and insulin resistance, which are common symptoms of lipodystrophic patients. Cachexia is considered a metabolic disorder and is characterized by loss of adipose tissue and skeletal muscle. Adipose tissue loss in cancer cachexia might be partly a

consequence of increased lipolysis, and this alteration in lipid metabolism is closely associated with adipose tissue inflammation (Batista et al., 2012; Das et al., 2011; Klein and Wolfe, 1990). These findings raise the possibility that dysregulated lipid metabolism of adipose tissue would affect systemic insulin resistance in lipodystrophic and cachectic subjects. Moreover, metabolically unhealthy lean individuals present impaired insulin sensitivity and exhibit higher serum TG, FFA levels than metabolically healthy lean individuals (Kim et al., 2013; Succurro et al., 2008). Serum levels of inflammatory markers including TNFα, IL-6, and MCP-1 are higher in metabolically unhealthy lean subjects than in metabolically healthy lean subjects (De Lorenzo et al., 2007; Indulekha et al., 2015). However, it is unclear how metabolically unhealthy lean individuals fail to maintain whole-body metabolic homeostasis due to the lack of proper animal models. Therefore, the present data indicate that *Plin1*$^{-/-}$ mice could be a suitable model to investigate the causality between insulin resistance and adipose tissue inflammation as well as lipid dysregulation in metabolically unhealthy lean subjects.

In conclusion, I identified novel roles of PLIN1 in adipose tissue inflammation and insulin sensitivity in lean animals. My data suggest that PLIN1 is a key regulator against adipose tissue inflammation and insulin resistance by restricting lipolysis. Taken together, PLIN1-mediated lipid metabolism might be a potential target to treat inflammation-linked metabolic

diseases as well as lipid dysregulation.

CHAPTER TWO:

Spatial regulation of reactive oxygen species via G6PD in brown adipocytes supports thermogenic function

1. Abstract

In brown adipocytes, reactive oxygen species (ROS) have been recently implicated in the regulation of thermogenic activity. Glucose-6-phosphate dehydrogenase (G6PD), a rate-limiting enzyme in the pentose phosphate pathway, plays essential roles in the control of cellular redox potential by producing NADPH. Although it has been reported that G6PD upregulates cellular ROS levels in white adipocytes, the role of G6PD in brown adipocytes is largely unknown. In this study, I found that G6PD defect in brown adipocytes impairs thermogenic function through excessive cytosolic ROS accumulation, unlike in white adipocytes. Upon cold stimulation, G6PD-deficient mutant ($G6PD^{mut}$) mice showed cold intolerance, accompanied by downregulated expression of thermogenic genes in brown adipose tissue (BAT). In addition, G6PD-deficient brown adipocytes exhibited increased levels of cytosolic ROS, potentially leading to ERK activation. In BAT of $G6PD^{mut}$ mice, administration of antioxidant, N-acetyl-L-cysteine (NAC), restored the levels of thermogenic gene expression and attenuated ERK activation. Furthermore, body temperature and thermogenic gene expression levels were elevated by ERK inhibition with PD98059 in BAT from cold-exposed $G6PD^{mut}$ mice, implying that elevated ERK activation would be attributable for cold intolerance in $G6PD^{mut}$ mice. Taken together, these data suggest that G6PD in brown adipocytes would relieve

cytosolic ROS to potentiate the thermogenic program.

2. Introduction

Adipose tissue is a key organ in the maintenance of systemic energy homeostasis by regulating energy storage and expenditure. Depending on morphology and function, mammalian adipose tissues are largely divided into white and brown adipose tissue (BAT). While white adipose tissue (WAT) plays major roles in energy storage and endocrine function, BAT is a specialized organ that converts chemical energy to heat and stimulates energy expenditure in response to cold or β-adrenergic stimuli (Cannon and Nedergaard, 2004). BAT contains brown adipocytes that have distinct intracellular features including composition of subcellular organelles and specific gene expression patterns compared to white adipocytes. For instance, brown adipocytes have multilocular lipid droplets and abundant mitochondria with brown adipocyte-specific protein, uncoupling protein 1 (UCP1). Thermogenic function of brown adipocytes primarily depends on UCP1 which is localized in mitochondrial inner membrane. In brown adipocytes, UCP1 mediates proton leaks across the inner membrane and uncouples oxidative phosphorylation from ATP synthesis, resulting in oxygen consumption and heat production (Klingenberg and Winkler, 1985; Nicholls, 1977).

Reactive oxygen species (ROS), a normal byproduct of metabolism, mediate various physiological processes, whereas excessive ROS

accumulation damages intracellular organelles and macromolecules to provoke pathological conditions (Schieber and Chandel, 2014). Cellular ROS is generated by non-enzymatic and enzymatic reactions in mitochondria, peroxisomes, and cytosol (Boveris et al., 1972; Finkel and Holbrook, 2000; Sandalio and Romero-Puertas, 2015; Schröder, 2020). Among them, mitochondria are a major source of cellular ROS production (Finkel and Holbrook, 2000). Since ROS are often produced during mitochondrial respiration, mitochondrial oxygen consumption leads to ROS accumulation in mitochondria and lysosomes (Ambrosio et al., 1993). Notably, cold exposure elevates mitochondrial ROS level with increased mitochondrial oxygen consumption in brown adipocytes (Chouchani et al., 2016; Gaikwad et al., 1990; Sekhar et al., 1987; Shabalina et al., 2014). In addition, it has been reported that the activity of antioxidant enzymes including superoxide dismutase, catalase, glutathione peroxidases and glutathione reductase as well as glutathione (GSH) level is increased (on a per weight basis) in BAT of cold-exposed rats (Barja de Quiroga et al., 1991). In this aspect, it is feasible to speculate that the balance between production and scavenging of ROS would be important for cold-induced BAT activation.

Glucose-6-phosphate dehydrogenase (G6PD), the first and rate-limiting enzyme of the pentose phosphate pathway, generates cytosolic nicotinamide adenine dinucleotide phosphate (NADPH). As a cofactor, NADPH mediates opposite roles for both pro-oxidative enzymes such as

NADPH oxidase and inducible nitric oxide synthase, and anti-oxidative enzymes such as glutathione peroxidase and thioredoxin reductase (Park et al., 2017; Spolarics, 1998). Thus, G6PD appears to have dual functions in the regulation of cellular oxidative levels, depending on cell and/or tissue types (Park et al., 2017). It has been shown that G6PD is highly expressed in WAT, and its overexpression in white adipocytes enhances oxidative stress and pro-inflammatory responses, leading to insulin resistance in obesity (Park et al., 2006; Park et al., 2005). Although it has been reported that enzymatic activity of G6PD in BAT is higher than in WAT and that G6PD activity is elevated in BAT upon cold (Carvalho et al., 1993; Swierczyński et al., 1981), the physiological roles of G6PD in BAT have not been fully elucidated.

In this study, I have studied G6PD-deficient mutant ($G6PD^{mut}$) mouse model to understand the roles of G6PD in BAT. Here, I found that G6PD in brown adipocytes is required for thermogenic activity by scavenging cellular ROS accumulation. Upon cold exposure, $G6PD^{mut}$ mice exhibited cold intolerance and downregulated thermogenic gene expression in BAT. Moreover, genetic and pharmacological inhibition of G6PD in brown adipocytes repressed thermogenic program and oxygen consumption rates in the presence of β-adrenergic activation. Mechanistically, G6PD deficiency in brown adipocytes elevated the level of cytosolic ROS, which suppressed thermogenic gene expression by activating ERK. Together, these data suggest

that G6PD play a pivotal role in the thermogenic regulation of brown adipocytes by restricting aberrant ROS accumulation and ERK activation.

3. Materials and Methods

Animals and treatments

The animal study was performed in accordance with the research guidelines of the Seoul National University Institutional Animal Care and Use Committee. G6PD^{mut} (C57BL/6) mice and their littermates were housed at 22–24°C in a 12-h light/12-h dark cycle and maintained on normal chow diet (Ham et al., 2016). For thermoneutral and cold-exposure experiments, 10–14-week-old male mice were placed at 30°C or 4–6°C (DBL Co., South Korea). For *in vivo* compound administration, mice were intraperitoneally injected with CL-316,243 (indicated dose), NAC (100 mg/kg), PD98059 (10 mg/kg), or an equivalent volume of vehicle.

Reagents and Chemicals

6-aminonicotinamide (6-AN), dehydroepiandrosterone (DHEA) and N-acetyl-L-cysteine (NAC) were purchased from Sigma. Chloromethyl-2', 7'-dichlorodihydrofluorescein diacetate (H_2DCFDA) and mitoSOX were purchased from Invitrogen. PD98059 was purchased from Enzo Life Sciences. siRNAs were purchased from Bioneer (Daejeon, Korea).

Cell Culture

BAC was kindly provided by Dr. Kai Ge (NIH). BAC preadipocytes were grown in Dulbecco's modified Eagle's medium (DMEM) supplemented

with 10% fetal bovine serum (FBS). BAC preadipocytes were grown to confluence (day 0) in induction medium consisting of DMEM, 10% FBS, 20 nM insulin, 1 nM 3,3′,5-triiodo-L-thyronine (T3), 125 μM indomethacin, 0.5 mM isobutylmethylxanthine, and 5.1 μM dexamethasone. After 2 day incubation in induction medium, the cells were transferred to differentiation medium (DMEM, 10% FBS, 20 nM insulin and 1 nM T3). Then, medium was changed with DMEM containing 10% FBS every other day. For siRNAs transfection, differentiated BAC were collected and washed with PBS. After wash, the cells were mixed with siRNA or plasmids and transfected with a single pulse of 1100 V for 30 ms using a Microporator MP-100 (Digital Bio, Seoul, Korea). For transient transfection of DNA plasmids, differentiated BAC were transfected by Lipofectamine 3000 (Thermo Fisher Scientific) according to the manufacturer's protocol. Adenoviral infection was performed as described previously (Park et al., 2006).

Thermal Imaging

The surface temperature of the mice was imaged using an infrared camera (CX320 Thermal Imaging Camera; COX Co., Seoul, Korea).

Whole-mount Immunohistochemistry

Whole-mounted BATs were incubated with DCFDA (10 μM) or

mitoSOX (2.5 μM) for 30 min. After staining, intracellular ROS level in BAT was visualized by coherent anti-Stokes Raman scattering (CARS) imaging using a model TCS SP8 CARS microscope (Leica Microsystems, Wetzlar, Germany). Pump and Stokes lasers were tuned to 14,140 cm^{-1} (or 707 nm) and 11,300 cm^{-1} (or 885 nm), respectively, to be in resonance with the CH_2 symmetric stretch vibration at 2,840 cm^{-1} (Kim et al., 2019).

Adipose tissue fractionation

Adipose tissue was fractionated as described previously (Sohn et al., 2018b). Briefly, BAT was dissected out, chopped, incubated in collagenase buffer (0.1 M HEPES, 0.125 M NaCl, 5 mM KCl, 1.3 mM $CaCl_2$, 5 mM glucose, 1.5% (w/v) glucose, and 0.1% (w/v) collagenase I) for 20 min at 37°C with shaking, and centrifuged. Supernatants containing adipocytes were used for primary cell culture or flow cytometry.

Flow cytometry

Flow cytometric analysis was performed as described previously (Boumelhem et al., 2017). For intracellular ROS measurement, adipocytes were incubated with H_2DCFDA (10 μM) or mitoSOX (2.5 μM) for 30 min. After a wash, fluorescent signals were analyzed using a FACS Canto II (BD Biosciences).

Cellular oxygen consumption assay

Cellular OCR of brown adipocytes were analyzed by Seahorse XFe24 extracellular flux analyzer (Seahorse Bioscience, North Billerica, MA) according to the manufacturer's instruction. Prior to analysis, adipocytes incubated in assay medium (25 mM glucose, 1 mM sodium pyruvate, 2 mM L-glutamine, 2% fatty acid-free BSA in Seahorse XF base medium at pH7.4). For mitochondrial stress tests, OCR was measured following treatment with 5 μM oligomycin, 7.5 μM FCCP and 6 μM antimycin A with 3 μM rotenone. For β-adrenergic stimulation, OCR was measured following acute treatment with 5 μM ISO or brown adipocytes were pretreated with 1 μM ISO for 3 h before OCR measurement. Protein concentration was measured using BCA assay to normalize OCR.

G6PD activity assay

In tissue homogenates, G6PD activity was determined by measuring NADPH production rate. NADPH level was detected using a fluorometric assay kit (Cayman Chemical, no.700300) according to the manufacturer's guidelines. Each enzymatic activity was normalized by tissue weights.

Quantitative reverse transcription (qRT)-PCR

Total RNA was isolated from BAT, iWAT, eWAT, liver, heart, lung, spleen, primary brown adipocytes and BAC. Then, qRT-PCR was performed

as described previously (Sohn et al., 2018a). Primers used were obtained from Bioneer (South Korea).

Western blot analysis

BAT, iWAT and BAC were lysed with modified RIPA buffer containing 50 mM Tris-HCl (pH 7.5), 150 mM NaCl, 2 mM EDTA, 1% (v/v) Triton X-100, 0.5% (w/v) sodium deoxycholate, 0.1% (w/v) SDS, 5 mM NaF, 1 mM Na_3VO_4, and a protease inhibitor mixture (GenDEPOT). Proteins in the lysates were separated by SDS-PAGE and transferred to polyvinylidene fluoride membranes (Millipore). The blots were blocked with 3% BSA and probed with anti-pERK (T202/Y204; Cell Signaling Technology), anti-pJNK (T183/Y185; Cell Signaling Technology), anti-pp38 (T180/Y182; BD science), anti-ERK1 (Santa Cruz Biotechnology), anti-p38 (Santa Cruz Biotechnology), anti-G6PD (Abcam) or anti-UCP1 (Abcam).

Statistical analysis

All data were analyzed using Student's *t*-test or analysis of variance (ANOVA) in GraphPad Prism 7 software (GraphPad Software, La Jolla, CA); *P* values of <0.05 were considered significant.

4. Results

In brown adipocytes, G6PD is elevated by cold exposure

It has been reported that there are intrinsic differences between transcriptomes of BAT and WAT (Hepler et al., 2017; Rosell et al., 2014). To elucidate distinct molecular features in BAT compared to WAT, we performed a large-scale gene function analysis using gene ontology. In BAT, enriched genes were associated with redox regulation pathways under both thermoneutral (TN, 28°C) and cold (4°C) conditions (Figure 26A and 26B). While the expression levels of anti-oxidative enzymes were increased in BAT, the expression levels of NADPH oxidase subunits were decreased in BAT compared to WAT (Figure 26B). Then, to identify the potential key factor(s) involved in the prominent functions of BAT, we analyzed the expression profile through KEGG pathway database. This analysis revealed that "pentose phosphate pathway" was significantly upregulated in BAT rather than WAT from cold-exposed or CL316,243-treated mice compared to each control mice (Figure 27).

Given that G6PD is a key enzyme in redox regulation as well as pentose phosphate pathway and is abundantly expressed in adipose tissue (Park et al., 2005), I hypothesized that G6PD might be involved in BAT function. To investigate whether G6PD expression might be altered in BAT upon cold stimuli, I examined the expression levels of BAT G6PD expression

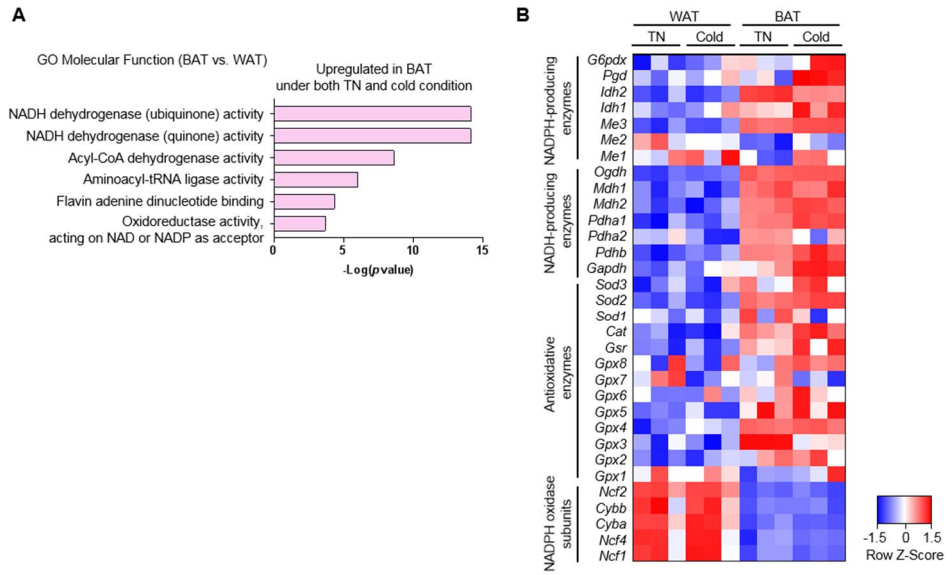

Figure 26. Molecular functions implicated in distinct roles of BAT different from WAT. (A) GO molecular function analysis for common upregulated genes in BAT compared to WAT under TN and cold conditions. (B) A heat map of redox control-related genes in BAT and WAT from TN- or cold-exposed mice. Bars represent Enrichr combined score. Data from GSE51080.

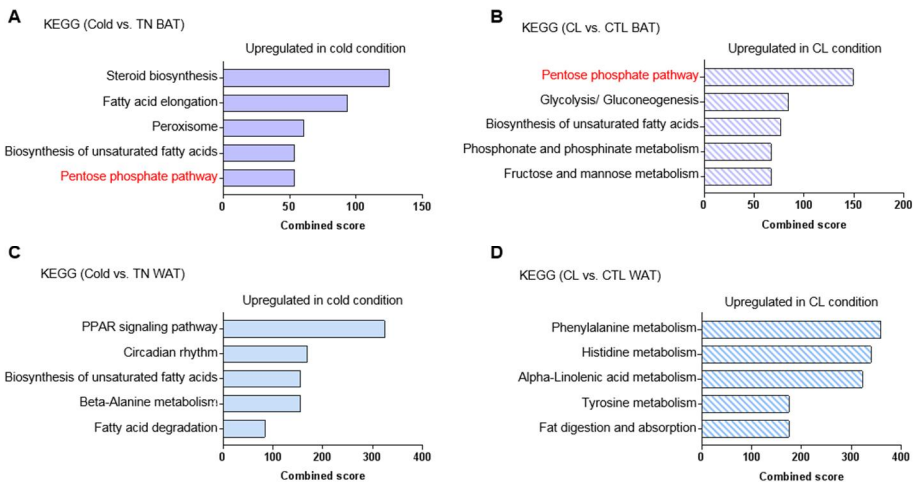

Figure 27. Biological pathways implicated in distinct roles of BAT different from WAT. (A-B) Biological pathway analysis for upregulated genes in BAT from cold-exposed or CL316,243-treated mice compared to control mice using KEGG pathways. (C-D) Biological pathway analysis for upregulated genes in WAT from cold-exposed or CL316,243-treated mice compared to control mice using KEGG pathways. All bars represent Enrichr combined score. Data from GSE51080 and GSE98132.

level under different temperatures such as TN, room temperature (RT, 22°C), and cold. As shown in Figure 28A, the level of *G6pd* mRNA was elevated in BAT during cold exposure. The level of *Ucp1* mRNA was studied as a positive control for cold-induced thermogenesis. Likewise, the level of G6PD protein in BAT was increased by cold exposure (Figure 28B). Moreover, I found that G6PD protein was more abundant in BAT than inguinal WAT (iWAT) (Figure 28C). Upon cold, the increased pattern of G6PD expression was more pronounced in BAT than in other tissues (Figure 28D). To further characterize the expression pattern of BAT G6PD, BATs were fractionated into adipocytes and stromal vascular cells (SVCs). Unlike in SVCs, the level of *G6pd* mRNA was further elevated in brown adipocytes from cold-exposed mice as compared to those from TN-exposed mice (Figure 28E). Although the increase in G6PD expression was prominent in chronic cold conditions, G6PD activity was increased in BAT, not WAT, even in acute cold conditions (Figure 29). In parallel, I examined the level of *G6pd* mRNA in BAT from obese mice where *G6pd* expression was upregulated in WAT. While the level of *G6pd* mRNA in WAT from HFD-fed or *db*/*db* mice was increased compared to NCD-fed or *db*/+ mice, that of *G6pd* mRNA was decreased in BAT from obese mice (Figure 30). Unlike white adipocytes, G6PD overexpression in brown adipocytes did not stimulate pro-inflammatory gene expression or pro-oxidative pathways (Figure 31). These results suggest that G6PD in brown adipocytes is activated in response to cold and might exert

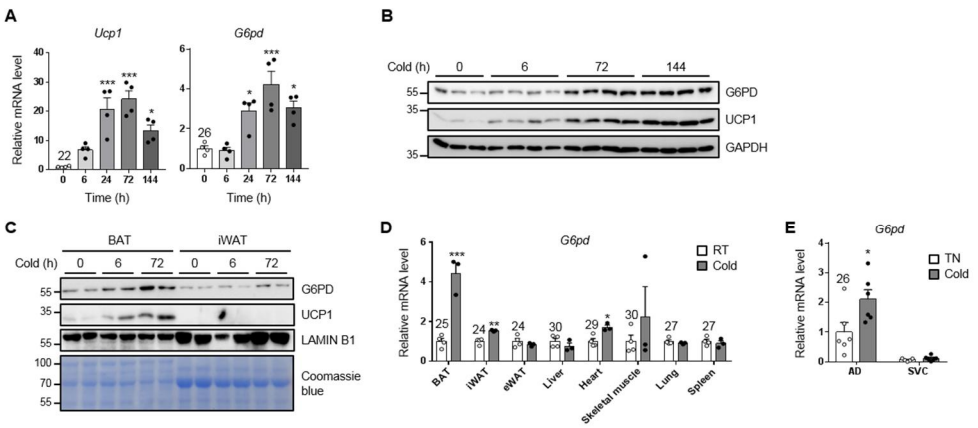

Figure 28. G6PD expression in BAT is induced during cold exposure. (A) The levels of *G6pd* mRNA were measured by qRT-PCR in BAT from WT mice exposed to room temperature (RT) or cold conditions. $^{*}P < 0.05$, $^{**}P < 0.01$, $^{***}P < 0.001$ vs. 0 h group by one-way ANOVA followed by Tukey's post-hoc test. (B) The levels of G6PD protein were determined by western blot analysis in BAT from WT mice exposed to thermoneutral (TN) or cold conditions. (C) The levels of G6PD protein were compared between BAT and iWAT from WT mice exposed to TN or cold conditions. (D) Tissue distribution patterns of *G6pd* mRNA expression were assessed in WT mice exposed to RT or 72 h cold condition. $^{*}P < 0.05$, $^{**}P < 0.01$, $^{***}P < 0.01$ vs. RT group by Student's *t*-test. (E) Relative mRNA level of *G6pd* in brown adipocytes (AD) and stromal vascular cells (SVC) of BAT from WT mice exposed to TN or 72 h cold conditions. $^{*}P < 0.05$ vs. TN group by two-way ANOVA followed by Tukey's post-hoc test. All data represent the mean ± SEM. All qRT-PCR data were normalized to the mRNA level of *36b4*.

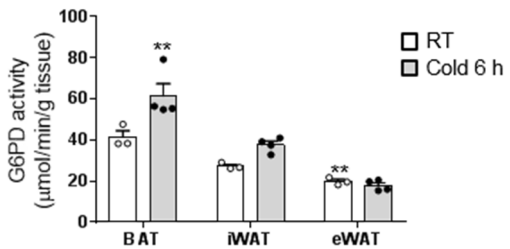

Figure 29. G6PD activity in BAT is induced during cold exposure. G6PD enzymatic activity in BAT, iWAT, and eWAT from WT mice exposed to RT or 6 h cold conditions. $^{**}P < 0.01$, $^{***}P < 0.001$ vs. RT, BAT group by two-way ANOVA followed by Tukey's post-hoc test. All data represent the mean ± SEM.

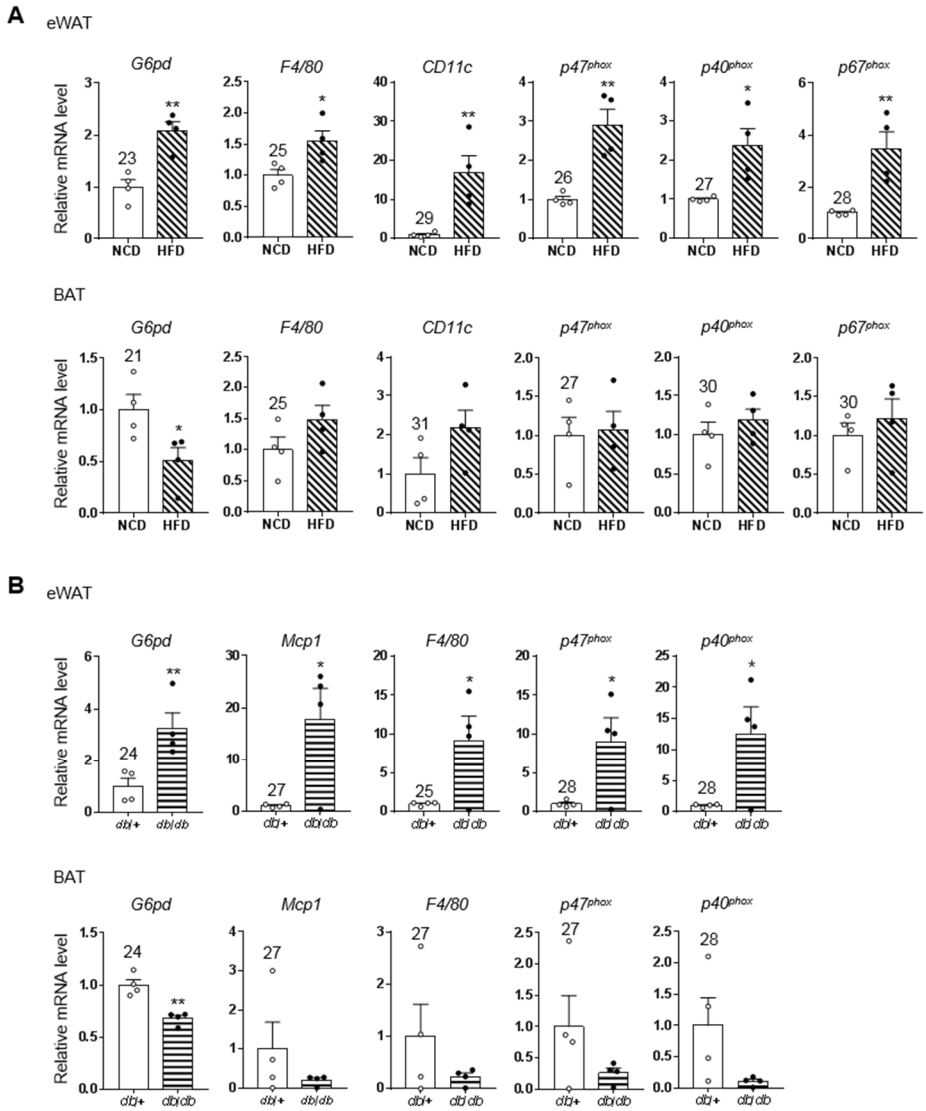

Figure 30. The expression levels of *G6pd*, inflammation- and oxidation-related genes in eWAT and BAT from obese mice. (A) The mRNA levels of *G6pd*, pro-inflammatory and pro-oxidative genes in eWAT and BAT from 8w HFD-fed mice compared with NCD-fed mice. (B) The mRNA levels of *G6pd*, pro-inflammatory and pro-oxidative genes in eWAT and BAT from *db*/*db* mice compared to *db*/+ mice. All data represent the mean ± SEM. All qRT-PCR data were normalized to the mRNA level of *cyclophilin*. $^{*}P < 0.05$, $^{**}P < 0.01$ vs. each control group by Student's *t*-test.

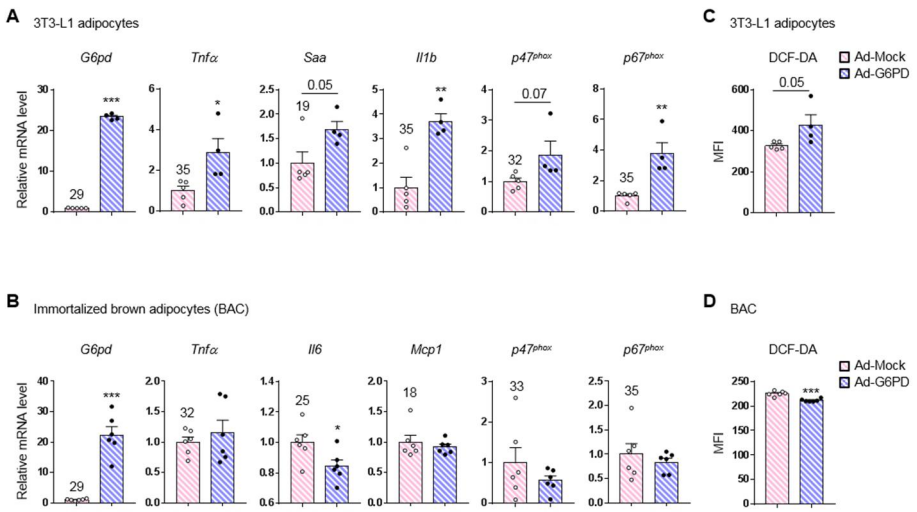

Figure 31. The mRNA levels of inflammatory and oxidative genes in white and brown adipocytes upon G6PD overexpression. (A-B) The mRNA levels of pro-inflammatory genes and NADPH oxidase subunit genes in 3T3-L1 adipocytes (A) or immortalized mouse brown adipocytes (BAC) (B) after G6PD overexpression using adenovirus. (C-D) Cellular ROS level in 3T3-L1 adipocytes (C) or BAC (D) after G6PD overexpression. All data represent the mean ± SEM. All qRT-PCR data were normalized to the mRNA level of *cyclophilin*. $^{*}P < 0.05$, $^{**}P < 0.01$, $^{***}P < 0.01$ vs. Ad-Mock group by Student's *t*-test.

distinct roles different from white adipocytes.

G6PD^{mut} mice show cold intolerance

To investigate the *in vivo* functions of G6PD in BAT, I examined the effects of cold exposure on thermogenic activity in WT and G6PD^{mut} mice. Body weight, adipose tissue mass and serum lipid levels were not significantly different between two genotypes under RT or cold condition (Figure 32). Interestingly, I found that G6PD^{mut} mice were more cold intolerant than WT mice (Figure 33A). Also, thermal imaging analysis revealed that cold-exposed G6PD^{mut} mice exhibited lower body temperature than cold-exposed WT mice (Figure 33B). Although thermogenic gene profiles and adipocyte morphology in BAT were not different between WT and G6PD^{mut} mice at RT (Figure 34), the mRNA levels of thermogenic marker genes including *Ucp1*, *Dio2* and *Ppargc1*α were decreased in BAT of G6PD^{mut} mice upon cold (Figure 34A). Moreover, G6PD-deficient BAT showed larger lipid droplets than WT BAT upon cold exposure (Figure 34B). Consistent with mRNA profile, the level of UCP1 protein in BAT of G6PD^{mut} mice was decreased upon cold (Figure 34C and 34D). However, the mRNA levels of thermogenic marker genes in iWAT were comparable between WT and G6PD^{mut} mice under either RT or cold (Figure 35). Next, I examined the metabolic activity of WT and G6PD^{mut} mice upon β-adrenergic activation. G6PD^{mut} mice displayed lower oxygen consumption and energy expenditure

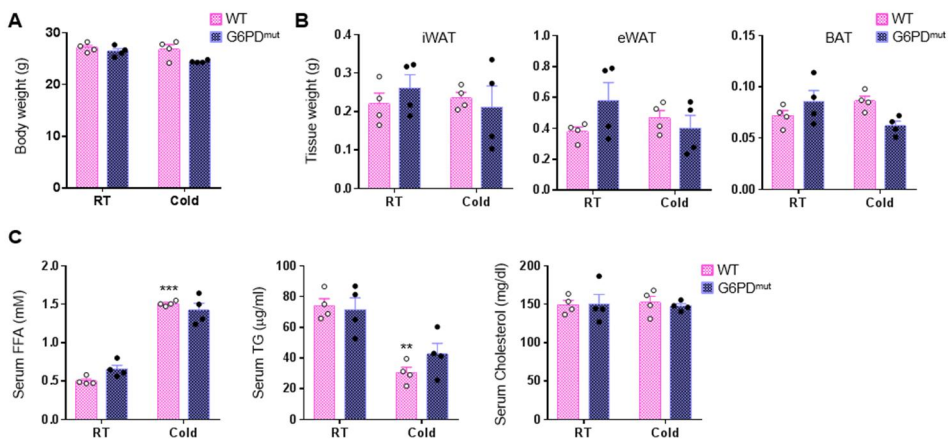

Figure 32. Body weight, tissue weights, and serum lipid profile from WT and G6PD^{mut} mice upon cold exposure. (A-B) Body weight (A) and the weights of adipose tissue (B) from WT and G6PD^{mut} mice exposed to RT or 6 h cold condition. (C) Serum lipid profile of WT and G6PD^{mut} mice upon 6 h cold exposure. All data represent the mean ± SEM. $^{**}P < 0.01$, $^{***}P < 0.001$ vs. WT, RT group by two-way ANOVA followed by Tukey's post-hoc test.

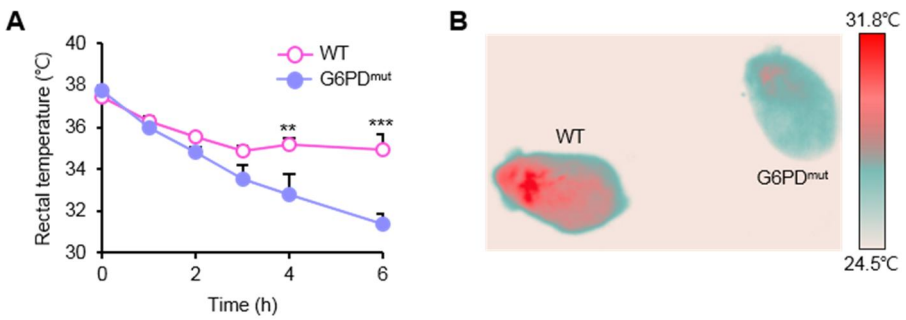

Figure 33. Cold-induced thermogenesis is attenuated in G6PD^{mut} mice. (A) Rectal temperature was measured during cold exposure. The data represent the mean ± SEM. $^{**}P < 0.01$, $^{***}P < 0.001$ vs. WT group by repeated-measures ANOVA (RM-ANOVA) followed by Tukey's post-hoc test. (B) Surface body temperature of WT and G6PD^{mut} mice was assessed by infrared camera after 4 h cold exposure.

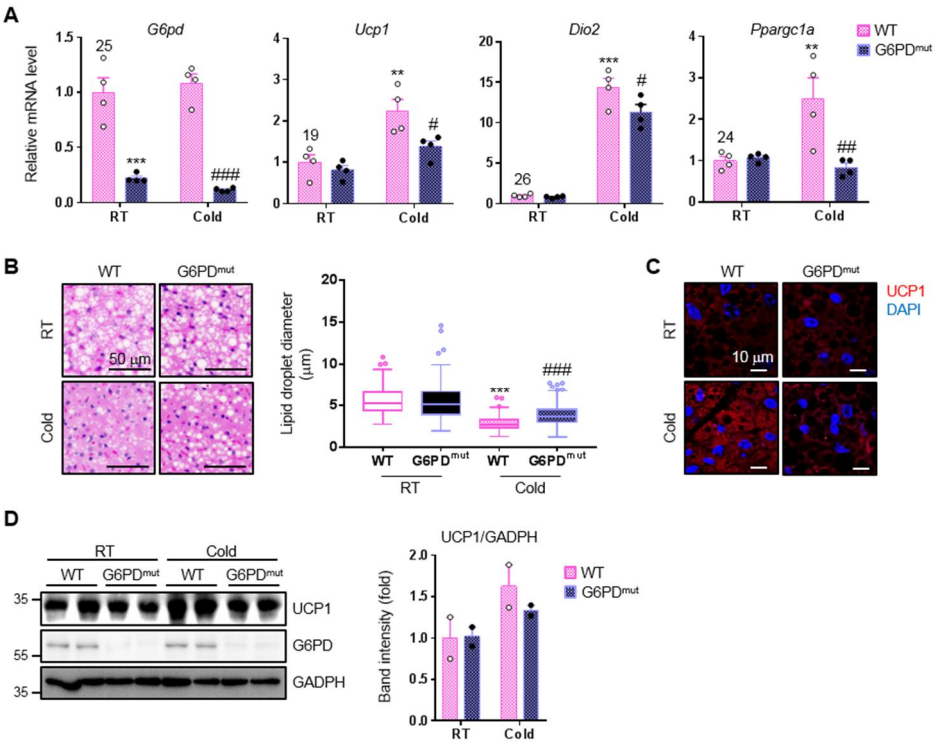

Figure 34. G6PD deficiency alleviates thermogenic action in BAT after cold stimulation. (A) Relative mRNA levels of thermogenic genes (*Ucp1*, *Dio2* and *Ppargc1a*) were measured in BAT by qRT-PCR. The data represent the mean ± SEM. $^{**}P < 0.01$, $^{***}P < 0.001$ vs. WT, RT group; $^{\#}P < 0.05$, $^{\#\#}P < 0.01$ vs. WT, cold group by two-way ANOVA followed by Tukey's post-hoc test. qRT-PCR data were normalized to the mRNA level of *36b4*. (B) Adipocyte morphology of BAT from WT and G6PD^{mut} mice exposed to RT or 12 h cold condition was assessed by hematoxylin and eosin (H&E) staining. Scale bars, 50 μm. Size of 100 lipid droplets were measured in each group. $^{***}P < 0.001$ vs. WT, RT group; $^{\#\#\#}P < 0.001$ vs. WT, cold group by one-way ANOVA followed by Tukey's post-hoc test. (C) UCP1 protein was detected in BAT from WT and G6PD^{mut} mice exposed to RT or 12 h cold condition. Immunohistochemistry analysis of the nuclei (blue) and UCP1 (red). Scale bars, 10 μm. (D) UCP1 protein levels were determined by western blot analysis in BAT from WT and G6PD^{mut} mice exposed to RT or 6 h cold condition. All data represent the mean ± SEM.

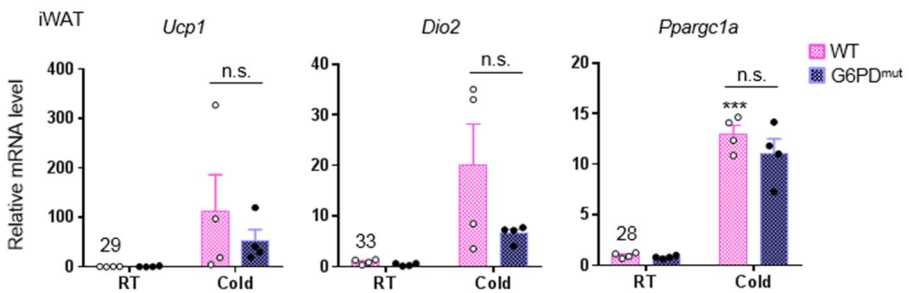

Figure 35. The expression level of thermogenic genes in iWAT is not different between WT and G6PD^{mut} mice upon cold exposure. The mRNA levels of thermogenic marker genes in iWAT of WT and G6PD^{mut} mice during 6 h cold exposure. qRT-PCR data were normalized to the mRNA level of *36b4*. Data represent the mean ± SEM. $^{**}P < 0.01$, $^{***}P < 0.001$ vs. WT, RT group by two-way ANOVA followed by Tukey's post-hoc test.

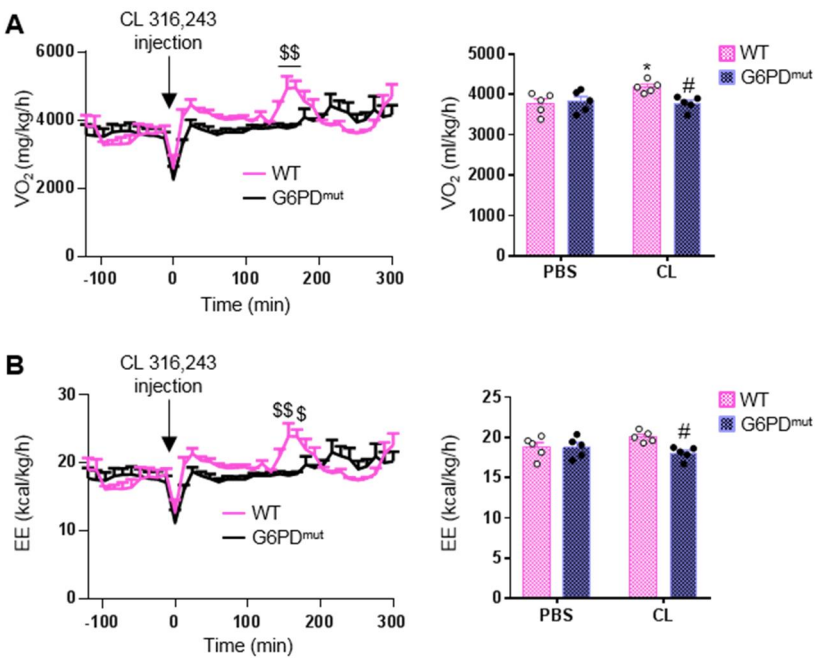

Figure 36. Systemic oxygen consumption and energy expenditure are decreased in G6PD^{mut} mice upon stimulation of β_3 adrenergic receptor. VO_2 (A), energy expenditure (EE) (B) of WT and G6PD^{mut} mice before and after CL316,243 (CL, 1 mg/kg) injection were determined. $^{\$}P < 0.05$, $^{\$\$}P < 0.01$ vs. WT group by RM-ANOVA by Sidak's post-hoc test. $^{*}P < 0.05$ vs. WT, PBS group; $^{\#}P < 0.05$ vs. WT, CL group by two-way ANOVA followed by Tukey's post-hoc test. All data represent the mean ± SEM.

than WT mice in the presence of CL316,243 (Figure 36). In WT and G6PD^{mut} mice, respiratory exchange rate (RER), locomotive activity and food intake were similarly decreased by CL316,243. However, there was no significant difference between two genotypes (Figure 37). Nevertheless, the mRNA levels of thermogenic genes were downregulated in BAT of G6PD^{mut} mice compared to WT mice with CL316,243 (Figure 38). Collectively, these results propose that G6PD in BAT might promote thermogenic action and energy expenditure upon cold or β-adrenergic stimulation.

In brown adipocytes, G6PD defect represses thermogenic gene expression and oxygen consumption upon β-adrenergic stimulation

Given that G6PD expression was upregulated in brown adipocytes (Figure 28) and G6PD deficiency repressed BAT activation upon cold or β-adrenergic stimuli (Figure 34 and 38), I asked whether G6PD defect in brown adipocytes might suppress thermogenic program in a cell-autonomous manner. Primary brown adipocytes isolated from WT and G6PD^{mut} mice were *ex vivo* cultured with isoproterenol (ISO) to stimulate β-adrenergic signaling. Compared to WT brown adipocytes, the mRNA levels of thermogenic genes were decreased in G6PD^{mut} brown adipocytes upon ISO treatment (Figure 39A). Moreover, the mRNA levels of thermogenic markers were downregulated in brown adipocytes treated with G6PD inhibitors such as DHEA and 6-AN in the presence of ISO (Figure 39B and 39C). To affirm

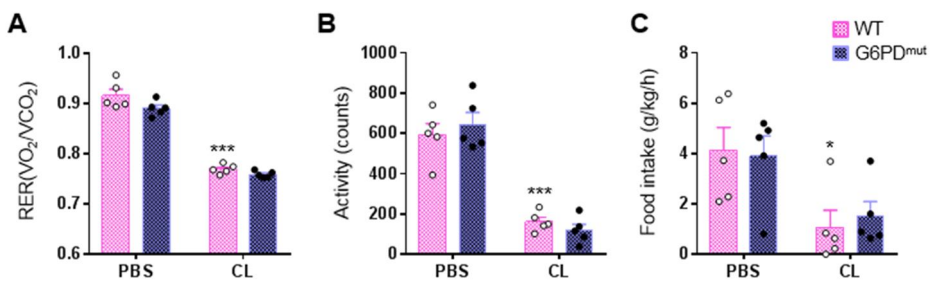

Figure 37. RER, physical activity, and food intake are not different between WT and G6PD^{mut} mice upon stimulation of β_3 adrenergic receptor. Respiratory exchange ratio (RER) (A), physical activity (B) and food intake (C) of WT and G6PD^{mut} mice before and after CL316,243 (CL, 1 mg/kg) injection were determined. $^{*}P < 0.05$, $^{***}P < 0.001$ vs. WT, PBS group by two-way ANOVA followed by Tukey's post-hoc test. All data represent the mean ± SEM.

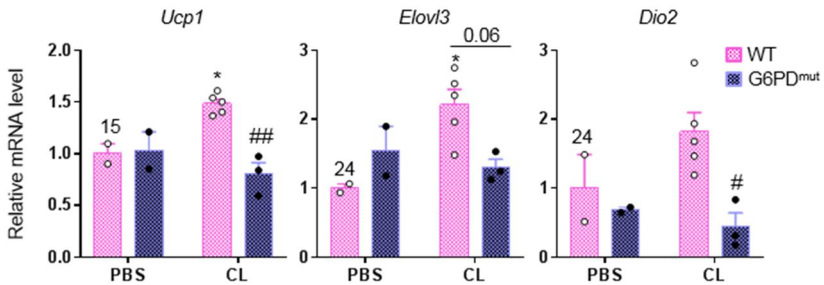

Figure 38. In BAT, G6PD^{mut} mice attenuate thermogenic program upon stimulation of β_3 adrenergic receptor. Relative mRNA levels of thermogenic genes (*Ucp1*, *Elovl3* and *Dio2*) were measured in BAT by qRT-PCR. $^{*}P < 0.05$ vs. WT, PBS group; $^{\#}P < 0.05$, $^{\#\#}P < 0.01$ vs. WT, CL group by two-way ANOVA followed by Tukey's post-hoc test. qRT-PCR data were normalized to the mRNA level of *36b4*. All data represent the mean ± SEM.

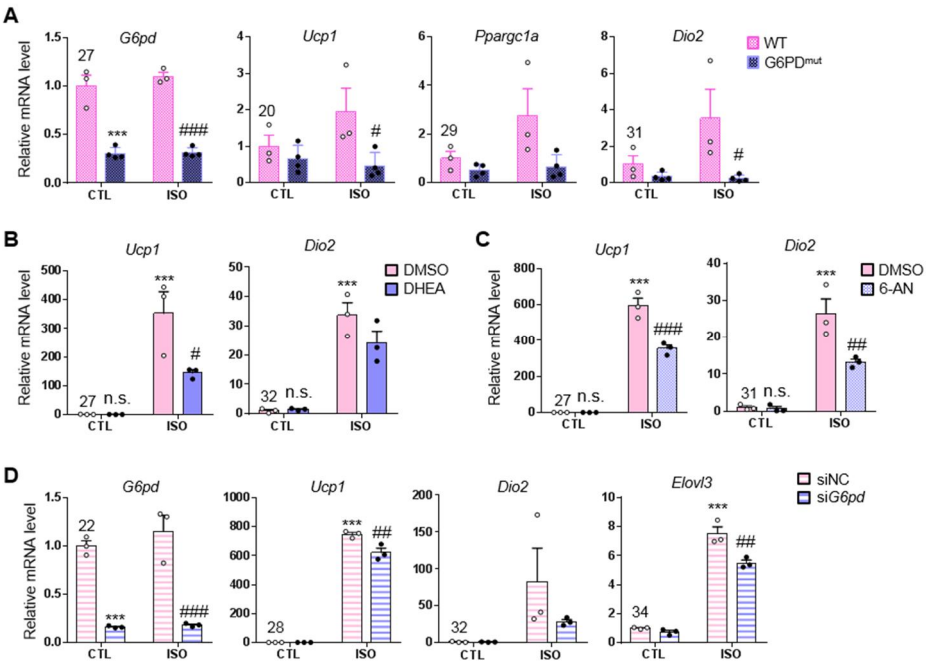

Figure 39. G6PD defect in brown adipocytes reduces thermogenic gene expression. (A) Relative mRNA levels of thermogenic genes (*Ucp1*, *Ppargc1a* and *Dio2*) were measured in primary brown adipocytes before and after 10 μM isoproterenol (ISO) treatment for 3 h. $^{***}P < 0.001$ vs. WT, CTL group; $^{\#}P < 0.05$, $^{\#\#\#}P < 0.001$ vs. WT, ISO group by two-way ANOVA followed by Tukey's post-hoc test. (B-C) Brown adipocyte cell-line (BAC) was pretreated with G6PD inhibitors, 100 μM DHEA (B) or 100 μM 6-AN (C) for 2 h. Relative mRNA levels of thermogenic genes (*Ucp1* and *Dio2*) were measured in BAC before and after 1 μM ISO treatment for 3 h. $^{***}P < 0.001$ vs. DMSO, CTL group; $^{\#}P < 0.05$, $^{\#\#}P < 0.01$, $^{\#\#\#}P < 0.001$ vs. DMSO, ISO group by two-way ANOVA followed by Tukey's post-hoc test. (D) qRT-PCR analyses of thermogenic genes in brown adipocytes transfected with siNC or si*G6pd*. All data represent the mean ± SEM. $^{**}P < 0.01$, $^{***}P < 0.001$ vs. DMSO, CTL group; $^{\#\#}P < 0.01$, $^{\#\#\#}P < 0.001$ vs. DMSO, ISO group by two-way ANOVA followed by Tukey's post-hoc test. All qRT-PCR data were normalized to the mRNA level of *cyclophilin*.

the effects of G6PD on thermogenic gene expression in brown adipocytes, I suppressed G6PD with siRNA. In brown adipocytes, suppression of G6PD via siRNA appeared to decrease the expression of thermogenic markers by ISO (Figure 39D). On the contrary, G6PD overexpression in brown adipocytes seemed to upregulate thermogenic gene expression with ISO (Figure 40). Next, to examine the effects of G6PD inhibition in brown adipocytes on mitochondrial activity or biogenesis, I analyzed oxygen consumption rates (OCRs) and mitochondrial DNA content with or without G6PD inhibitors. While G6PD inhibition in brown adipocytes did not alter OCRs in the absence of ISO (Figure 41A), G6PD inhibition reduced OCRs under basal- and FCCP-treated condition in the presence of ISO (Figure 41B). However, mitochondrial DNA/genomic DNA ratio was not significantly different by ISO treatment (Figure 41C). Together, these data suggest that G6PD in brown adipocytes would be crucial for activation of thermogenic gene expression and mitochondrial oxygen consumption upon β-adrenergic stimulation.

In BAT, oxidative stress induced by G6PD defect disrupts thermogenic function

G6PD produces NADPH, which is a critical cofactor in the regulation of cellular redox (Park et al., 2017; Spolarics, 1998). To verify whether

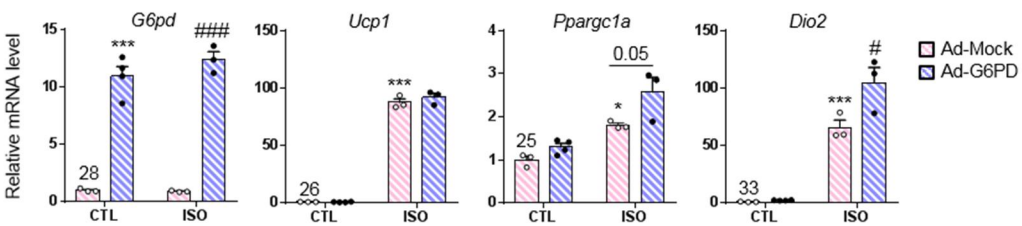

Figure 40. G6PD overexpression in brown adipocytes upregulates thermogenic gene expression. BAC infected with an adenovirus containing GFP (Ad-Mock) or G6PD (Ad-G6PD). Relative mRNA levels of thermogenic genes (*Ucp1*, *Ppargc1a* and *Dio2*) were analyzed before and after 1 μM ISO treatment for 3 h. $^{*}P < 0.05$, $^{***}P < 0.001$ vs. Ad-Mock, CTL group; $^{\#}P < 0.05$, $^{\#\#\#}P < 0.001$ vs. Ad-Mock, ISO group by two-way ANOVA followed by Tukey's post-hoc test. All data represent the mean ± SEM. qRT-PCR data were normalized to the mRNA level of *cyclophilin*.

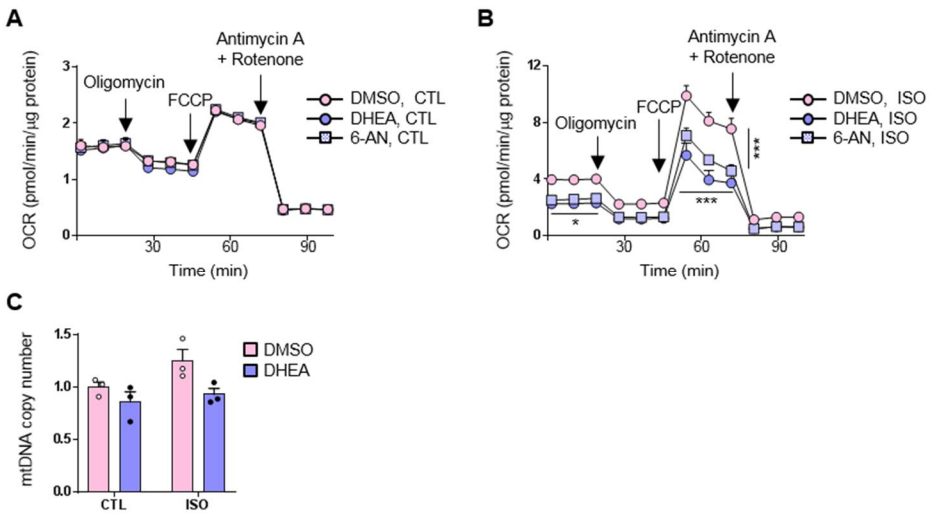

Figure 41. G6PD defect in brown adipocytes reduces mitochondrial oxygen consumption after β-adrenergic stimulation. (A-B) Oxygen consumption rate (OCR) was assessed without (A) or with 1 μM ISO (B) in BAC pretreated G6PD inhibitors. $^{*}P < 0.05$, $^{***}P < 0.001$ vs. DMSO, ISO group by RM-ANOVA followed by Tukey's post-hoc test. (C) Mitochondrial DNA (mtDNA) contents (mtDNA/nuclear DNA ratio) in brown adipocytes upon G6PD inhibition followed by ISO treatment. All data represent the mean ± standard error of the mean (SEM).

decreased thermogenic programing in brown adipocytes by G6PD defect might be associated with ROS, the level of cellular ROS was determined. As shown in Figure 42A, the basal level of cellular ROS was elevated by G6PD inhibitor, DHEA. Stimulation with ISO further augmented cellular ROS level in brown adipocytes treated with DHEA. I also found that cellular ROS accumulation was higher in primary brown adipocytes from $G6PD^{mut}$ mice under either RT or cold condition, despite no difference in eWAT between two genotypes (Figure 42B and 42C). In BAT of $G6PD^{mut}$ mice, cellular ROS level was further elevated compared with WT mice upon CL316,243 (Figure 42D). Nonetheless, the levels of mitochondrial superoxide in BAT and brown adipocytes from two genotypes were not different under either RT or cold (Figure 43A and 43B). Also, G6PD deficiency did not affect the expression the levels of NADPH oxidase subunits ($p47^{phox}$, $p67^{phox}$ and *Nox2*) and antioxidative genes (*Sod2*, *Catalase* and *Gpx1*) in BAT (Figure 44). The fact that most G6PD is localized in cytosol led me to investigate whether G6PD might regulate cytosolic ROS level rather than mitochondrial ROS level in brown adipocytes upon β-adrenergic stimulation. To measure the cytosolic ROS level in brown adipocytes, I used engineered ascorbate peroxidase (APEX)-generated biotin labeling system. Subcellular compartment-targeting APEX produces biotin-phenoxyl radicals in the presence of hydrogen peroxide and then the radicals biotinylate nearby proteins (Lee et al., 2016). For quantifying cytosolic ROS or mitochondrial ROS levels,

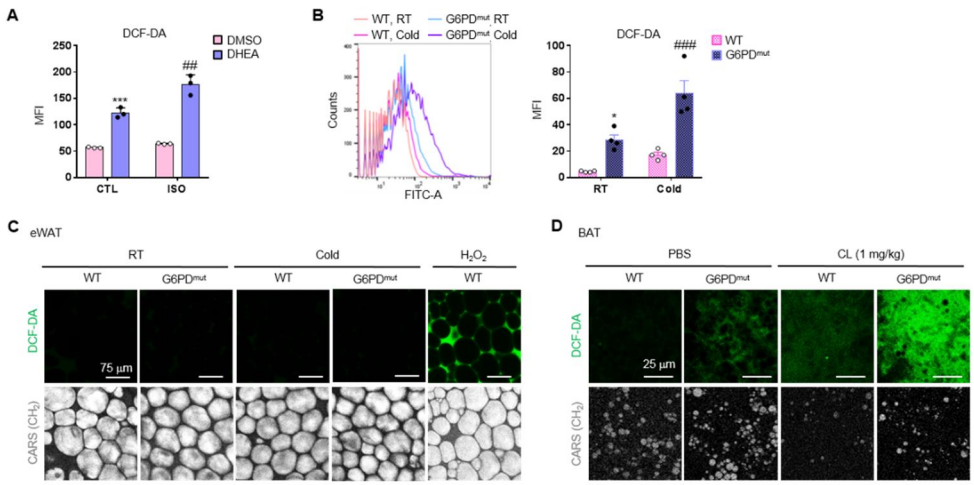

Figure 42. G6PD defect in brown adipocytes induces cellular ROS level. (A) Cellular ROS accumulation was measured in BAC by flow cytometric analysis. After treatment with DMSO or DHEA, BAC were treated with 1 μM ISO for 3 h. The cells were then incubated with the redox-sensitive fluorescent dye DCFDA for 30 min. $^{***}P < 0.001$ vs. DMSO, CTL group; $^{\#\#}P < 0.01$ vs. DMSO, ISO group by two-way ANOVA followed by Tukey's post-hoc test. (B) Using flow cytometric analysis, cellular ROS level was detected in primary brown adipocytes from WT and G6PD^{mut} mice exposed to RT or 3 h cold condition. $^{*}P < 0.05$ vs. WT, RT group; $^{\#\#\#}P < 0.001$ vs. WT, Cold group by two-way ANOVA followed by Tukey's post-hoc test. All data represent the mean ± SEM. (C) Cellular ROS level in eWAT from WT and G6PD^{mut} mice upon cold exposure as measured DCF-DA staining. Scale bars, 75 μm. (D) Cellular ROS level in BAT from WT and G6PD^{mut} mice before and after 4 h CL316,243 (CL, 1 mg/kg) injection detected by whole-mount immunofluorescence analysis. Scale bars, 25 μm.

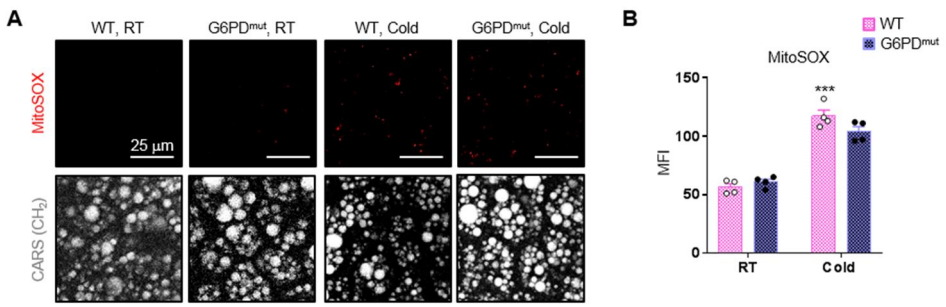

Figure 43. G6PD defect does not change in mitochondrial superoxide levels in brown adipocytes. (A) Using whole-mount immunofluorescence analysis, mitochondrial superoxide level in BAT from WT and G6PD^{mut} mice exposed to RT or 3 h cold condition was detected by MitoSOX staining. Scale bars, 25 μm. Data represent the mean ± SEM. (B) Mitochondrial superoxide level was measured in primary brown adipocytes from WT and G6PD^{mut} mice exposed to RT or 3 h cold condition by flow cytometric analysis. $^{***}P < 0.001$ vs. WT, RT group by two-way ANOVA followed by Tukey's post-hoc test.

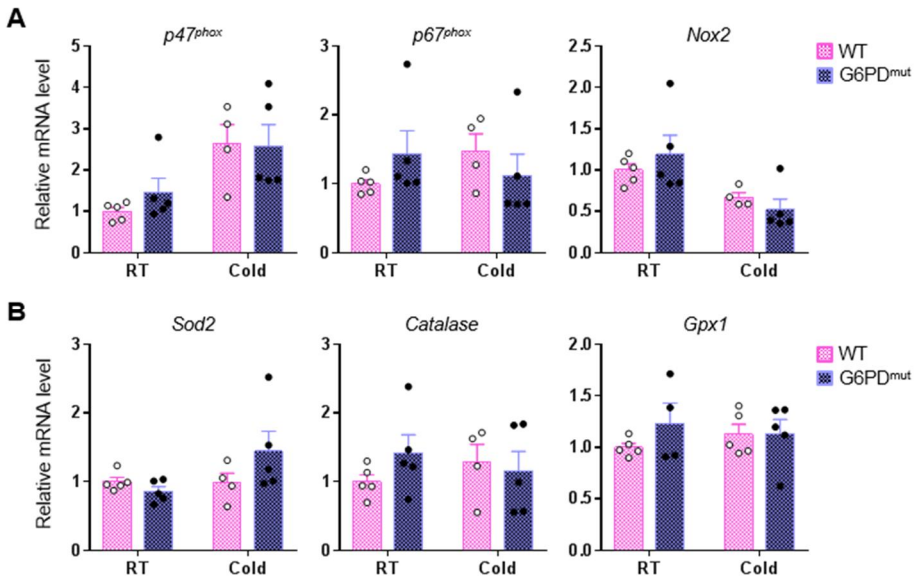

Figure 44. Oxidative gene expressions in BAT are not different between WT and G6PD^{mut} mice. (A-B) qRT-PCR analyses of NADPH oxidase subunits (A) and anti-oxidative genes (B) in BAT of WT and G6PD^{mut} mice after 6 h cold exposure. qRT-PCR data were normalized to the mRNA level of *36b4*. All data represent the mean ± SEM. $^{*}P < 0.05$ vs. WT, RT group by two-way ANOVA followed by Tukey's post-hoc test.

brown adipocytes were transfected with NES-APEX (cytosol) or Matrix-APEX (mitochondrial matrix) constructs and treated with vehicle or DHEA in the absence or presence ISO. As shown in Figure 45, G6PD inhibition in brown adipocytes accelerated cytosolic ROS accumulation, whereas it did not affect mitochondrial ROS level after β-adrenergic stimulation. These results propose that G6PD would modulate cytosolic ROS in brown adipocytes.

To investigate whether impaired thermogenic regulation in G6PD-deficient brown adipocytes might be attributable to oxidative stress, brown adipocytes were treated with antioxidant N-acetyl cysteine (NAC). NAC decreased cellular ROS level in brown adipocytes (Figure 46A). In DHEA-treated brown adipocytes, NAC increased OCR and thermogenic gene expression in the presence of ISO (Figure 46B and 46C). Furthermore, to verify whether accumulated cellular ROS could be responsible for BAT inactivation in $G6PD^{mut}$ mice, $G6PD^{mut}$ mice were intraperitoneally administered with NAC (100 mg/kg body weight), followed by CL316,243 injection. Cellular ROS levels were decreased in NAC-treated $G6PD^{mut}$ mice compared to PBS-treated $G6PD^{mut}$ mice (Figure 47A). In BAT of $G6PD^{mut}$ mice, NAC treatment stimulated the expression of thermogenic genes such as UCP1, PPARGC1A, and CIDEA and promoted small lipid droplet formation (Figure 47B and 47C). Furthermore, NAC in $G6PD^{mut}$ mice elevated UCP1 protein in BAT (Figure 47D). Together, these data indicate that oxidative stress mediated by G6PD defect would exacerbate thermogenesis in brown

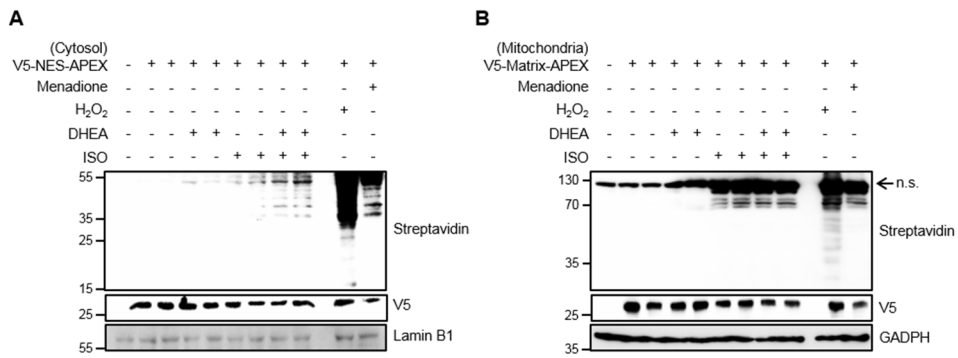

Figure 45. G6PD defect increases cytosolic ROS level in brown adipocytes. (A-B) The level of protein biotinylation mediated by APEX were analyzed by western blot analysis. After transiently transfected with NES-APEX (A) or mitochondria matrix-APEX (B), BAC were treated with DHEA, followed by ISO treatment for 3 h.

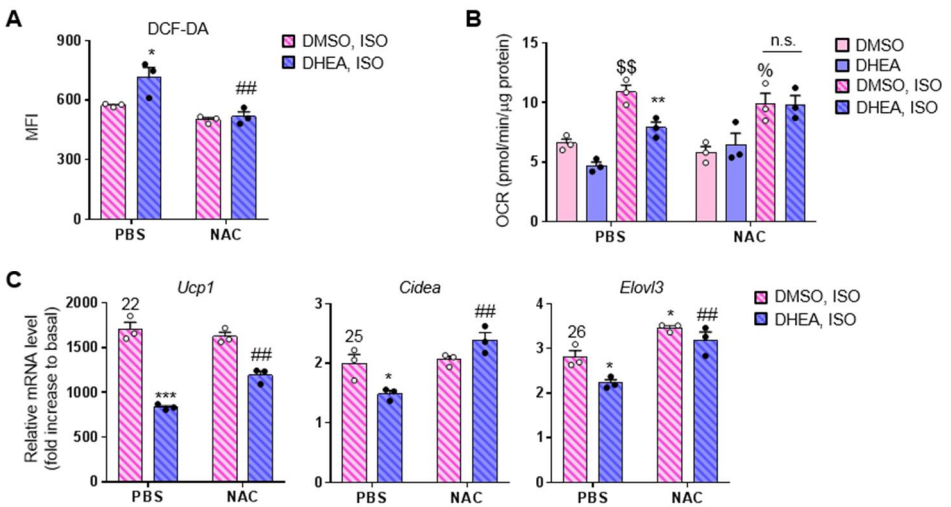

Figure 46. Antioxidant restores thermogenic function impaired by G6PD defect in brown adipocytes. (A-C) BAC was pretreated with 100 μM DHEA and 10 mM N-acetyl cysteine (NAC) for 2 h, followed by 1 μM ISO treatment for 3 h. Cellular ROS level (A), OCR (B) and relative mRNA levels of thermogenic genes (*Ucp1*, *Cidea* and *Elovel3*) (C) were determined. $^{*}P < 0.05$, $^{**}P < 0.001$, $^{***}P < 0.001$ vs. DMSO, ISO, PBS group; $^{\#\#}P < 0.01$ vs. DMSO, ISO, NAC group; $^{\$\$}P < 0.01$ vs. DMSO, PBS group; $^{\%}P < 0.05$ vs. DMSO, NAC group by two-way ANOVA followed by Tukey's post-hoc test. All data represent the mean ± SEM. qRT-PCR data were normalized to the mRNA level of *cyclophilin.*

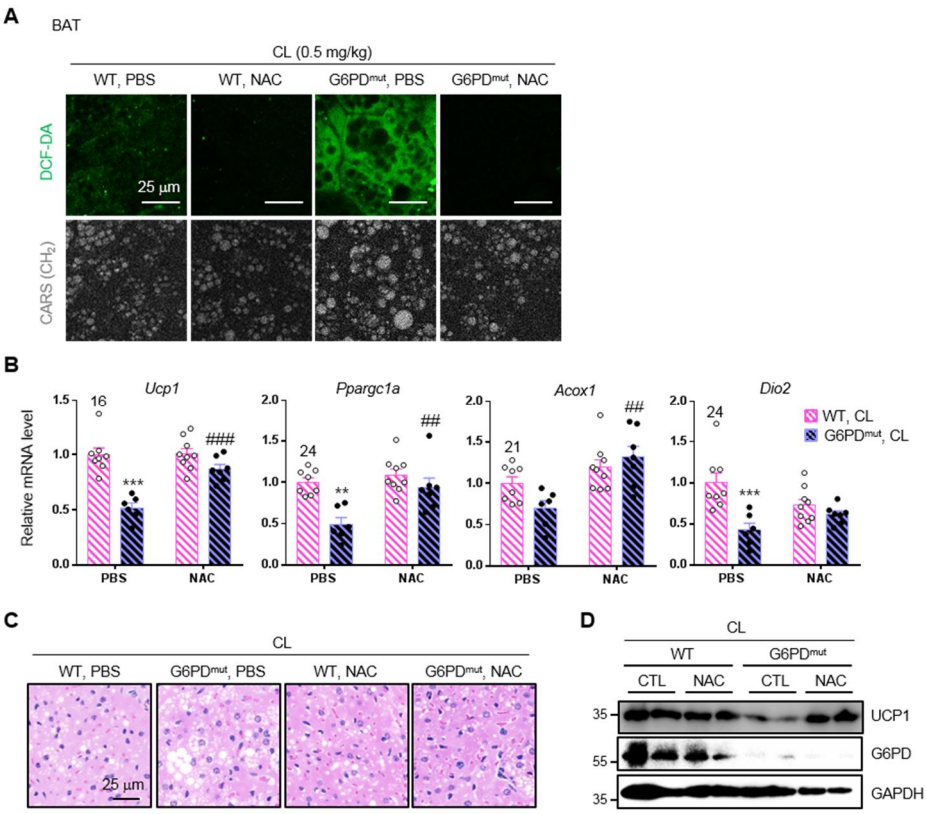

Figure 47. Antioxidant restores thermogenic function in BAT from G6PD^{mut} mice. (A-D) NAC (100 mg/kg) was intraperitoneally (i.p.) injected to WT or G6PD^{mut} mice. After 10 min, CL316,243 (0.5 mg/kg) was i.p. administered. Cellular ROS level (A), relative mRNA levels of thermogenic genes (*Ucp1*, *Ppargc1a*, *Acox1*, and *Dio2*) (B) and adipocyte morphology (C) in BAT from WT and G6PD^{mut} mice was assessed. Scale bars, 25 μm. $^{**}P <$ 0.01, $^{***}P < 0.001$ vs. WT, CL, PBS group; $^{\#\#}P < 0.01$, $^{\#\#\#}P < 0.001$ vs. G6PD^{mut}, CL, PBS group by two-way ANOVA followed by Tukey's post-hoc test. (D) UCP1 protein levels were assessed in BAT from WT and G6PD^{mut} mice treated with NAC after CL316,243 administration. All data represent the mean ± SEM. All qRT-PCR data were normalized to the mRNA level of *cyclophilin.*

adipocytes.

In G6PD-deficienct brown adipocytes, ERK activation suppresses the expression of thermogenic genes.

It has been demonstrated that oxidative stress potentiates the signaling cascades of mitogen-activated protein kinases (MAPKs) including ERK, p38 MAPK, and JNK to regulate gene expression (Torres and Forman, 2003; Yang et al., 2003). To decipher the underlying mechanisms by which G6PD-deficient brown adipocytes would decrease thermogenic program, I have focused on MAPK signaling upon cold. As indicated in Figures 48A and 48B, phosphorylation of ERK, not p38 MAPK and JNK, was enhanced in BAT of $G6PD^{mut}$ mice upon cold or CL316,243. In brown adipocytes, suppression of G6PD with DHEA upregulated the level of ERK phosphorylation in the presence of ISO and such increase was downregulated by NAC (Figure 49A and 49B). Similarly, inhibitory effects of NAC on ERK activation were observed in BAT of $G6PD^{mut}$ mice (Figure 49C). To clarify the involvement of ERK in decreased thermogenic program by G6PD defect, G6PD-deficient brown adipocytes were treated with an ERK inhibitor, PD98059. ERK inhibition in DHEA-treated brown adipocytes significantly upregulated thermogenic gene expression in the presence of ISO (Figure 50). Next, to investigate whether ERK activation would be responsible for impaired thermogenic activity in $G6PD^{mut}$ mice, mice were treated with

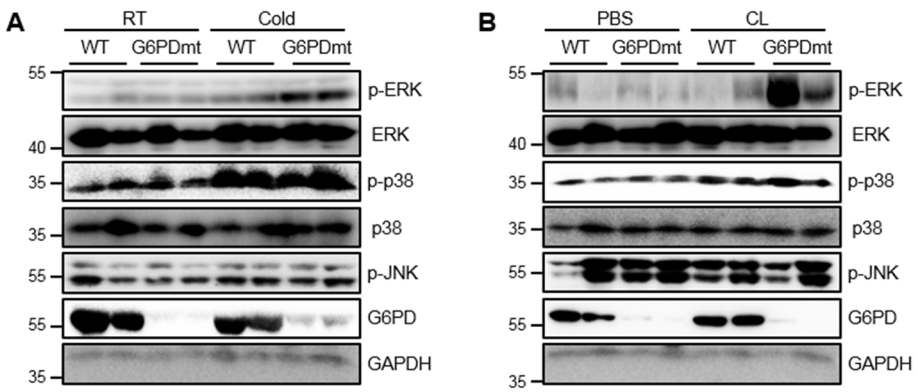

Figure 48. G6PD^{mut} mice show increased ERK activation in BAT after cold exposure or β-adrenergic stimulation. (A) Phosphorylation of MAPKs, i.e., p38 MAPK (T180/Y182), ERK (T202/Y204), and JNK (T183/Y185) was measured in BAT from WT or G6PD^{mut} mice upon 6 h cold exposure. (B) MAPK activation in BAT from WT and G6PD^{mut} mice after CL316,243 (1 mg/kg) injection.

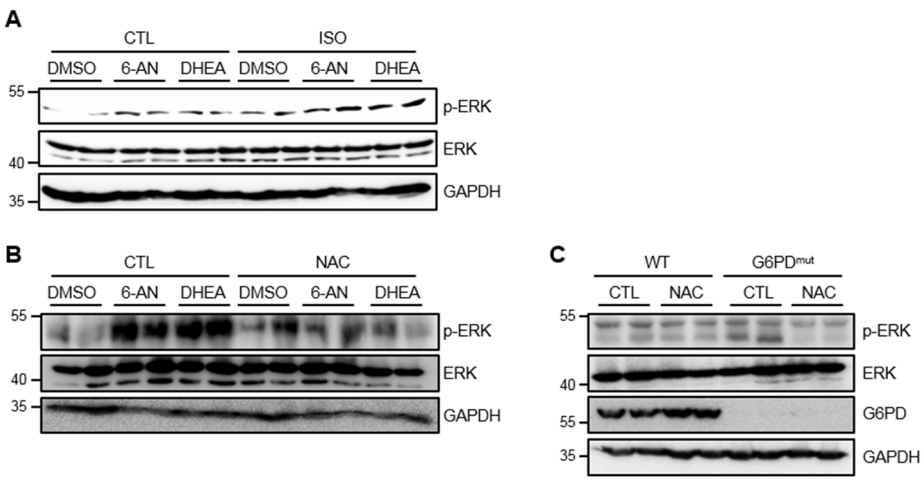

Figure 49. G6PD defect induces ROS-induced ERK activation in brown adipocytes. (A) ERK phosphorylation in brown adipocytes upon G6PD inhibition followed by ISO treatment. (B) ERK phosphorylation in G6PD-inhibited brown adipocytes upon NAC treatment in the presence of ISO. (C) NAC was administrated to WT and G6PD^{mut} mice and then CL316,243 was injected. ERK phosphorylation level was determined in BATs.

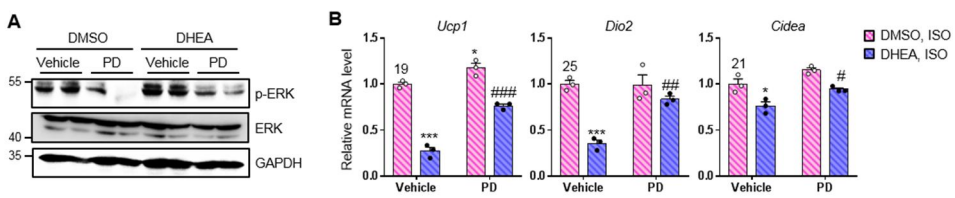

Figure 50. ERK activation by G6PD defect inhibits thermogenic gene expression after β-adrenergic stimulation. (A) BAC was pretreated with G6PD inhibitors (100 μM) and 50 μM PD98059 for 2 h, followed by 1 μM ISO treatment for 3 h. The level of ERK phosphorylation was assessed (B) qRT-PCR analyses of thermogenic genes. All data represent the mean ± SEM. All qRT-PCR data were normalized to the mRNA level of *cyclophilin.*

PD98059 (10 mg/kg body weight), followed by cold exposure. PD98059 administration not only inhibited ERK activation in BAT (Figure 51A), but also elevated body temperature in G6PD^{mut} mice during cold exposure (Figure 51B and 51C). In BAT of G6PD^{mut} mice, ERK suppression with PD98059 stimulated small lipid droplet formation and expression of thermogenic marker genes (Figure 51D and 51E). These data indicate that ERK in brown adipocytes would mediate the deleterious effects of G6PD defect on thermogenic program.

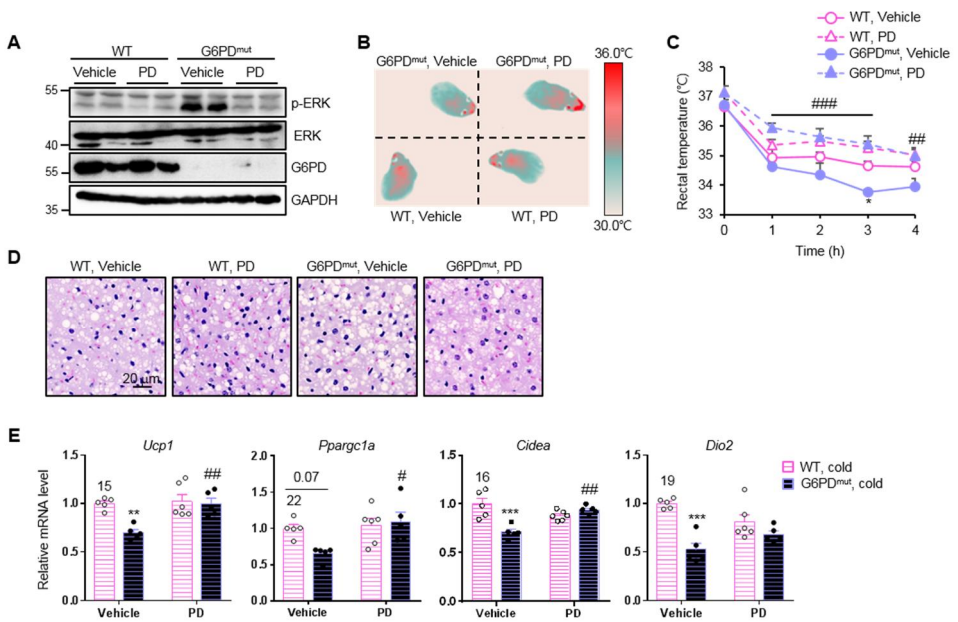

Figure 51. ERK activation represses thermogenic function in BAT of G6PD^{mut} mice. PD98059 (10 mg/kg) was i.p. injected to WT or G6PDmt mice. After 30 min, mice were exposed to cold condition for 4 h. (A) The level of ERK phosphorylation in BAT of G6PD^{mut} mice upon PD98059 treatment. (B-E) Surface body temperature (B), rectal temperature (C), brown adipocyte morphology (D) and thermogenic gene profile in BAT (E) were assessed. Scale bars, 20 μm. $^{**}P < 0.01$, $^{***}P < 0.001$ vs. WT, cold, Veh group; $^{\#}P < 0.05$, $^{\#\#}P < 0.01$, $^{\#\#\#}P < 0.001$ vs. G6PD^{mut}, cold, Veh group by two-way ANOVA followed by Tukey's post-hoc test. All data represent the mean ± SEM. qRT-PCR data were normalized to the mRNA level of *cyclophilin.*

5. Discussion

It has been suggested that cellular ROS is closely associated with thermogenic activity in brown adipocytes (Chouchani et al., 2016; Cui et al., 2019; Lee et al., 2020; Mills et al., 2018; Ro et al., 2014; Shimizu et al., 2014). In BAT, increased mitochondrial ROS contributes to thermogenesis (Chouchani et al., 2016; Mills et al., 2018; Ro et al., 2014), whereas age- or obesity-induced oxidative stress impairs BAT function (Cui et al., 2019; Lee et al., 2020; Shimizu et al., 2014). Nevertheless, it remains largely unknown by which cellular ROS in brown adipocytes would be maintained without oxidative stress. In this study, several lines of evidence supports the idea that G6PD in brown adipocytes is critical for thermogenic function by restricting cytosolic oxidative stress during cold exposure. First, the level of cytosolic ROS was boosted in brown adipocytes of $G6PD^{mut}$ mice and was further augmented after cold or β-adrenergic stimulation. Second, G6PD defect downregulated the expression of thermogenic genes in brown adipocytes upon cold or β-adrenergic stimulation. Third, antioxidant treatment in G6PD-inhibited brown adipocytes upregulated thermogenic gene expression and OCRs, accompanied with reduced cellular ROS level. Moreover, I observed that antioxidant administration promoted mRNA levels of thermogenic genes and small lipid droplet formation in BAT of $G6PD^{mut}$ mice.

It has been demonstrated that G6PD in WAT acts as a pro-oxidative

enzyme by generating NADPH, which supports NADPH oxidase-mediated ROS production (Ham et al., 2016; Park et al., 2006). In white adipocytes, G6PD overexpression stimulates cellular ROS accumulation and promotes oxidative stress-induced inflammatory responses (Park et al., 2006). Moreover, G6PD defect attenuates chronic inflammation and insulin resistance in obese WAT upon HFD (Ham et al., 2016). However, it is well known that NADPH is a key electron donor for anti-oxidative enzymes such as glutathione reductase, leading to ameliorate oxidative stress (Jain et al., 2003; Leopold et al., 2007; Xu et al., 2010). Thus, it is plausible that the roles of G6PD in the regulation of ROS homeostasis might depend on different intracellular properties. In this study, I discovered that physiological roles of G6PD in the regulation of cellular ROS level would differ in white adipocytes and brown adipocytes. Compared to white adipocytes, brown adipocytes contain more mitochondria which could make them more susceptible to cellular ROS accumulation. Here, bioinformatics analyses suggest that redox control system and anti-oxidative pathway might alleviate excessive ROS accumulation in brown adipocytes compared to white adipocytes during evolution. While the expression levels of electron donor-producing enzymes and anti-oxidative enzymes were upregulated in BAT compared to WAT, the mRNA levels of NADPH oxidase subunits were higher in WAT than BAT (Figure 26). Also, G6PD overexpression in brown adipocytes did not regulate the expression levels of pro-oxidative enzymes which were downstream

targets of G6PD in white adipocytes and reduced cellular ROS level (Figure 31). In addition, G6PD defect in brown adipocytes significantly augmented cytosolic ROS level which could increase oxidative damage (Figure 45). Thus, current findings suggest that G6PD plays pro-oxidative roles in white adipocytes, while G6PD has anti-oxidative functions in brown adipocytes, probably, due to distinct intracellular environments.

Cellular ROS are produced in several subcellular compartments (Tafani et al., 2016). For instance, cytosol and mitochondria are major compartments producing ROS (Hernández-García et al., 2010). In particular, cytosolic ROS are produced by NADPH oxidase and xanthine oxidase (Gorrini et al., 2013). Mitochondrial ROS are generated by electron transport chain and can diffuse into cytosol through channels such as voltage-dependent anion channel or aquaporin (Chauvigné et al., 2015; Han et al., 2003). Recently, it has been reported that subcellular organelle-specific spatial regulation of ROS is crucial for physiological processes such as lifespan and endothelial function (Aldosari et al., 2018; Schaar et al., 2015; Shafique et al., 2017). For example, cytosolic ROS and mitochondrial ROS play opposite roles in the aspects of longevity (Schaar et al., 2015). In brown adipocytes, mitoSOX level was chronically elevated by β-adrenergic stimulation, whereas the extent of total cellular ROS was acutely (10 min) increased upon β-adrenergic stimulation (Figure 52). These observations imply that brown adipocytes might have spatial regulatory mechanisms of

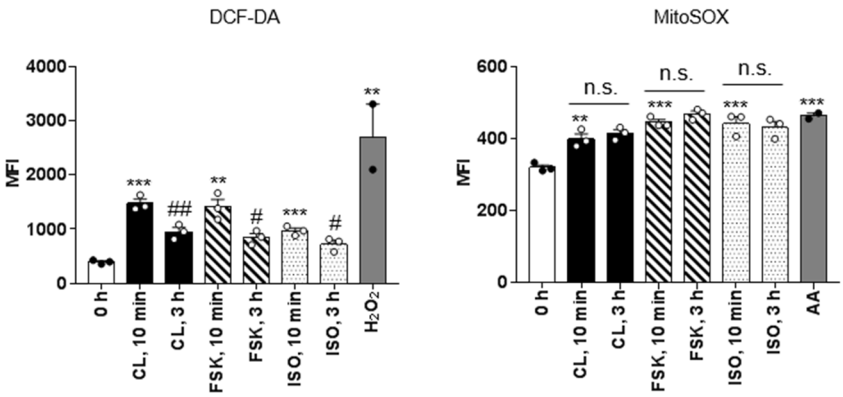

Figure 52. Cellular ROS and mitochondrial ROS level upon duration of β-adrenergic stimulation. Cellular ROS and mitochondrial superoxide level in BAC upon CL316,243 (2.5 μM), forskolin (10 μM), and ISO (5 μM) treatment as measured DCF-DA and mitoSOX staining. All data represent the mean ± SEM. $^{**}P < 0.01$, $^{***}P < 0.001$ vs. 0 h group; $^{\#}P < 0.05$, $^{\#\#}P < 0.01$ vs. each stimuli, 10 min group by one-way ANOVA followed by Tukey's post-hoc test

cellular ROS homeostasis. It led me to investigate whether G6PD would regulate thermogenic function in brown adipocytes via spatial regulation of cellular ROS. Given that G6PD produces cytosolic NADPH, I speculated that G6PD defect in brown adipocytes might affect cytosolic ROS level rather than mitochondrial ROS level. Although DCF-DA intensity was enhanced in G6PD defective brown adipocytes (Figure 42), mitoSOX intensity was indifferent in brown adipocytes of $G6PD^{mut}$ mice when compared with WT littermates (Figure 43). Using subcellular compartment-specific APEX systems, I found that G6PD inhibition could alter cytosolic ROS rather than mitochondrial ROS in brown adipocytes upon ISO (Figure 45). These data suggest that G6PD would preferentially decrease cytosolic ROS in brown adipocytes, thereby preventing oxidative damages and, probably supporting thermogenic function in brown adipocytes. To date, it remains unclear whether increased cytosolic ROS level due to G6PD defect would be primarily produced in cytosol or released from mitochondria. Thus, it would be important to investigate the roles of subcellular compartment-specific ROS generation for thermogenic regulation in brown adipocytes.

MAPK signaling pathways regulate gene expression through phosphorylation of several transcriptional regulators (Whitmarsh, 2007). Pro-oxidative stimulation activates MAPKs, whereas suppression of cellular ROS level with antioxidants attenuates MAPK signaling cascades (Yue et al., 2019; Zhang et al., 1998). Thus, it appears that MAPKs are one of the key mediators

via ROS for physiological or pathological processes. It has been shown that MAPKs could regulate thermogenic marker gene, UCP1 in brown adipocytes (Porras et al., 2002; Valladares et al., 2001). Although p38 MAPK is a positive regulator of UCP1 expression, ERK inhibits UCP1 expression upon TNFα treatment in brown adipocytes (Valladares et al., 2001). Meanwhile, PD98059 upregulates UCP1 expression in TNFα-treated brown adipocytes (Porras et al., 2002). In this work, I found that G6PD defect selectively activated ERK in brown adipocytes upon cold or β-adrenergic stimulation. In addition, the activation of ERK by G6PD defect was mitigated by NAC treatment. Furthermore, ERK inhibition with PD98059 elevated thermogenic marker expression in G6PD-suppressed brown adipocytes and restored body temperature of cold-exposed $G6PD^{mut}$ mice. Collectively, these data suggest that ROS-induced ERK activation by G6PD defect would mediate impaired thermogenesis in brown adipocytes (Figure 53). Nevertheless, transcription factor(s) involved in the suppression of thermogenic genes in brown adipocytes upon G6PD defect are still unclear. ERK modulates activation of several transcription factors including AP-1, c-MYC, and ELK1 (Chen et al., 1993; Marais et al., 1993; Morton et al., 2003; Sears et al., 2000). It has been reported that c-JUN in brown adipocytes binds to UCP1 promoter and suppresses UCP1 gene expression (Yubero et al., 1998). In addition, I preliminarily observed that c-MYC overexpression in brown

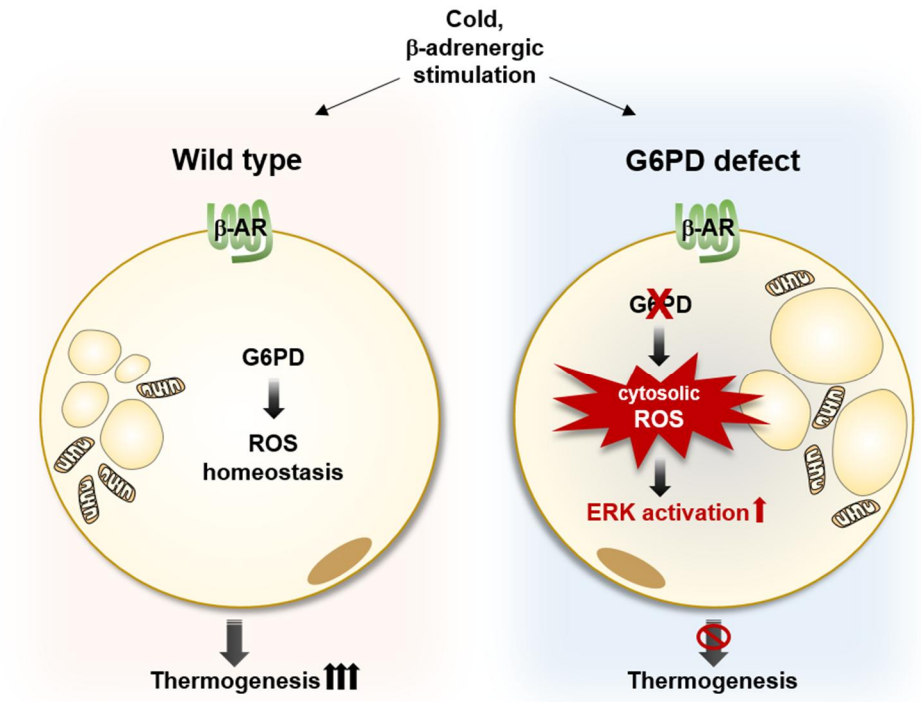

Figure 53. Proposed model of chapter two. In G6PD-deficient brown adipocytes, cytosolic ROS stimulates ERK activation, contributing to impaired cold-induced thermogenesis.

adipocytes reduced thermogenic gene expression upon β-adrenergic stimulation (data not shown). Thus, it is possible to speculate that downstream target(s) of ERK might act as a repressor to inhibit thermogenic gene expression in G6PD-defective brown adipocytes.

Metabolic roles of ERK in adipocyte biology have been well studied (Taniguchi et al., 2006). Recently, Hong et al. reported that WT mice treated with ERK inhibitor fail to activate cold-induced thermogenesis due to lack of lipid availability (Hong et al., 2018). On the contrary, this study revealed that increased ERK activation in BAT would mediate impaired thermogenesis in cold-exposed $G6PD^{mut}$ mice, while there was no significant change in BAT of WT mice upon ERK inhibition. Also, other groups have reported that ERK would have detrimental effects on the regulation of thermogenic gene expression and thermogenic adipocyte formation (Chung et al., 2017; Ye et al., 2012). Although it is unclear whether ERK activation has positive or negative roles in thermogenic function, it seems that this discrepancy might be resulted from several factors such as different animal models, animal facilities, and MEK/ERK inhibitors.

In conclusion, I identified distinct roles of G6PD in the regulation of ROS in brown adipocytes, which might be attributed to its unique properties that distinguish it from white adipocytes. In brown adipocytes, G6PD would positively contribute to thermogenic activity by preventing oxidative stress-induced ERK activation upon cold or β-adrenergic stimulation. Collectively,

these data suggest that removal of harmful cytosolic ROS by G6PD in brown adipocytes could be a key process to maintain thermal homeostasis.

CONCLUSION

Adipocytes modulate systemic energy metabolism through diverse functions including energy storage, energy expenditure, thermogenesis, hormone secretion, and immune response control. Adipocyte dysfunction is associated with various metabolic disorders. Adipocytes are largely divided into white and brown subtypes. White and brown adipocytes have distinct characteristics in terms of subcellular organelles, gene expression profiles, and lipid metabolism. Lipid metabolism in adipocytes is crucial for maintaining systemic energy homeostasis. Dysregulation of lipid metabolism in white and brown adipocytes is closely related to metabolic disorders. However, the meditators involved in lipid metabolism that regulate adipocyte functions and systemic energy homeostasis are not well understood. In this study, I have investigated the underlying mechanisms by which products of lipid metabolism such as lipid metabolites and ROS regulate adipocyte functions, eventually, affecting whole-body energy homeostasis (Figure 54). In the first chapter, I have elucidated novel roles of lipid metabolites such as prostaglandins in the regulation of adipose tissue inflammation, resulting in whole-body insulin resistance. In the second chapter, I have revealed the roles of cytosolic ROS-dependent thermogenic regulation in brown adipocytes.

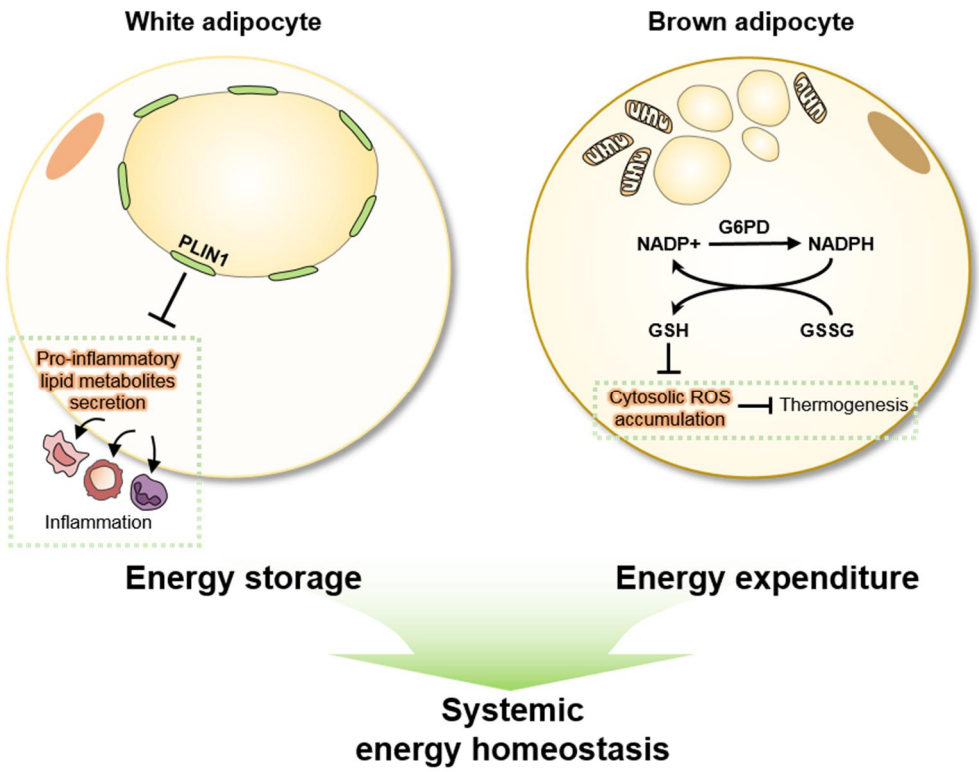

Figure 54. Conclusion. Proper regulation of lipid metabolites and cellular ROS in adipocytes is crucial for maintaining adipocyte functions which contribute to systemic energy homeostasis.

1. Lipolysis and adipose tissue inflammation

In adipocytes, lipolysis is closely associated with inflammatory responses in adipose tissue. Upon fasting or β-adrenergic stimulation, lipolysis in adipocytes is enhanced and accumulation of ATMs is increased (Kosteli et al., 2010; Schoiswohl et al., 2015). In contrast, suppression of lipolysis in ATGL-deficient adipocytes reduces ATM accumulation (Schoiswohl et al., 2015). Despite these observations, the molecular mechanisms by which lipolysis in adipocytes regulates ATMs have not been properly addressed. Here, uncontrolled lipolytic activation in PLIN1-deficient adipocytes aggravates adipose tissue inflammation, leading to systemic insulin resistance. It has been reported that increased lipolysis in adipocytes upon β-adrenergic stimuli increases metabolite production from cyclooxygenase (COX), lipoxygenases, and epoxygenases (Gartung et al., 2016). It appears that pro-inflammatory lipid metabolites might be products of futile lipolysis. Therefore, I suggest that precise regulation of lipolysis mediated by PLIN1 in adipocytes would help adipose tissue to maintain immune balance by restricting the aberrant production of pro-inflammatory lipid metabolites.

2. Lipid metabolites and adipose tissue inflammation

Several lipid metabolites are produced by adipocytes or adipose tissues during lipid metabolic processes (Cao et al., 2008; Gartung et al., 2016; Mazid et al., 2006; Yore et al., 2014). Palmitoleate (C16:1n7), a long-chain monounsaturated FA, is produced through *de novo* lipogenesis in adipose tissue (Cao et al., 2008) and downregulates pro-inflammatory gene expression in macrophages *in vitro* (Chan et al., 2015; Cimen et al., 2019; Talbot et al., 2014). In addition, palmitic acid esters of hydroxyl stearic acids (PAHSAs) synthesized by carbohydrate response element binding protein (ChREBP) in adipocytes regulate adipose tissue inflammation. While adipocyte-specific ChREBP knockout (ChREBP AKO) mice exhibit decreased PAHSA levels and increased ATMs in adipose tissue, PAHSA administration ameliorates pro-inflammatory responses in the adipose tissue of ChREBP AKO mice (Vijayakumar et al., 2017).

In addition to *de novo* lipogenesis, lipid metabolites that regulate adipose tissue inflammation can be produced during lipolysis. It has been reported that serum palmitoleate levels are reduced in adipose tissue-specific ATGL KO mice during exercise (Foryst-Ludwig et al., 2015). In this study, I have demonstrated that PLIN1 inhibits futile prostaglandin secretion to restrict pro-inflammatory responses in adipose tissue. PLIN1 deficiency in adipocytes impairs lipid storage into LDs and stimulates lipolysis, contributing to fat loss and leakage of pro-inflammatory lipid metabolites.

Pro-inflammatory gene expression and M1-type ATM accumulation are increased in adipose tissue of PLIN1 KO mice, while the abolishment of lipolysis through knockdown of key lipases attenuates the effects of PLIN1-deficient adipocytes on monocyte migration. Moreover, the increased adipose tissue inflammation is mediated by excess PGE_2 secreted from PLIN1-deficient adipocytes, as observed through lipidomic analysis and administration of a COX inhibitor. These findings indicate that certain pro-inflammatory lipid metabolites that can be produced from lipolysis in adipocytes could promote adipose tissue inflammation.

3. ROS and thermogenic function in brown adipocyte

The roles of cellular ROS in thermogenic execution of brown adipocytes are somewhat controversial. Mitochondrial ROS generated in brown adipocytes under normal physiological conditions, such as cold exposure, support thermogenesis (Chouchani et al., 2016; Mills et al., 2018; Ro et al., 2014; Schneider et al., 2016). However, paradoxically, increased mitochondrial ROS under pathological conditions, such as aging and obesity, impair thermogenic activity in brown adipocytes (Cui et al., 2019; Lee et al., 2020; Shimizu et al., 2014). These findings suggest that proper production of mitochondrial ROS would be crucial for brown adipocyte function. However, it is also necessary to remove excess ROS to prevent oxidative stress. Here, I

have shown that the anti-oxidative pathway mediated by G6PD in brown adipocytes would be required for thermogenic regulation in response to cold exposure or β-adrenergic stimulation. In brown adipocytes, anti-oxidative reactions regulated by G6PD are specific to cytosol because G6PD is main source of cytosolic NADPH (Stanton et al., IUBMB life, 2012). Given that cytosolic ROS is generated by enzymatic reactions and/or come from mitochondria by diffusion, it is not clear whether cellular ROS removed by G6PD would be originated from cytosol or mitochondria. Nevertheless, current observations suggest that brown adipocytes could regulate and scavenge cytosolic ROS to execute thermgenic programing upon cold exposure.

In conclusion, I have investigated two novel mechanisms of adipocyte biology by dysregulation of lipid metabolites in white adipocytes and cellular ROS in brown adipocytes. In white adipocytes, PLIN1 plays a pivotal role in the control of lipolysis and secretion of futile lipid metabolites, which would affect inflammatory responses of WAT. Furthermore, I elucidated that G6PD protects thermogenic programs against oxidative stress in brown adipocytes. Taken together, this work would provide important clues to understand novel regulatory mechanisms of “adipocytes” for whole-body energy homeostasis.

ACKNOWLEDGEMENTS

Chapter one in this thesis study was published in Journal of Biological Chemistry, 2018. **293**(36):13974-13988. Also, parts of conclusion in this thesis study were published in Frontiers in Immunology, 2021. **11**:598566.

REFERENCES

Aldosari, S., Awad, M., Harrington, E.O., Sellke, F.W., and Abid, M.R. (2018). Subcellular Reactive Oxygen Species (ROS) in Cardiovascular Pathophysiology. Antioxidants (Basel, Switzerland) *7*.

Ambrosio, G., Zweier, J.L., Duilio, C., Kuppusamy, P., Santoro, G., Elia, P.P., Tritto, I., Cirillo, P., Condorelli, M., Chiariello, M.*, et al.* (1993). Evidence that mitochondrial respiration is a source of potentially toxic oxygen free radicals in intact rabbit hearts subjected to ischemia and reflow. The Journal of biological chemistry *268*, 18532-18541.

Ayache, S., Panelli, M.C., Byrne, K.M., Slezak, S., Leitman, S.F., Marincola, F.M., and Stroncek, D.F. (2006). Comparison of proteomic profiles of serum, plasma, and modified media supplements used for cell culture and expansion. Journal of translational medicine *4*, 40.

Barja de Quiroga, G., López-Torres, M., Pérez-Campo, R., Abelenda, M., Paz Nava, M., and Puerta, M.L. (1991). Effect of cold acclimation on GSH, antioxidant enzymes and lipid peroxidation in brown adipose tissue. The Biochemical journal *277 (Pt 1)*, 289-292.

Batista, M.L., Jr., Henriques, F.S., Neves, R.X., Olivan, M.R., Matos-Neto, E.M., Alcantara, P.S., Maximiano, L.F., Otoch, J.P., Alves, M.J., and Seelaender, M. (2016). Cachexia-associated adipose tissue morphological rearrangement in gastrointestinal cancer patients. Journal of cachexia, sarcopenia and muscle *7*, 37-47.

Batista, M.L., Jr., Peres, S.B., McDonald, M.E., Alcantara, P.S., Olivan, M., Otoch, J.P., Farmer, S.R., and Seelaender, M. (2012). Adipose tissue inflammation and cancer cachexia: possible role of nuclear transcription factors. Cytokine *57*, 9-16.

Bensinger, S.J., and Tontonoz, P. (2008). Integration of metabolism and inflammation by lipid-activated nuclear receptors. Nature *454*, 470-477.
Bolisetty, S., and Jaimes, E.A. (2013). Mitochondria and reactive oxygen species: physiology and pathophysiology. International journal of molecular sciences *14*, 6306-6344.

Boumelhem, B.B., Assinder, S.J., Bell-Anderson, K.S., and Fraser, S.T. (2017). Flow cytometric single cell analysis reveals heterogeneity between adipose depots. Adipocyte *6*, 112-123.

Boveris, A., Oshino, N., and Chance, B. (1972). The cellular production of hydrogen peroxide. The Biochemical journal *128*, 617-630.

Brasaemle, D.L., Levin, D.M., Adler-Wailes, D.C., and Londos, C. (2000). The lipolytic stimulation of 3T3-L1 adipocytes promotes the translocation of hormone-sensitive lipase to the surfaces of lipid storage droplets. Biochim Biophys Acta *1483*, 251-262.

Cannon, B., and Nedergaard, J. (2004). Brown adipose tissue: function and physiological significance. Physiological reviews *84*, 277-359.

Cao, H., Gerhold, K., Mayers, J.R., Wiest, M.M., Watkins, S.M., and Hotamisligil, G.S. (2008). Identification of a lipokine, a lipid hormone linking adipose tissue to systemic metabolism. Cell *134*, 933-944.

Carman, G.M. (2012). Thematic minireview series on the lipid droplet, a dynamic organelle of biomedical and commercial importance. J Biol Chem *287*, 2272.

Carrière, A., Fernandez, Y., Rigoulet, M., Pénicaud, L., and Casteilla, L. (2003). Inhibition of preadipocyte proliferation by mitochondrial reactive oxygen species. FEBS letters *550*, 163-167.

Carvalho, S.D., Negrão, N., and Bianco, A.C. (1993). Hormonal regulation of malic enzyme and glucose-6-phosphate dehydrogenase in brown adipose tissue. The American journal of physiology *264*, E874-881.

Cedikova, M., Kripnerová, M., Dvorakova, J., Pitule, P., Grundmanova, M., Babuska, V., Mullerova, D., and Kuncova, J. (2016). Mitochondria in White, Brown, and Beige Adipocytes. Stem cells international *2016*, 6067349.

Chakrabarti, S.K., Cole, B.K., Wen, Y., Keller, S.R., and Nadler, J.L. (2009). 12/15-lipoxygenase products induce inflammation and impair insulin signaling in 3T3-L1 adipocytes. Obesity (Silver Spring, Md) *17*, 1657-1663.

Chan, K.L., Pillon, N.J., Sivaloganathan, D.M., Costford, S.R., Liu, Z., Théret, M., Chazaud, B., and Klip, A. (2015). Palmitoleate Reverses High Fat-induced Proinflammatory Macrophage Polarization via AMP-activated Protein Kinase (AMPK). The Journal of biological chemistry *290*, 16979-16988.

Chaurasia, B., and Summers, S.A. (2015). Ceramides - Lipotoxic Inducers of Metabolic Disorders. Trends in endocrinology and metabolism: TEM *26*,

538-550.

Chauvigné, F., Boj, M., Finn, R.N., and Cerdà, J. (2015). Mitochondrial aquaporin-8-mediated hydrogen peroxide transport is essential for teleost spermatozoon motility. Scientific reports *5*, 7789.

Chen, R.H., Abate, C., and Blenis, J. (1993). Phosphorylation of the c-Fos transrepression domain by mitogen-activated protein kinase and 90-kDa ribosomal S6 kinase. Proceedings of the National Academy of Sciences of the United States of America *90*, 10952-10956.

Choe, S.S., Shin, K.C., Ka, S., Lee, Y.K., Chun, J.S., and Kim, J.B. (2014). Macrophage HIF-2alpha Ameliorates Adipose Tissue Inflammation and Insulin Resistance in Obesity. Diabetes *63*, 3359-3371.

Chouchani, E.T., Kazak, L., Jedrychowski, M.P., Lu, G.Z., Erickson, B.K., Szpyt, J., Pierce, K.A., Laznik-Bogoslavski, D., Vetrivelan, R., Clish, C.B., *et al.* (2016). Mitochondrial ROS regulate thermogenic energy expenditure and sulfenylation of UCP1. Nature *532*, 112-116.

Chung, K.J., Chatzigeorgiou, A., Economopoulou, M., Garcia-Martin, R., Alexaki, V.I., Mitroulis, I., Nati, M., Gebler, J., Ziemssen, T., Goelz, S.E., *et al.* (2017). A self-sustained loop of inflammation-driven inhibition of beige adipogenesis in obesity. Nature immunology *18*, 654-664.

Cimen, I., Yildirim, Z., Dogan, A.E., Yildirim, A.D., Tufanli, O., Onat, U.I., Nguyen, U., Watkins, S.M., Weber, C., and Erbay, E. (2019). Double bond configuration of palmitoleate is critical for atheroprotection. Molecular metabolism *28*, 58-72.

Cinti, S. (2009). Transdifferentiation properties of adipocytes in the adipose organ. American journal of physiology Endocrinology and metabolism *297*, E977-986.

Cui, X., Xiao, W., You, L., Zhang, F., Cao, X., Feng, J., Shen, D., Li, Y., Wang, Y., Ji, C., *et al.* (2019). Age-induced oxidative stress impairs adipogenesis and thermogenesis in brown fat. The FEBS journal *286*, 2753-2768.

Cypess, A.M., Lehman, S., Williams, G., Tal, I., Rodman, D., Goldfine, A.B., Kuo, F.C., Palmer, E.L., Tseng, Y.H., Doria, A., *et al.* (2009). Identification and importance of brown adipose tissue in adult humans. The New England journal of medicine *360*, 1509-1517.

Das, S.K., Eder, S., Schauer, S., Diwoky, C., Temmel, H., Guertl, B., Gorkiewicz, G., Tamilarasan, K.P., Kumari, P., Trauner, M., *et al.* (2011). Adipose triglyceride lipase contributes to cancer-associated cachexia. Science (New York, NY) *333*, 233-238.

De Lorenzo, A., Del Gobbo, V., Premrov, M.G., Bigioni, M., Galvano, F., and Di Renzo, L. (2007). Normal-weight obese syndrome: early inflammation? The American journal of clinical nutrition *85*, 40-45.

de Matos-Neto, E.M., Lima, J.D., de Pereira, W.O., Figueredo, R.G., Riccardi, D.M., Radloff, K., das Neves, R.X., Camargo, R.G., Maximiano, L.F., Tokeshi, F., *et al.* (2015). Systemic Inflammation in Cachexia - Is Tumor Cytokine Expression Profile the Culprit? Frontiers in immunology *6*, 629.

Donath, M.Y., and Shoelson, S.E. (2011). Type 2 diabetes as an inflammatory disease. Nature reviews Immunology *11*, 98-107.

Endemann, G., Stanton, L.W., Madden, K.S., Bryant, C.M., White, R.T., and Protter, A.A. (1993). CD36 is a receptor for oxidized low density lipoprotein. The Journal of biological chemistry *268*, 11811-11816.

Faveeuw, C., Gosset, P., Bureau, F., Angeli, V., Hirai, H., Maruyama, T., Narumiya, S., Capron, M., and Trottein, F. (2003). Prostaglandin D2 inhibits the production of interleukin-12 in murine dendritic cells through multiple signaling pathways. European journal of immunology *33*, 889-898.

Feng, B., Jiao, P., Nie, Y., Kim, T., Jun, D., van Rooijen, N., Yang, Z., and Xu, H. (2011). Clodronate liposomes improve metabolic profile and reduce visceral adipose macrophage content in diet-induced obese mice. PLoS One *6*, e24358.

Finkel, T., and Holbrook, N.J. (2000). Oxidants, oxidative stress and the biology of ageing. Nature *408*, 239-247.

Folch, J., Lees, M., and Sloane Stanley, G.H. (1957). A simple method for the isolation and purification of total lipides from animal tissues. J Biol Chem *226*, 497-509.

Foryst-Ludwig, A., Kreissl, M.C., Benz, V., Brix, S., Smeir, E., Ban, Z., Januszewicz, E., Salatzki, J., Grune, J., Schwanstecher, A.K., *et al.* (2015). Adipose Tissue Lipolysis Promotes Exercise-induced Cardiac Hypertrophy Involving the Lipokine C16:1n7-Palmitoleate. The Journal of biological chemistry *290*, 23603-23615.

Fujisaka, S., Usui, I., Bukhari, A., Ikutani, M., Oya, T., Kanatani, Y., Tsuneyama, K., Nagai, Y., Takatsu, K., Urakaze, M., *et al.* (2009). Regulatory mechanisms for adipose tissue M1 and M2 macrophages in diet-induced obese mice. Diabetes *58*, 2574-2582.

Funk, C.D. (2001). Prostaglandins and leukotrienes: advances in eicosanoid biology. Science (New York, NY) *294*, 1871-1875.

Furukawa, S., Fujita, T., Shimabukuro, M., Iwaki, M., Yamada, Y., Nakajima, Y., Nakayama, O., Makishima, M., Matsuda, M., and Shimomura, I. (2004). Increased oxidative stress in obesity and its impact on metabolic syndrome. The Journal of clinical investigation *114*, 1752-1761.

Gaidhu, M.P., Anthony, N.M., Patel, P., Hawke, T.J., and Ceddia, R.B. (2010). Dysregulation of lipolysis and lipid metabolism in visceral and subcutaneous adipocytes by high-fat diet: role of ATGL, HSL, and AMPK. American journal of physiology Cell physiology *298*, C961-971.

Gaikwad, A.S., Ramasarma, T., and Kurup, C.K. (1990). Decrease of oxidative activities in brown adipose tissue mitochondria of cold acclimated rats on short term exposure to heat stress. Biochimica et biophysica acta *1017*, 242-250.

Gandotra, S., Le Dour, C., Bottomley, W., Cervera, P., Giral, P., Reznik, Y., Charpentier, G., Auclair, M., Delepine, M., Barroso, I., *et al.* (2011). Perilipin deficiency and autosomal dominant partial lipodystrophy. The New England journal of medicine *364*, 740-748.

Garg, A. (2004). Acquired and inherited lipodystrophies. The New England journal of medicine *350*, 1220-1234.

Gartung, A., Zhao, J., Chen, S., Mottillo, E., VanHecke, G.C., Ahn, Y.H., Maddipati, K.R., Sorokin, A., Granneman, J., and Lee, M.J. (2016). Characterization of Eicosanoids Produced by Adipocyte Lipolysis: IMPLICATION OF CYCLOOXYGENASE-2 IN ADIPOSE INFLAMMATION. The Journal of biological chemistry *291*, 16001-16010.

Gorrini, C., Harris, I.S., and Mak, T.W. (2013). Modulation of oxidative stress as an anticancer strategy. Nature reviews Drug discovery *12*, 931-947.

Granneman, J.G., Moore, H.P., Krishnamoorthy, R., and Rathod, M. (2009). Perilipin controls lipolysis by regulating the interactions of AB-hydrolase containing 5 (Abhd5) and adipose triglyceride lipase (Atgl). J Biol Chem *284*,

34538-34544.

Greenberg, A.S., Egan, J.J., Wek, S.A., Garty, N.B., Blanchette-Mackie, E.J., and Londos, C. (1991). Perilipin, a major hormonally regulated adipocyte-specific phosphoprotein associated with the periphery of lipid storage droplets. J Biol Chem *266*, 11341-11346.

Ham, M., Choe, S.S., Shin, K.C., Choi, G., Kim, J.-W., Noh, J.-R., Kim, Y.-H., Ryu, J.-w., Yoon, K.-H., Lee, C.-H., *et al.* (2016). Glucose-6-phosphate dehydrogenase deficiency improves insulin resistance with reduced adipose tissue inflammation in obesity. Diabetes.

Han, C.Y., Umemoto, T., Omer, M., Den Hartigh, L.J., Chiba, T., LeBoeuf, R., Buller, C.L., Sweet, I.R., Pennathur, S., Abel, E.D., *et al.* (2012). NADPH oxidase-derived reactive oxygen species increases expression of monocyte chemotactic factor genes in cultured adipocytes. The Journal of biological chemistry *287*, 10379-10393.

Han, D., Antunes, F., Canali, R., Rettori, D., and Cadenas, E. (2003). Voltage-dependent anion channels control the release of the superoxide anion from mitochondria to cytosol. The Journal of biological chemistry *278*, 5557-5563.

Han, Y.H., Buffolo, M., Pires, K.M., Pei, S., Scherer, P.E., and Boudina, S. (2016). Adipocyte-Specific Deletion of Manganese Superoxide Dismutase Protects From Diet-Induced Obesity Through Increased Mitochondrial Uncoupling and Biogenesis. Diabetes *65*, 2639-2651.

Hepler, C., Shao, M., Xia, J.Y., Ghaben, A.L., Pearson, M.J., Vishvanath, L., Sharma, A.X., Morley, T.S., Holland, W.L., and Gupta, R.K. (2017). Directing visceral white adipocyte precursors to a thermogenic adipocyte fate improves insulin sensitivity in obese mice. eLife *6*.

Hernández-García, D., Wood, C.D., Castro-Obregón, S., and Covarrubias, L. (2010). Reactive oxygen species: A radical role in development? Free radical biology & medicine *49*, 130-143.

Herrero, L., Shapiro, H., Nayer, A., Lee, J., and Shoelson, S.E. (2010). Inflammation and adipose tissue macrophages in lipodystrophic mice. Proc Natl Acad Sci U S A *107*, 240-245.

Hong, S., Song, W., Zushin, P.H., Liu, B., Jedrychowski, M.P., Mina, A.I., Deng, Z., Cabarkapa, D., Hall, J.A., Palmer, C.J., *et al.* (2018). Phosphorylation of Beta-3 adrenergic receptor at serine 247 by ERK MAP

kinase drives lipolysis in obese adipocytes. Molecular metabolism *12*, 25-38.

Hoo, R.L., Shu, L., Cheng, K.K., Wu, X., Liao, B., Wu, D., Zhou, Z., and Xu, A. (2017). Adipocyte Fatty Acid Binding Protein Potentiates Toxic Lipids-Induced Endoplasmic Reticulum Stress in Macrophages via Inhibition of Janus Kinase 2-dependent Autophagy. Sci Rep *7*, 40657.

Hotamisligil, G.S., Shargill, N.S., and Spiegelman, B.M. (1993). Adipose expression of tumor necrosis factor-alpha: direct role in obesity-linked insulin resistance. Science (New York, NY) *259*, 87-91.

Hu, X., Cifarelli, V., Sun, S., Kuda, O., Abumrad, N.A., and Su, X. (2016). Major role of adipocyte prostaglandin E2 in lipolysis-induced macrophage recruitment. J Lipid Res *57*, 663-673.

Huang-Doran, I., Sleigh, A., Rochford, J.J., O'Rahilly, S., and Savage, D.B. (2010). Lipodystrophy: metabolic insights from a rare disorder. J Endocrinol *207*, 245-255.

Huh, J.Y., Park, J., Kim, J.I., Park, Y.J., Lee, Y.K., and Kim, J.B. (2017). Deletion of CD1d in Adipocytes Aggravates Adipose Tissue Inflammation and Insulin Resistance in Obesity. Diabetes *66*, 835-847.

Indulekha, K., Surendar, J., Anjana, R.M., Geetha, L., Gokulakrishnan, K., Pradeepa, R., and Mohan, V. (2015). Metabolic obesity, adipocytokines, and inflammatory markers in Asian Indians--CURES-124. Diabetes technology & therapeutics *17*, 134-141.

Iyer, A., Fairlie, D.P., Prins, J.B., Hammock, B.D., and Brown, L. (2010). Inflammatory lipid mediators in adipocyte function and obesity. Nature reviews Endocrinology *6*, 71-82.

Jain, M., Brenner, D.A., Cui, L., Lim, C.C., Wang, B., Pimentel, D.R., Koh, S., Sawyer, D.B., Leopold, J.A., Handy, D.E.*, et al.* (2003). Glucose-6-phosphate dehydrogenase modulates cytosolic redox status and contractile phenotype in adult cardiomyocytes. Circulation research *93*, e9-16.

Kahn, B.B., and Flier, J.S. (2000). Obesity and insulin resistance. J Clin Invest *106*, 473-481.

Kanda, H., Tateya, S., Tamori, Y., Kotani, K., Hiasa, K., Kitazawa, R., Kitazawa, S., Miyachi, H., Maeda, S., Egashira, K.*, et al.* (2006). MCP-1 contributes to macrophage infiltration into adipose tissue, insulin resistance,

and hepatic steatosis in obesity. J Clin Invest *116*, 1494-1505.

Kim, J.I., Park, J., Ji, Y., Jo, K., Han, S.M., Sohn, J.H., Shin, K.C., Han, J.S., Jeon, Y.G., Nahmgoong, H., *et al.* (2019). During Adipocyte Remodeling, Lipid Droplet Configurations Regulate Insulin Sensitivity through F-Actin and G-Actin Reorganization. Mol Cell Biol *39*.

Kim, M., Paik, J.K., Kang, R., Kim, S.Y., Lee, S.H., and Lee, J.H. (2013). Increased oxidative stress in normal-weight postmenopausal women with metabolic syndrome compared with metabolically healthy overweight/obese individuals. Metabolism: clinical and experimental *62*, 554-560.

Kimmel, A.R., and Sztalryd, C. (2016). The Perilipins: Major Cytosolic Lipid Droplet-Associated Proteins and Their Roles in Cellular Lipid Storage, Mobilization, and Systemic Homeostasis. Annual review of nutrition *36*, 471-509.

Klein, S., and Wolfe, R.R. (1990). Whole-body lipolysis and triglyceride-fatty acid cycling in cachectic patients with esophageal cancer. J Clin Invest *86*, 1403-1408.

Klingenberg, M., and Winkler, E. (1985). The reconstituted isolated uncoupling protein is a membrane potential driven H+ translocator. The EMBO journal *4*, 3087-3092.

Kono, T., Robinson, F.W., Blevins, T.L., and Ezaki, O. (1982). Evidence that translocation of the glucose transport activity is the major mechanism of insulin action on glucose transport in fat cells. The Journal of biological chemistry *257*, 10942-10947.

Kosteli, A., Sugaru, E., Haemmerle, G., Martin, J.F., Lei, J., Zechner, R., and Ferrante, A.W., Jr. (2010). Weight loss and lipolysis promote a dynamic immune response in murine adipose tissue. The Journal of clinical investigation *120*, 3466-3479.

Kwon, H., and Pessin, J.E. (2013). Adipokines mediate inflammation and insulin resistance. Front Endocrinol (Lausanne) *4*, 71.

Lackey, D.E., and Olefsky, J.M. (2016). Regulation of metabolism by the innate immune system. Nature reviews Endocrinology *12*, 15-28.

Langlois, D., Forcheron, F., Li, J.Y., del Carmine, P., Neggazi, S., and Beylot, M. (2011). Increased atherosclerosis in mice deficient in perilipin1. Lipids in

health and disease *10*, 169.

Lee, H., Lee, Y.J., Choi, H., Ko, E.H., and Kim, J.W. (2009). Reactive oxygen species facilitate adipocyte differentiation by accelerating mitotic clonal expansion. The Journal of biological chemistry *284*, 10601-10609.

Lee, J.H., Go, Y., Kim, D.Y., Lee, S.H., Kim, O.H., Jeon, Y.H., Kwon, T.K., Bae, J.H., Song, D.K., Rhyu, I.J., *et al.* (2020). Isocitrate dehydrogenase 2 protects mice from high-fat diet-induced metabolic stress by limiting oxidative damage to the mitochondria from brown adipose tissue. Experimental & molecular medicine *52*, 238-252.

Lee, S.Y., Kang, M.G., Park, J.S., Lee, G., Ting, A.Y., and Rhee, H.W. (2016). APEX Fingerprinting Reveals the Subcellular Localization of Proteins of Interest. Cell reports *15*, 1837-1847.

Leopold, J.A., Dam, A., Maron, B.A., Scribner, A.W., Liao, R., Handy, D.E., Stanton, R.C., Pitt, B., and Loscalzo, J. (2007). Aldosterone impairs vascular reactivity by decreasing glucose-6-phosphate dehydrogenase activity. Nature medicine *13*, 189-197.

Li, P., Oh, D.Y., Bandyopadhyay, G., Lagakos, W.S., Talukdar, S., Osborn, O., Johnson, A., Chung, H., Maris, M., Ofrecio, J.M., *et al.* (2015). LTB4 promotes insulin resistance in obese mice by acting on macrophages, hepatocytes and myocytes. Nature medicine *21*, 239-247.

Little, S.A., and de Haën, C. (1980). Effects of hydrogen peroxide on basal and hormone-stimulated lipolysis in perifused rat fat cells in relation to the mechanism of action of insulin. The Journal of biological chemistry *255*, 10888-10895.

Lumeng, C.N., DelProposto, J.B., Westcott, D.J., and Saltiel, A.R. (2008). Phenotypic switching of adipose tissue macrophages with obesity is generated by spatiotemporal differences in macrophage subtypes. Diabetes *57*, 3239-3246.

Lumeng, C.N., Deyoung, S.M., Bodzin, J.L., and Saltiel, A.R. (2007). Increased inflammatory properties of adipose tissue macrophages recruited during diet-induced obesity. Diabetes *56*, 16-23.

Marais, R., Wynne, J., and Treisman, R. (1993). The SRF accessory protein Elk-1 contains a growth factor-regulated transcriptional activation domain. Cell *73*, 381-393.

Martin, S., Fernandez-Rojo, M.A., Stanley, A.C., Bastiani, M., Okano, S., Nixon, S.J., Thomas, G., Stow, J.L., and Parton, R.G. (2012). Caveolin-1 deficiency leads to increased susceptibility to cell death and fibrosis in white adipose tissue: characterization of a lipodystrophic model. PLoS One *7*, e46242.

May, J.M., and de Haën, C. (1979). The insulin-like effect of hydrogen peroxide on pathways of lipid synthesis in rat adipocytes. The Journal of biological chemistry *254*, 9017-9021.

Mazid, M.A., Chowdhury, A.A., Nagao, K., Nishimura, K., Jisaka, M., Nagaya, T., and Yokota, K. (2006). Endogenous 15-deoxy-Delta(12,14)-prostaglandin J(2) synthesized by adipocytes during maturation phase contributes to upregulation of fat storage. FEBS letters *580*, 6885-6890.

McManaman, J.L., Bales, E.S., Orlicky, D.J., Jackman, M., MacLean, P.S., Cain, S., Crunk, A.E., Mansur, A., Graham, C.E., Bowman, T.A.*, et al.* (2013). Perilipin-2-null mice are protected against diet-induced obesity, adipose inflammation, and fatty liver disease. J Lipid Res *54*, 1346-1359.

Merkel, M., Eckel, R.H., and Goldberg, I.J. (2002). Lipoprotein lipase: genetics, lipid uptake, and regulation. Journal of lipid research *43*, 1997-2006.

Mills, E.L., Pierce, K.A., Jedrychowski, M.P., Garrity, R., Winther, S., Vidoni, S., Yoneshiro, T., Spinelli, J.B., Lu, G.Z., Kazak, L.*, et al.* (2018). Accumulation of succinate controls activation of adipose tissue thermogenesis. Nature *560*, 102-106.

Miyoshi, H., Souza, S.C., Zhang, H.H., Strissel, K.J., Christoffolete, M.A., Kovsan, J., Rudich, A., Kraemer, F.B., Bianco, A.C., Obin, M.S.*, et al.* (2006). Perilipin promotes hormone-sensitive lipase-mediated adipocyte lipolysis via phosphorylation-dependent and -independent mechanisms. J Biol Chem *281*, 15837-15844.

Montgomery, M.K., Mokhtar, R., Bayliss, J., Parkington, H.C., Suturin, V.M., Bruce, C.R., and Watt, M.J. (2018). Perilipin 5 Deletion Unmasks an Endoplasmic Reticulum Stress-Fibroblast Growth Factor 21 Axis in Skeletal Muscle. Diabetes *67*, 594-606.

Morton, S., Davis, R.J., McLaren, A., and Cohen, P. (2003). A reinvestigation of the multisite phosphorylation of the transcription factor c-Jun. The EMBO journal *22*, 3876-3886.

Najt, C.P., Senthivinayagam, S., Aljazi, M.B., Fader, K.A., Olenic, S.D., Brock, J.R., Lydic, T.A., Jones, A.D., and Atshaves, B.P. (2016). Liver-specific loss of Perilipin 2 alleviates diet-induced hepatic steatosis, inflammation, and fibrosis. American journal of physiology Gastrointestinal and liver physiology *310*, G726-738.

Nicholls, D.G. (1977). The effective proton conductance of the inner membrane of mitochondria from brown adipose tissue. Dependency on proton electrochemical potential gradient. European journal of biochemistry *77*, 349-356.

Nicholls, D.G., and Locke, R.M. (1984). Thermogenic mechanisms in brown fat. Physiological reviews *64*, 1-64.

Oh, D.Y., Morinaga, H., Talukdar, S., Bae, E.J., and Olefsky, J.M. (2012). Increased macrophage migration into adipose tissue in obese mice. Diabetes *61*, 346-354.

Olefsky, J.M., and Glass, C.K. (2010). Macrophages, inflammation, and insulin resistance. Annual review of physiology *72*, 219-246.

Park, A., Kim, W.K., and Bae, K.H. (2014). Distinction of white, beige and brown adipocytes derived from mesenchymal stem cells. World journal of stem cells *6*, 33-42.

Park, J., Choe, S.S., Choi, A.H., Kim, K.H., Yoon, M.J., Suganami, T., Ogawa, Y., and Kim, J.B. (2006). Increase in glucose-6-phosphate dehydrogenase in adipocytes stimulates oxidative stress and inflammatory signals. Diabetes *55*, 2939-2949.

Park, J., Rho, H.K., Kim, K.H., Choe, S.S., Lee, Y.S., and Kim, J.B. (2005). Overexpression of glucose-6-phosphate dehydrogenase is associated with lipid dysregulation and insulin resistance in obesity. Mol Cell Biol *25*, 5146-5157.

Park, Y.J., Choe, S.S., Sohn, J.H., and Kim, J.B. (2017). The role of glucose-6-phosphate dehydrogenase in adipose tissue inflammation in obesity. Adipocyte *6*, 147-153.

Pereira, P.A.T., Assis, P.A., Prado, M.K.B., Ramos, S.G., Aronoff, D.M., de Paula-Silva, F.W.G., Sorgi, C.A., and Faccioli, L.H. (2018). Prostaglandins D(2) and E(2) have opposite effects on alveolar macrophages infected with Histoplasma capsulatum. Journal of lipid research *59*, 195-206.

Petersen, K.F., and Shulman, G.I. (2002). Pathogenesis of skeletal muscle insulin resistance in type 2 diabetes mellitus. The American journal of cardiology *90*, 11g-18g.

Porporato, P.E. (2016). Understanding cachexia as a cancer metabolism syndrome. Oncogenesis *5*, e200.

Porras, A., Valladares, A., Alvarez, A.M., Roncero, C., and Benito, M. (2002). Differential role of PPAR gamma in the regulation of UCP-1 and adipogenesis by TNF-alpha in brown adipocytes. FEBS letters *520*, 58-62.

Rigoulet, M., Yoboue, E.D., and Devin, A. (2011). Mitochondrial ROS generation and its regulation: mechanisms involved in H(2)O(2) signaling. Antioxidants & redox signaling *14*, 459-468.

Ro, S.H., Nam, M., Jang, I., Park, H.W., Park, H., Semple, I.A., Kim, M., Kim, J.S., Park, H., Einat, P*., et al.* (2014). Sestrin2 inhibits uncoupling protein 1 expression through suppressing reactive oxygen species. Proceedings of the National Academy of Sciences of the United States of America *111*, 7849-7854.

Rosell, M., Kaforou, M., Frontini, A., Okolo, A., Chan, Y.W., Nikolopoulou, E., Millership, S., Fenech, M.E., MacIntyre, D., Turner, J.O*., et al.* (2014). Brown and white adipose tissues: intrinsic differences in gene expression and response to cold exposure in mice. American journal of physiology Endocrinology and metabolism *306*, E945-964.

Samuel, V.T., and Shulman, G.I. (2012). Mechanisms for insulin resistance: common threads and missing links. Cell *148*, 852-871.

Sandalio, L.M., and Romero-Puertas, M.C. (2015). Peroxisomes sense and respond to environmental cues by regulating ROS and RNS signalling networks. Annals of botany *116*, 475-485.

Saponaro, C., Gaggini, M., Carli, F., and Gastaldelli, A. (2015). The Subtle Balance between Lipolysis and Lipogenesis: A Critical Point in Metabolic Homeostasis. Nutrients *7*, 9453-9474.

Savage, D.B. (2009). Mouse models of inherited lipodystrophy. Disease models & mechanisms *2*, 554-562.

Schaar, C.E., Dues, D.J., Spielbauer, K.K., Machiela, E., Cooper, J.F., Senchuk, M., Hekimi, S., and Van Raamsdonk, J.M. (2015). Mitochondrial

and cytoplasmic ROS have opposing effects on lifespan. PLoS genetics *11*, e1004972.

Scherer, P.E., Williams, S., Fogliano, M., Baldini, G., and Lodish, H.F. (1995). A novel serum protein similar to C1q, produced exclusively in adipocytes. The Journal of biological chemistry *270*, 26746-26749.

Schieber, M., and Chandel, N.S. (2014). ROS function in redox signaling and oxidative stress. Current biology : CB *24*, R453-462.

Schneider, K., Valdez, J., Nguyen, J., Vawter, M., Galke, B., Kurtz, T.W., and Chan, J.Y. (2016). Increased Energy Expenditure, Ucp1 Expression, and Resistance to Diet-induced Obesity in Mice Lacking Nuclear Factor-Erythroid-2-related Transcription Factor-2 (Nrf2). The Journal of biological chemistry *291*, 7754-7766.

Schoiswohl, G., Stefanovic-Racic, M., Menke, M.N., Wills, R.C., Surlow, B.A., Basantani, M.K., Sitnick, M.T., Cai, L., Yazbeck, C.F., Stolz, D.B.*, et al.* (2015). Impact of Reduced ATGL-Mediated Adipocyte Lipolysis on Obesity-Associated Insulin Resistance and Inflammation in Male Mice. Endocrinology *156*, 3610-3624.

Schröder, K. (2020). NADPH oxidases: Current aspects and tools. Redox biology *34*, 101512.

Scott, J.P., and Peters-Golden, M. (2013). Antileukotriene agents for the treatment of lung disease. American journal of respiratory and critical care medicine *188*, 538-544.

Sears, R., Nuckolls, F., Haura, E., Taya, Y., Tamai, K., and Nevins, J.R. (2000). Multiple Ras-dependent phosphorylation pathways regulate Myc protein stability. Genes Dev *14*, 2501-2514.

Sekhar, B.S., Kurup, C.K., and Ramasarma, T. (1987). Generation of hydrogen peroxide by brown adipose tissue mitochondria. Journal of bioenergetics and biomembranes *19*, 397-407.

Shabalina, I.G., Vrbacký, M., Pecinová, A., Kalinovich, A.V., Drahota, Z., Houštěk, J., Mráček, T., Cannon, B., and Nedergaard, J. (2014). ROS production in brown adipose tissue mitochondria: the question of UCP1-dependence. Biochimica et biophysica acta *1837*, 2017-2030.

Shafique, E., Torina, A., Reichert, K., Colantuono, B., Nur, N., Zeeshan, K.,

Ravichandran, V., Liu, Y., Feng, J., Zeeshan, K., *et al.* (2017). Mitochondrial redox plays a critical role in the paradoxical effects of NAPDH oxidase-derived ROS on coronary endothelium. Cardiovascular research *113*, 234-246.

Shi, H., Kokoeva, M.V., Inouye, K., Tzameli, I., Yin, H., and Flier, J.S. (2006). TLR4 links innate immunity and fatty acid-induced insulin resistance. The Journal of clinical investigation *116*, 3015-3025.

Shimizu, I., Aprahamian, T., Kikuchi, R., Shimizu, A., Papanicolaou, K.N., MacLauchlan, S., Maruyama, S., and Walsh, K. (2014). Vascular rarefaction mediates whitening of brown fat in obesity. The Journal of clinical investigation *124*, 2099-2112.

Shimizu, T. (2009). Lipid mediators in health and disease: enzymes and receptors as therapeutic targets for the regulation of immunity and inflammation. Annual review of pharmacology and toxicology *49*, 123-150.

Shimizu, T., and Wolfe, L.S. (1990). Arachidonic acid cascade and signal transduction. Journal of neurochemistry *55*, 1-15.

Shulman, G.I. (2014). Ectopic fat in insulin resistance, dyslipidemia, and cardiometabolic disease. The New England journal of medicine *371*, 2237-2238.

Sidossis, L., and Kajimura, S. (2015). Brown and beige fat in humans: thermogenic adipocytes that control energy and glucose homeostasis. The Journal of clinical investigation *125*, 478-486.

Sohn, J.H., Kim, J.I., Jeon, Y.G., Park, J., and Kim, J.B. (2018a). Effects of Three Thiazolidinediones on Metabolic Regulation and Cold-Induced Thermogenesis. Molecules and cells *41*, 900-908.

Sohn, J.H., Lee, Y.K., Han, J.S., Jeon, Y.G., Kim, J.I., Choe, S.S., Kim, S.J., Yoo, H.J., and Kim, J.B. (2018b). Perilipin 1 (Plin1) deficiency promotes inflammatory responses in lean adipose tissue through lipid dysregulation. Journal of Biological Chemistry *293*, 13974-13988.

Song, Z., Xiaoli, A.M., and Yang, F. (2018). Regulation and Metabolic Significance of De Novo Lipogenesis in Adipose Tissues. Nutrients *10*.

Spolarics, Z. (1998). Endotoxemia, pentose cycle, and the oxidant/antioxidant balance in the hepatic sinusoid. Journal of leukocyte biology *63*, 534-541.

Succurro, E., Marini, M.A., Frontoni, S., Hribal, M.L., Andreozzi, F., Lauro, R., Perticone, F., and Sesti, G. (2008). Insulin secretion in metabolically obese, but normal weight, and in metabolically healthy but obese individuals. Obesity (Silver Spring, Md) *16*, 1881-1886.

Suganami, T., Tanimoto-Koyama, K., Nishida, J., Itoh, M., Yuan, X., Mizuarai, S., Kotani, H., Yamaoka, S., Miyake, K., Aoe, S., *et al.* (2007). Role of the Toll-like receptor 4/NF-kappaB pathway in saturated fatty acid-induced inflammatory changes in the interaction between adipocytes and macrophages. Arterioscler Thromb Vasc Biol *27*, 84-91.

Swierczyński, J., Scisłowski, P.W., Aleksandrowicz, Z., and Zydowo, M. (1981). Malic enzyme in brown adipose tissue--purification, some properties and possible physiological role. The International journal of biochemistry *13*, 365-372.

Tafani, M., Sansone, L., Limana, F., Arcangeli, T., De Santis, E., Polese, M., Fini, M., and Russo, M.A. (2016). The Interplay of Reactive Oxygen Species, Hypoxia, Inflammation, and Sirtuins in Cancer Initiation and Progression. Oxidative medicine and cellular longevity *2016*, 3907147.

Talbot, N.A., Wheeler-Jones, C.P., and Cleasby, M.E. (2014). Palmitoleic acid prevents palmitic acid-induced macrophage activation and consequent p38 MAPK-mediated skeletal muscle insulin resistance. Molecular and cellular endocrinology *393*, 129-142.

Taniguchi, C.M., Emanuelli, B., and Kahn, C.R. (2006). Critical nodes in signalling pathways: insights into insulin action. Nature reviews Molecular cell biology *7*, 85-96.

Tansey, J.T., Sztalryd, C., Gruia-Gray, J., Roush, D.L., Zee, J.V., Gavrilova, O., Reitman, M.L., Deng, C.X., Li, C., Kimmel, A.R., *et al.* (2001). Perilipin ablation results in a lean mouse with aberrant adipocyte lipolysis, enhanced leptin production, and resistance to diet-induced obesity. Proc Natl Acad Sci U S A *98*, 6494-6499.

Tormos, K.V., Anso, E., Hamanaka, R.B., Eisenbart, J., Joseph, J., Kalyanaraman, B., and Chandel, N.S. (2011). Mitochondrial complex III ROS regulate adipocyte differentiation. Cell metabolism *14*, 537-544.

Torres, M., and Forman, H.J. (2003). Redox signaling and the MAP kinase pathways. BioFactors (Oxford, England) *17*, 287-296.

Valladares, A., Roncero, C., Benito, M., and Porras, A. (2001). TNF-alpha inhibits UCP-1 expression in brown adipocytes via ERKs. Opposite effect of p38MAPK. FEBS letters *493*, 6-11.

Vane, J.R., Bakhle, Y.S., and Botting, R.M. (1998). Cyclooxygenases 1 and 2. Annual review of pharmacology and toxicology *38*, 97-120.

Vijayakumar, A., Aryal, P., Wen, J., Syed, I., Vazirani, R.P., Moraes-Vieira, P.M., Camporez, J.P., Gallop, M.R., Perry, R.J., Peroni, O.D.*, et al.* (2017). Absence of Carbohydrate Response Element Binding Protein in Adipocytes Causes Systemic Insulin Resistance and Impairs Glucose Transport. Cell reports *21*, 1021-1035.

Virtanen, K.A., Lidell, M.E., Orava, J., Heglind, M., Westergren, R., Niemi, T., Taittonen, M., Laine, J., Savisto, N.J., Enerbäck, S.*, et al.* (2009). Functional brown adipose tissue in healthy adults. The New England journal of medicine *360*, 1518-1525.

Wallace, J.L. (2001). Prostaglandin biology in inflammatory bowel disease. Gastroenterology clinics of North America *30*, 971-980.

Wang, C.H., Wang, C.C., Huang, H.C., and Wei, Y.H. (2013). Mitochondrial dysfunction leads to impairment of insulin sensitivity and adiponectin secretion in adipocytes. The FEBS journal *280*, 1039-1050.

Weisberg, S.P., McCann, D., Desai, M., Rosenbaum, M., Leibel, R.L., and Ferrante, A.W., Jr. (2003). Obesity is associated with macrophage accumulation in adipose tissue. J Clin Invest *112*, 1796-1808.

Whitmarsh, A.J. (2007). Regulation of gene transcription by mitogen-activated protein kinase signaling pathways. Biochimica et biophysica acta *1773*, 1285-1298.

Wu, Q., Ortegon, A.M., Tsang, B., Doege, H., Feingold, K.R., and Stahl, A. (2006). FATP1 is an insulin-sensitive fatty acid transporter involved in diet-induced obesity. Mol Cell Biol *26*, 3455-3467.

Xu, H., Barnes, G.T., Yang, Q., Tan, G., Yang, D., Chou, C.J., Sole, J., Nichols, A., Ross, J.S., Tartaglia, L.A.*, et al.* (2003). Chronic inflammation in fat plays a crucial role in the development of obesity-related insulin resistance. J Clin Invest *112*, 1821-1830.

Xu, Y., Zhang, Z., Hu, J., Stillman, I.E., Leopold, J.A., Handy, D.E., Loscalzo,

J., and Stanton, R.C. (2010). Glucose-6-phosphate dehydrogenase-deficient mice have increased renal oxidative stress and increased albuminuria. FASEB journal : official publication of the Federation of American Societies for Experimental Biology *24*, 609-616.

Yamamoto, K., Miyoshi, H., Cho, K.Y., Nakamura, A., Greenberg, A.S., and Atsumi, T. (2018). Overexpression of perilipin1 protects against atheroma progression in apolipoprotein E knockout mice. Atherosclerosis *269*, 192-196.

Yang, J., Schmelzer, K., Georgi, K., and Hammock, B.D. (2009). Quantitative profiling method for oxylipin metabolome by liquid chromatography electrospray ionization tandem mass spectrometry. Analytical chemistry *81*, 8085-8093.

Yang, S.H., Sharrocks, A.D., and Whitmarsh, A.J. (2003). Transcriptional regulation by the MAP kinase signaling cascades. Gene *320*, 3-21.

Ye, L., Kleiner, S., Wu, J., Sah, R., Gupta, R.K., Banks, A.S., Cohen, P., Khandekar, M.J., Boström, P., Mepani, R.J., *et al.* (2012). TRPV4 is a regulator of adipose oxidative metabolism, inflammation, and energy homeostasis. Cell *151*, 96-110.

Yeop Han, C., Kargi, A.Y., Omer, M., Chan, C.K., Wabitsch, M., O'Brien, K.D., Wight, T.N., and Chait, A. (2010). Differential effect of saturated and unsaturated free fatty acids on the generation of monocyte adhesion and chemotactic factors by adipocytes: dissociation of adipocyte hypertrophy from inflammation. Diabetes *59*, 386-396.

Yore, M.M., Syed, I., Moraes-Vieira, P.M., Zhang, T., Herman, M.A., Homan, E.A., Patel, R.T., Lee, J., Chen, S., Peroni, O.D., *et al.* (2014). Discovery of a class of endogenous mammalian lipids with anti-diabetic and anti-inflammatory effects. Cell *159*, 318-332.

Yubero, P., Barberá, M.J., Alvarez, R., Viñas, O., Mampel, T., Iglesias, R., Villarroya, F., and Giralt, M. (1998). Dominant negative regulation by c-Jun of transcription of the uncoupling protein-1 gene through a proximal cAMP-regulatory element: a mechanism for repressing basal and norepinephrine-induced expression of the gene before brown adipocyte differentiation. Molecular endocrinology (Baltimore, Md) *12*, 1023-1037.

Yue, L., Zhao, W., Wang, D., Meng, M., Zheng, Y., Li, Y., Qiu, J., Yu, J., Yan, Y., Lu, P., *et al.* (2019). Silver nanoparticles inhibit beige fat function and promote adiposity. Molecular metabolism *22*, 1-11.

Zhang, J., Jin, N., Liu, Y., and Rhoades, R.A. (1998). Hydrogen peroxide stimulates extracellular signal-regulated protein kinases in pulmonary arterial smooth muscle cells. American journal of respiratory cell and molecular biology *19*, 324-332.

Zhang, S., Liu, G., Xu, C., Liu, L., Zhang, Q., Xu, Q., Jia, H., Li, X., and Li, X. (2018). Perilipin 1 Mediates Lipid Metabolism Homeostasis and Inhibits Inflammatory Cytokine Synthesis in Bovine Adipocytes. Frontiers in immunology *9*, 467.

Zhang, Y., Proenca, R., Maffei, M., Barone, M., Leopold, L., and Friedman, J.M. (1994). Positional cloning of the mouse obese gene and its human homologue. Nature *372*, 425-432.

Zhou, P.L., Li, M., Han, X.W., Bi, Y.H., Zhang, W.G., Wu, Z.Y., and Wu, G. (2017). Plin5 deficiency promotes atherosclerosis progression through accelerating inflammation, apoptosis and oxidative stress. Journal of cellular biochemistry.

Zoccal, K.F., Sorgi, C.A., Hori, J.I., Paula-Silva, F.W., Arantes, E.C., Serezani, C.H., Zamboni, D.S., and Faccioli, L.H. (2016). Opposing roles of LTB4 and PGE2 in regulating the inflammasome-dependent scorpion venom-induced mortality. Nat Commun *7*, 10760.

Zou, L., Wang, W., Liu, S., Zhao, X., Lyv, Y., Du, C., Su, X., Geng, B., and Xu, G. (2016). Spontaneous hypertension occurs with adipose tissue dysfunction in perilipin-1 null mice. Biochim Biophys Acta *1862*, 182-191.

국문 초록

지방세포 기능 조절에 있어
지방대사물 및 활성산소의 역할 규명

지방세포는 지방 대사에 특화되어 있으며, 이는 전신적 에너지대사 항상성과 밀접하게 연관되어 있다. 백색지방세포는 체내 에너지 상태를 인지하여 지방대사물의 저장 및 분해를 관장하는 반면, 갈색지방세포는 추위 자극에 반응하여 지방산 산화를 통해 열 생성 및 에너지 소비를 촉진한다. 지방세포에서 지방대사의 조절 결함은 이상 지질혈증, 제 2 형 당뇨병, 지방간 및 다양한 염증성 질환을 포함한 에너지대사 이상과 밀접하게 연관되어 있다. 지방세포 내 지방대사의 정밀한 조절이 전신적 에너지대사 항상성에 중요하다는 것이 잘 알려져 있지만, 지방대사 과정에서 생성되는 매개물들의 역할에 대해서는 거의 알려진 바 없다. 최근, 지방대사 과정의 산물 혹은 부산물인 지방대사물과 활성산소가 신호분자로 작용한다는 것이 제안되고 있다. 포화지방산이나 류코트리엔(leukotriene)B_4와 같은 지방대사물이 백색지방조직에서 염증반응을 촉진하여 전신적 인슐린 민감도를 손상시킨다. 뿐만 아니

라, 갈색지방세포 내 활성산소가 열 발생 기능에 반대되는 영향력을 미칠 수 있다는 것이 보고되었다. 예를 들면, 미토콘드리아 활성산소는 저온 노출 시 갈색지방세포의 열 생성을 매개하는 반면, 오히려 과도한 활성산소는 갈색지방세포의 열 생성 작용을 방해한다. 이러한 보고에도 불구하고, 지방대사물 및 활성산소가 지방세포의 기능 및 전신적 에너지대사를 조절하는 상세한 기전에 대한 이해가 부족하다.

본 학위논문의 1장에서는 백색지방세포 내 지방대사물의 비정상적인 분해가 염증성 지방대사물의 분비를 촉진시켜 지방조직 염증반응과 전신적 인슐린 저항성을 유발함을 다루고 있다. 백색지방세포에서 PLIN1 결손에 의한 지방대사물의 분해 증가는 지방대사물 중 하나인 프로스타글란딘(prostaglandin) 분비를 촉진하며, 이를 통해 지방조직 내 대식세포 축적이 증가함으로써 전신적 인슐린 저항성이 유발되었다. 그러므로, 본 연구는 백색지방세포에서 지방대사물 분해 제어 결함이 지방대사물의 부적절한 분비를 통해 지방조직의 면역반응 균형과 전신적 에너지대사 항상성 조절과정을 손상시킬 수 있음을 의미한다.

본 학위논문의 2장에서는 갈색지방세포에서 활성산소를 제거하는 항산화 과정을 통한 열 발생 조절기전을 연구하였다. 산화

환원 조절과 항산화 경로가 백색지방조직보다 갈색지방조직에서 더 활발함을 관찰하였다. 또한, NADPH 생산 효소인 G6PD는 갈색지방조직과 백색지방조직에서 다르게 조절되는 것을 관찰하였다. 갈색지방세포에서 G6PD 결손은 세포질 특이적 활성산소의 과도한 증가에 의해 ERK 활성화를 유도하여 열 발생 과정에서 손상을 야기하였다. 이상의 결과들은 갈색지방세포에서 G6PD에 의한 세포질 내 활성산소의 제거가 열 생성을 촉진할 것임을 암시한다.

본 연구를 통하여 지방세포 내 지방대사물 및 활성산소의 조절이 전신적 에너지대사 항상성 유지에 중요한 지방세포의 기능을 위해 필수적임을 제안한다.

주요어: 백색 지방세포, 갈색 지방세포, 지질 분해, 지방대사물, 염증반응, 인슐린 저항성, 열 생성, 산화 스트레스

학번: 2012-20314